SYNTHESIS AND CHARACTERIZATION OF COPPER DOPED ZINC OXIDE THIN FILMS DEPOSITED BY SPRAY PYROLYSIS TECHNIQUE

M. Phil. Thesis

BY
MAKSUDA AKHTER
ROLL NO. 1009143008 F
SESSION: October, 2009

DEPARTMENT OF PHYSICS
BANGLADESH UNIVERSITY OF ENGINEERING AND TECHNOLOGY
DHAKA-1000, BANGLADESH

May, 2012

SYNTHESIS AND CHARACTERIZATION OF COPPER DOPED ZINC OXIDE THIN FILMS DEPOSITED BY SPRAY PYROLYSIS TECHNIQUE

A Dissertation Submitted to the department of Physics, Bangladesh University of Engineering and Technology (BUET), Dhaka, Bangladesh, in Partial Fulfillment of Requirement for the Degree of Master of Philosophy (M. Phil) in Physics

BY
MAKSUDA AKHTER
ROLL NO. 1009143008 F
SESSION: October, 2009

DEPARTMENT OF PHYSICS
BANGLADESH UNIVERSITY OF ENGINEERING AND TECHNOLOGY
DHAKA-1000, BANGLADESH
May, 2012

CANDIDATE'S DECLARATION

It is hereby declared that this thesis or any part of it has not been submitted elsewhere for the award of any degree or diploma.

_____

MAKSUDA AKHTER

DEDICATED TO
MY
BELOVED PARENTS

CHAPTER-I

INTRODUCTION

CHAPTER-II

THEORETICAL BACKGROUND

Part A: Formation of Thin Films

Part B: Theoretical Principles of Film Characterization

CHAPTER-III

THIN FILM DEPOSITION TECHNIQUES

CHAPTER-IV

EXPERIMENTAL DETAILS

Part A: Film Deposition

Part B: Measurement Details

CHAPTER- V

RESULTS AND DISCUSSION

CHAPTER- VI

CONCLUSIONS AND SUGGESTIONS FOR FUTURE WORK

CONTENTS

CHAPTER-III: THIN FILM DEPOSITION TECHNIQUES

CHAPTER-IV: EXPERIMENTAL DETAILS

CHAPTER-V: RESULTS AND DISCUSSION

List of Figures

List of Tables

ACKNOWLEDGEMENTS

At first I express my gratefulness to the Almighty Allah-Rabbul Alamin, who gives me the strength and energy to fulfill this research work.

It is a great pleasure for me to express my profound sense of gratitude, indebtedness and deep appreciation to my reverend and respectable teacher Professor Dr. Jiban Podder, Department of Physics, Bangladesh University of Engineering & Technology, Dhaka. I am most grateful to his constant supervision, inspiring guidance, sagacious advice, active help, enthusiastic encouragement, co-operation, fruitful suggestions and encouragements throughout the entire course of my research work. Due to his constant guidance and inspiring collaboration, I have very much benefited from his vast knowledge and experience.

I am deeply indebted to my respected teacher Professor Dr. Md. Mostak Hossain Head, Department of Physics, BUET, Dhaka for providing necessary facilities to carry out this research work and valuable suggestions regarding my thesis.

I like to express my gratitude to, Professor Dr. Md. Abu Hashan Bhuiyan, Professor Dr. Feroz Alam Khan, Professor Dr. A. K. M. Akther Hossain, Dr. Afia Begum, Dr. Forhad Mina, Dr. Rafi Uddin, Dr. Nasreen Akhter and all other teachers of the Physics Department, for their corporation and valuable discussion on various points.

I am very much grateful to Dr. Dilip Kumar Saha, Chief Scientific Officer, Atomic Energy Centre, Dhaka, for his kind help to take XRD patterns. I am grateful to Dr. Md. Abdul Gafur, Senior Engineer, BCSIR, for UV-VIS measurements and Md. Al-Mamun, Engineer, AECD for SEM and EDX analysis.

I am really thankful to Jewel Kumar Saha, Muslima Zahan, Mahjabin Taskin, Mr. Khorshed Alam, Mr. Sanjoy Das, for their continuous cooperation and valuable suggestions during my research work in the solid state physics laboratory of the Department of Physics, BUET.

I am very grateful to Mr. Idris Munsi, Mr.Liakot Ali, Abu Taher and all other official staff of this department for their sincere help. I am also thankful to the technicians of the mechanical workshop of BUET for their technical support during this research work.

I am thankful to the authority of Bangladesh University of Engineering & Technology, Dhaka for giving me necessary permission and providing financial support for this work.

Finally, I would like to express my deep gratitude to my parents and brother for their multifaceted support through all these years. Last, but not least I am very grateful to my husband Lieutenant M Jahurul Haque, BN for her constant support and encouragement during my research work. Thanks are also given to all my relatives and friends who are always appreciating me to doing this work.

The Author

Maksuda Akhter

Abstract

Zinc Oxide (ZnO) is one of the most important candidates for a II-VI room-temperature diluted magnetic semiconductor (DMS) by doping with a transition metal. ZnO based DMSs are particularly attractive as candidates for integrating optical and electronic properties into a single substance. ZnO and copper (Cu) doped ZnO thin films were synthesized from the precursors $Zn(CH_3COO)_2.2H_2O$ and $Cu(CH_3COO)_2.H_2O$ by using a "Spray Pyrolysis Deposition" technique at 623K substrate temperature containing 0, 5, 9, 15, 20 and 25 at% Cu concentrations. The surface morphological, structural, electrical and optical properties of the as-deposited ZnO films have been investigated as a function of Cu-doping level. The thickness of the films was estimated by Fizeau fringes interference method which varied from 195 to 198 nm.

The scanning electron microscopy (SEM) micrographs of as-deposited films shows that all the films are found well covered on the glass substrate. Nanofibers are observed around the nucleation center in pure ZnO thin film. Due to interstitial holes of ZnO are filled with copper, the fiber has broken and transform into grain. The size of the grain decreases with the increase of Cu concentration. Energy Dispersive Analysis of X-ray (EDAX) results clearly showed that the grains are typically comprised of both Zn and O for pure and Zn, O, and Cu for Cu doped films. From EDAX data it is found that atomic weight % of Cu is increased with the increase of Cu concentration in Cu doped ZnO films.

X-ray diffraction studies showed the amorphous polycrystalline nature of the films with preferential orientation along the (100), (002), (101), (102), (110), (103) and (112) planes. Structure of the material has been identified as hexagonal wurtzite. The peaks are found to shift from their standard positions in the presence of the Cu dopant due to the positioning of dopant atoms into interstitial lattice sites.

Various optical constants such as absorbance, transmittance, refractive index and dielectric constant of the films have been studied for the as-deposited films are recorded in the wavelength ranges from 300 to 1100 nm. For as-deposited $Zn_{1-x}Cu_xO$ films, the band gap varies from 3.21 to 3.05 eV as Cu increases. The resistivity gradually decreases with the increase of temperature, which indicates the semiconducting nature of the materials. The activation energy is increasing up to 9% and then it decreases with the higher percentage of copper concentration.

CHAPTER-I
INTRODUCTION

1.1 Introduction

'Thin Solid Film' is the new branch of science has become a great demand of microelectronics in science and technology has greatly stimulated due to the development of thin film and the expansion. Experimental work on thin films has been continued in different parts of the world for successful applications of their properties in scientific, engineering and industrial purposes. The increasing demands for microelectronics and micro structural components in different branches of science and technology have greatly expanded the sphere of thin film research [1-2]. Thin films mean a thin layer or coating of a material on another material. The definition of thin film means a thin layer of solid material is deposited on the substrate. The thickness of the thin film is comparable with the mean free path of the conduction electron.

A solid crystalline material whose electrical conductivity is between that of a conductors and an insulator is known as a semiconductor. Good conductors have resistivity between 10^{-7} Ωm to 10^{-8} Ωm at room temperature while the resistivity of insulators is in the range 10^{10} Ωm and 10^{14} Ωm. Semiconductors fall in resistivity between 10^{-6} Ωm to 10^{7} Ωm. Pure semiconductors behave like insulators at 0 Kelvin, however at normal temperatures, in contrast to metals, semiconductors have a negative coefficient of resistance due to the increase in the concentration of charge carriers as the temperature rises. The conductivity of a semiconductor material can be varied under an external electrical field. Devices made from semiconductor materials are the foundation of modern electronics, including radio, computers, telephones, and many other devices. Semiconductor devices include the transistor, many kinds of diodes including the light-emitting diode (LED), laser diode (LD)[3], the silicon controlled rectifier, and digital and analog integrated circuits. Solar photovoltaic panels are large semiconductor devices that directly convert light energy into electrical energy [4].

The property of semiconductors that makes them most useful for constructing electronic devices is that their conductivity may easily be modified by introducing impurities into their crystal lattice. The process of adding controlled impurities to a semiconductor is known as doping. The amount of impurity, or dopant, added to an intrinsic (pure) semiconductor varies its level of conductivity. Doped semiconductors are often referred to as extrinsic. By adding impurity to pure semiconductors, the electrical conductivity may be varied not only by the number of impurity atoms but also, by the type of impurity atom.

The materials chosen as suitable dopants depend on the atomic properties of both the dopant and the material to be doped. In general, dopants that produce the desired controlled changes are classified as either electron acceptors or donors. A donor atom that activates donates weakly bound valence electrons to the material, creating excess negative charge carriers. These weakly bound electrons can move about in the crystal lattice relatively freely and can facilitate conduction in the presence of an electric field. The donor atoms introduce some states under, but very close to the conduction band edge. Electrons at these states can be easily excited to the conduction band, becoming free electrons, at room temperature. Conversely, an activated acceptor produces a hole. Semiconductors doped with donor impurities are called n-type, while those doped with acceptor impurities are known as p-type. The n and p type designations indicate which charge carrier acts as the material's majority carrier. The opposite carrier is called the minority carrier, which exists due to thermal excitation at a much lower concentration compared to the majority carrier.

Transistors operate by controlling the flow of carriers through the semiconductor by applied electric fields. Spin, on the other hand, is used for the magnetic data storage. The word "spin electronics" refers to devices that manipulate the freedom of spin degree [5]. In traditional electronic devices, charge and spin are used separately. Charge, on one hand, is used for the computing. A new generation of devices based on the manipulation of spins may have completely new functionality, therefore drastically improves the computation speed and reduces power consumption.

1.2 Characteristics of Thin Films

The properties of thin film changes appreciably when it is cooled to a very low temperature or heated at a higher temperature (above room temperature). The study of the changes in the properties of thin film with temperature provides a great deal of information about the properties of thin films. In general the physical properties of thin film are determined by a number of factors, such as

i) The nature of substrates

It may be non-crystalline solids e.g., glass of vitreous silica or crystalline such as cleavage plates of rock salt or mica. To select a particular substrate one has to take into consideration of the lattice parameter of the substrate so that it matches to the lattice parameter of the grown film, otherwise structural mismatch may create mechanical fracture in the film. It is also necessary to consider the melting point of the substrate material. It should be comparable with that of the film materials.

ii) Substrate temperature

The temperature of substrate during deposition of film may affect the film properties. At low temperature polycrystalline films with high densities of structural imperfections are formed on both vitreous and crystalline substrate, but a high temperature oriented single crystal films are formed on crystalline substrates.

iii) Deposition rate and film thickness

The temperature at which epitaxy occurs is dependent on the deposition rate. Substrate temperature decreases with increasing deposition rate. Film thickness mainly depends on deposition rate and deposition time. If the deposition rate increases, the film thickness also increases having the same deposition time.

iv) Post-deposition annealing of the films

Heating the film to a higher temperature after deposition and cooling it back to room temperature is known as annealing. Properties of the deposited films are related to the annealing temperature. The post-annealing process removes some defects of the films. It plays an important role in the surface mobility of the atoms.

1.3 Application Areas of Thin Films

Thin films are widely used in today's technology, and their applications are expected to be even more widespread in future. It is not possible to give an exhaustive survey over thin film applications, but a listing may, nevertheless, be of some interest. The application areas for thin films are:

A. Optical functional

1. Solar absorbing coatings
2. Anti- reflection layers on optical components
3. Coatings for laser optics
4. Display devices (CD)

B. Electrically functional

1. Conductors, Insulators (resistors, capacitors)
2. Semiconductor, Super-conductors devices
3. Microelectronic devices
4. Solar cells

C. Magnetically functional

1. Computer memories, Computer logic elements
2. Radio-frequency and microwave

D. Chemically functional

1. Gas/liquid sensors

F. Decorative

1. Eyeglass frames
2. Costume jewelry

G. Optoelectronic applications:

Thin films are of current interest owing to their potential use in light emitting diodes and laser diodes. Besides this other photo-electronic device e.g., photovoltaic solar cells, photoconductive devices, light-emitting diodes, coatings, sensors, integrated components for telecommunication etc., are now under active consideration of the

experimental physicists. In recent time popular utilization of this films as the absorber of the solar cells.

1.4 General Properties of Zinc Oxide

The II-VI compound semiconductors are of great importance due to their applications in various electro-optic devices. In materials science, Zinc oxide (ZnO) is called II-VI semiconductor because zinc and oxygen belong to the 2^{nd} and 6^{th} groups of the periodic table, respectively. It usually appears as a white powder, nearly insoluble in water. Zinc oxide (ZnO) is a wide bandgap (3.3 eV at room temperature) semiconductor that is desirable for many applications. It is attractive for forming various forms of nanostructures, such as nanorods, nanowires, and nanobelts [6]. Transparent transistors fabricated from ZnO have been reported. With its high exciton binding energy, ZnO is a good candidate for room temperature UV lasers. Its large piezoelectric constant is promising for ultrasonic transducers. ZnO is transparent and electrically conductive, making it an ideal material for solar cell windows. The mineral form of ZnO can be found in nature and is known as Zincite. Zinc oxide has the hexagonal wurtzite structure.

ZnO nanomaterials are promising candidates for nanoelectronic, optoelectronic and solar cells devices [7]. Compared with other semiconductor materials, ZnO has higher exciton binding energy (60 meV), is more resistant to radiation, and is multifunctional with uses in the areas as a piezoelectric, ferroelectric and ferromagnetic. ZnO based semiconductor and nanowire devices are also promising for the integration on a single chip. So far, the various applications of ZnO nano-materials such as biosensors and UV detectors [8].

Some important physical properties of ZnO semiconductors are given below:

- Molecular formula: ZnO
- Crystal structure: Hexagonal
- Molecular weight (g/mole) : 81.4084
- Band gap : 3.3 eV (direct)
- Appearance : White solid
- Density (g/cm^3) : 5.606

- Melting point (°C) : ≈ 1975
- Solubility in water (g/L) : 1.6 (at 28 °C)
- Dielectric constant : 8.5
- Lattice energy (Kcal/mole) : 965

Crystal structure zinc oxide

Zinc oxide crystallizes in three forms: hexagonal wurtzite, cubic zincblende, and the rarely observed cubic rocksalt. The wurtzite structure is most stable at ambient conditions and thus most common. The zincblende form can be stabilized by growing ZnO on substrates with cubic lattice structure. In both cases, the zinc and oxide centers are tetrahedral. Hexagonal and zincblende polymorphs have no inversion symmetry . This and other lattice symmetry properties result in piezoelectricity of the hexagonal and zincblende ZnO [9].

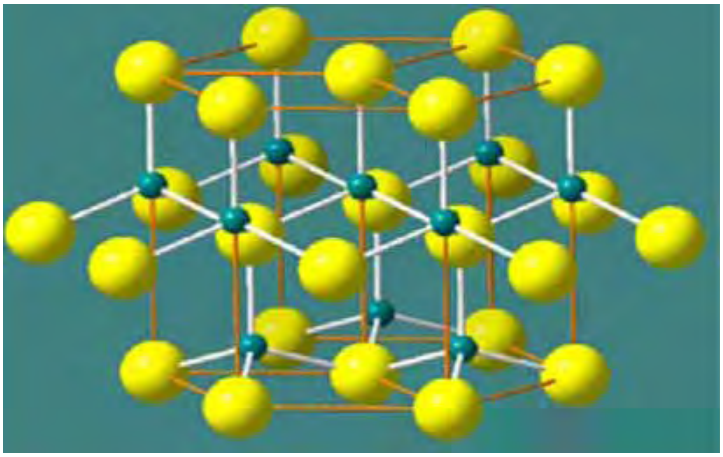

Fig.1.1: Wurtzite structure of ZnO (lagre ball-Zn, small ball-O)

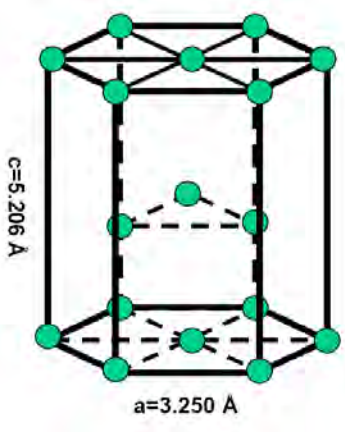

Fig.1.2:Hexagonal close packed (hcp) structure of ZnO.

1.5 General Properties of Copper

Copper is a chemical element with the chemical symbol Cu and atomic number 29. Cu as a group IB element can assume a valency of either +1 or +2 depending on its chemical configuration, for example in the compounds CuO and Cu_2O respectively. The radii of Cu+ (98pm) and Cu^{2+} (80pm) ions are similar to that of Zn^{2+} ion (83pm) [10]. The electronic structure of Cu is $1s^2 2s^2 2p^6 3s^2 3p^6 3d^{10} 4s^1$. Copper (Cu) atoms in unionized state have an outer cell electronic configuration of $3d^{10}4s^1$ and hence Cu^+ and Cu^{2+} ions are expected to posses $3d^{10}$ and $3d^9$ configurations respectively. In $3d^{10}$ configuration, all the d electrons are paired and Cu^+ ions does not posses any magnetic moment. On the other hand, in the case of Cu^{2+} ions with $3d^9$ configuration, one unpaired electron is available. This will give rise to a spin angular momentum of ½ which can result in a net magnetic moment.

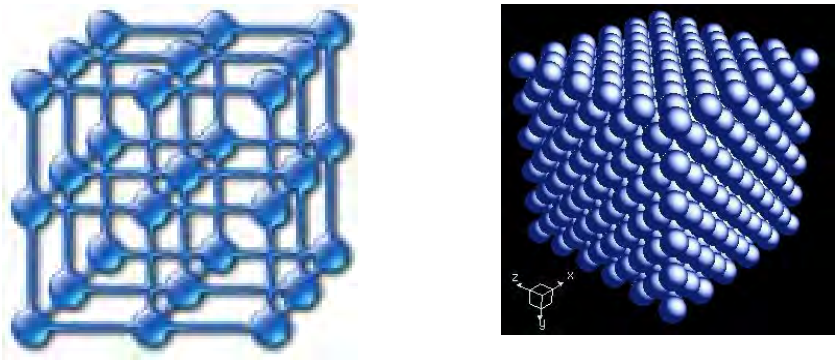

Fig.1.3: Crystal Structure of Cu

The standard values relating to the physical properties of copper are mentioned below:

- Moleular Formula: Cu
- Atomic Number: 29
- Type of metal: Transition metal
- Atomic Weight**:** 63.54
- Density**:** 8960 Kg/m^3
- Melting Point**:** 1356K
- Crystal Structure**:** Face centered Cubic
- Thermal Conductivity**:** 394 W/mK
- Specific heat at 293K**:** 0.383 KJ/Kg-K

1.6 Diluted magnetic semiconductors (DMS)

Transitional metal doped semiconductors are called diluted magnetic semiconductors (DMS) [11]. Transition metal doped II-VI compounds are the most common DMSs studied in the early period. DMS materials are semiconductors in which a fraction of the host cations can be substitutionally replaced by transition metal ions. The partially filled 3d states contain unpaired electrons, which are responsible for localized magnetic moments. The diluted magnetic semiconductors exhibit simultaneously ferromagnetic and semiconducting properties and focused on a new practical technology namely "spintronics" (spin-electronics). Spintronics is a new branch of electronics in which electron spin, in addition to charge, is manipulated to yield a desired electronic outcome. All spintronic devices act according to the simple scheme:

(1) Information is stored (written) into spins as a particular spin orientation (up or down),

(2) The spins, being attached to mobile electrons, carry the information along a wire, and

(3) The information is read at a terminal.

Spin orientation of conduction electrons survives for a relatively long time which makes spintronic devices particularly attractive for memory storage and magnetic sensors applications and potentially for quantum computing where electron spin would represent a bit of information. It was in this context that the concept of diluted magnetic semiconductor (DMS) emerged.

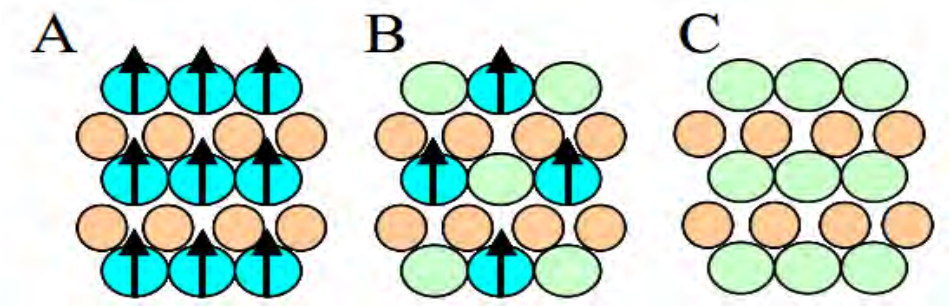

Fig.1.4: The different types of semiconductor : (A) a magnetic semiconductor, (B) a DMS and (C) a non-magnetic semiconductor.

1.7 A brief review of ZnO and $Zn_{1-x}Cu_xO$ Thin Films

Islam et al [12] deposited good homogeneous and stoichiometric ZnO nanofiber thin films onto cleaned glass substrate by a simple spray pyrolysis technique under atmospheric pressure using zinc acetate precursor at temperature 200^0 C. They obtained films of various thickness by varying the deposition time, while all other deposition parameters such as spray rate, carrier gas pressure and distance between spray nozzle to substrate were kept constant.They studied surface morphplogy and optical properties of the as deposited thin films by Scanning electron Microscopy (SEM) attached with and EDX and UV visible spectroscopy. From EDX data, atomic weight % of zinc and oxygen were found to be 49.22% and 49.62% respectively. The SEM micrograph of the film showed uniform deposition and scattered nano fiber around the nucleation centers. The optical band gap of the ZnO thin films was found to be in the range 3.3 to 3.4 eV and the band gap decreased with thickness of the film. Optical constants such as refractive index, extinction coefficient, real and imaginary parts of dielectric constants evaluated from reflectance and absorbance spectra.

Sahay et al [13] were prepared ZnO thin films by spray pyrolytic decomposition of zinc acetate onto glass substrate. These films were analyzed for the optical and electrical properties. Optical studies show that in these films the electronic transition is of the direct transition type. The optical energy gap for the film of different thicknesses is estimated to be in the range 2.98-3.09 eV. Electrical studies indicate that the films exhibit thermally activated electronic conduction and the activation energies are found to be dependent on the film thickness. The complex impedence measurement was carried out over a wide range of frequencies at room temperature. All the impedence spectra contain only a single arc, but the arc has a non-zero intersection with the real axis in the high frequency region. Also the arc has its centre lying below with the real axis which indicates the multirelaxation behavior of the films.

Studenikin et al [14] was investigated undoped ZnO films were deposited by spray pyrolysis using aqueous zinc nitrate solution at different substrate temperatures. The effect of the growth temperature on the structural, optical, electrical, and relaxation properties has been studied. It was found that there was a critical temperature Tc=180

°C below which the thermal decomposition to ZnO did not occur or was incomplete. Films grown above *Tc* showed strong preferred orientation of polycrystals along the *c*-axis, while the films grown at *Tc* or below showed a powder-like, non-oriented polycrystalline structure when they were converted afterwards to zinc oxide by annealing. A slight increase of the optical band gap was observed for as-prepared films as the substrate temperature was decreased near the critical temperature. Annealing brought all the samples to the same band gap 3.30 eV measured at a half height of the maximum absorption. After illumination, the steady-state photoconductivity decayed very slowly with a time constant of about a week for as-grown samples. The steady-state photoconductivity in daylight was very close to saturation. Steady-state photoconductivity in the daylight can be as much as four orders in magnitude larger than the dark value. Annealing in nitrogen at 400 °C brought all samples to the same conductivity of 10^{-3} (ohm- cm)$^{-1}$ in daylight and 10^{-4} (ohm-cm)$^{-1}$ in the dark. The photoconductivity transients were complicated and changed from a power law to multiexponential time dependence after annealing. The data are discussed on the basis of model in which hole traps located at the grain boundaries play the major role.

Ueda et al [15] formed 3d-transition-metal-doped ZnO films on sapphire substrates using a palsed laser deposition technique and there magnetic and electric properties are examined. The Cu doped ZnO films showed the maximum solubility limits. Some of the Cu-doped ZnO films exhibit ferromagnetic behaviors with the Curie temperature higher than room temperature. The magnetic properties of Cu-doped ZnO films depend on the concentration of Cu ions and carriers.

Rahmani et al [10] investigated the structural, optical, and gas-sensing properties of spray pyrolysis deposited Cu doped ZnO thin films. Gas response of the undoped and doped films to NO_2 (oxidizing) gas shows an increase and decrease in resistance, respectively, indicating p-type conduction indoped samples. The UV-Vis spectra of the films show decrease in the bandgap with increasing Cu concentration in ZnO. The observed p-type conductivity is attributed to the holes generated by incorporated Cu atoms on Zn sites in ZnO thin films. The X-ray diffraction spectra showed that samples are polycrystalline with the hexagonal wurtzite structure and increasing the

concentration of Cu caused a decrease in the intensity of the dominant (002) peak. The surface morphology of films was studied by scanning electron microscopy and the presence of Cu was also confirmed by X-ray photoelectron spectroscopy. Seebeck effect measurements were utilized to confirm the p-type conduction of Cu doped ZnO thin films.

Das et al [16] deposited well crystallized Cu doped (1, 3 and 5 molar%) ZnO films on quartz substrates by sol-gel technique. The microstructural, optical and photoluminescence properties of the films have been studied. It has been observed that the band gap (3.38 eV) of ZnO films did not vary up to 5 molar % of cu doping. The preffered orientation along (002) was observed for all the films. The X-ray diffraction (XRD) measurement confirmed the decrease of degree of orientation of (002) plane with increasing molar % of Cu in the films. The atomic force microscopy (AFM) measurements have been performed to examine the surface morphologies of the films. It has been observed that the surface roughness of 1molar % Cu doped film is smaller (6nm) than those of 3 and 5 molar % of Cu. The photoluminescence of the films shows prominent peaks between 2.27 to 3.11 eV due to excitonic as well as defect related transitions. A possible mechanism of carrier transitions between shallow and deep impurity levels in the photoluminescence has also been studied.

Jeon et al [17] deposited epitaxial Cu-doped (0.2, 0.4, 0.6, 0.8, 1, 2, 3 mol%) ZnO (CZO) films on Al_2O_3(006) substrates. The substrate temperature during deposition was maintained at temperatures ranging from room temperature (R.T.) to 600^0C and the oxygen ow rate was10 sccm. The full width at half maximum (FWHM) of the CZO films was $<0.18^0$, which was attributed to the low lattice-mismatch of 0.19 % between the film and the substrate according to the extended atomic distance mismatch (EADM) relationships. The '-scan of the CZO (112) reflection showed six-fold-like symmetric peaks, indicating specific c in-plane epitaxial growth patterns of the CZO/Al_2O_3 substrate. The depth profiles of the CZO films confirmed the presence of zinc, oxygen and copper distributed uniformly throughout the entire film. The CZO films showed a high transmittance (>90 %) at a 600-nm wavelength. The variations in the band gap energy (Eg = 3.13 - 3.28 eV) and the deep level emission (DLE) for the CZO films with the deposition temperature and the Cu doping content ratio are also discussed.

Hou et al [18] prepared a series of *n*-type $Zn_{1-x}Cu_xO$ (x=0.02, 0.06, 0.10, and 0.12) films using direct current reactive magnetron sputtering. Magnetic measurements indicate that all the films are ferromagnetic at room temperature and the moment per Cu ion decreases with increasing copper concentration and nitrogen doping. The observed magnetic moment was 1.8 μ_B/Cu for $Zn_{0.98}Cu_{0.02}O$ film and the transition temperature of about 350 K decreased to 320 K due to nitrogen doping. It can be concluded that itinerant electrons play an important role in ferromagnetism. The resistivity increased with increasing copper concentration and nitrogen doping. The anomalous Hall effect has been found for ferromagnetic materials.

1.8 Aim of the Present Work

The spray pyrolysis method for the deposition of thin solid films is a good method for the preparation of thin films suitable for scientific studies and for many applications in technology and industry. This method was used for the preparation of thin films of the important semiconductors II-VI.

In the recent years, the II-VI binary semiconductor nanomaterials have attracted much attention due to their potential technological applications such as storage devices, high-speed electronics, nanoelectronics, optoelectronic and solar cells devices. Zinc Oxide (ZnO) is potentially useful because of attractive properties like non-toxicity, good electrical, optical and piezoelectric behavior [12]. It's wide band gap 3.3 eV makes it attractive for the development of light-emitting diodes, coatings, sensors, integrated components for telecommunication, solar cells, etc.[12]. The crystal structure of zinc oxide is hexagonal (a=3.2498, c=5.2066). Transitional metal doped semiconductors are called diluted magnetic semiconductors (DMS). The diluted magnetic semiconductors exhibit simultaneously ferromagnetic and semiconducting properties and focused on a new practical technology namely "spintronics" (spin-electronics). It has vast demand for integrated optoelectronic applications such as light emitters and UV detectors. Cu doped ZnO has combine ferromagnetic order at room temperature with semiconducting properties for spintronic devices such as magneto-optical devices and magnetic sensors applications. Small amount of Cu can make attractive effect of structural, optical and electrical properties of ZnO. This has motivated to investigate the influence of transition metals Cu dopants on the transport and optical properties of ZnO thin film in

the present work. Although much work has been done on the electronic and optical properties of ZnO thin films but insufficient information is available on the $Zn_{1-x}Cu_xO$ thin films by spray pyrolysis deposition technique. Spray pyrolysis deposition technique is a simple, economical, viable technique and capable of producing good quality films for device application. From practical point of view, the focus of this work is to prepare $Zn_{1-x}Cu_xO$ thin film on glass substrate by spray pyrolysis deposition and its structural, optical and electrical properties to be studied in details.

Based of these research challenges, the objectives of this work are as follows:

i. The thickness of the films are measured by interferometer method (Fizeau fringes)
ii. By SEM, EDX and XRD the surface morphology, structures and phase of the deposited films are analyzed.
iii. The optical transmission and absorption, optical band gap (E_g), refractive index, etc. are determined by UV visible spectrophotometer.
iv The electrical measurement is carried out by four probe method.

References:

1. Kumar, A., Chung, Y.W., Moore, J.J. and Smugeresky, J. E., "Surface Engineering Science and Technology", The Minerals, Metals & Materials Society, Warrendale, 1999.

2. Gloker, D. A., and Shah, S. I., "Hand Book of Thin Film Process Technology", Institute of Physics Publishing, Bristol and Philadelphia, 1998.

3. Lim, B. J. H., Kang, C. K., Kim, K. K., Park, L. K., Hwang, D. K., and Park, S. J., "UV Electroluminescence Emission from ZnO Light-Emitting Diodes Grown by High-Temperature Radiofrequency Sputtering", DOI: 10.1002/adma.200502633.

4. Fortunato, E., Ginley, D., Hosono, H., and Paine, D. C., "Transparent Conducting Oxides for Photovoltaics" MRS Bulletin, Vol. 32, pp 242-247, 2007.

5. Licu C., Yun, and Morkoc H.,"Ferromagnetism of ZnO and GaN: A Review" Journal Of Materials Science: Materials In Electronics Vol. 16, pp 555– 597, 2005.

6. He, J. H., Lao, C. S., Chen, L . J., Davidovic, D. and Wang, Z. L. J., "Large-Scale Ni-Doped ZnO Nanowire Arrays and Electrical and Optical Properties" AM. CHEM. SOC. Vol. 127, pp 16376-16377, 2005.

7. Hwang, D. K,, Oh, M. S., Lim, J. H., and ParkJuan, S. J., HaiAn, S., Weii, Z., "ZnO thin films and light-emitting diodes" Phys. D: Appl. Phys. Vol. 40, pp 87–R412, 2007.

8. Sathananthan, S., Fan, S.W., and Dravid, V.P., "Hydrogen-Sensing Characteristics of Palladium-Doped Zinc-Oxide Nanostructures" Nanoscape Vol. 6, Issue 1, 2009.

9. Zhou, L., Gu, P., and Zhou, Y., "Piezoelectric f ilm electro-deposition for optical fiber sensor with ZnO coating" Chinese Optics Letters Vol. 6, No. 6, 2008.

10. Rahmani, M. B., Keshmiri, S. H., Shafiei1, M., Latham, K., Wlodarski1, W., Plessis, J.and Zadeh, K. K., "Transition from n- to p-Type of Spray Pyrolysis Deposited Cu Doped ZnO Thin Films for NO_2 Sensing", American Scientific Publishers, Sensor Letters, Vol-7, pp 1–8, 2009.

11. Wu, D., Xu, Q.Y., Zhang, F.M., Liu, X. S., Du, Y. W., "Diluted Magnetic Semiconductors and Spin Transport in Organic Materials" AAPPS Bulletin, Vol. 18, No. 5, 2008.

12. Islam, M. R., and Podder, J., "Optical Properties Of ZnO nano fiber thin films grows by spray pyrolysis of zince acetate precursor" Cryst. Res.Techno.Vol. 44, No.3, pp 286-292, 2009.

13. Sahay, P. P., Tewari, S. and Nath, R. K., "Optical and Electrical Studies on Spray Deposited ZnO Thin Films", Cryst. Res. Techn., Vol-42, No. 7, pp 723-729, 2007.

14. Studenikin, S. A., Golego, N. and Cocivera, M., "Optical and Electrical Properties of Undoped ZnO films grown by spray pyrolysis of zinc nitrate solution", J. Appl. Phys., V. 83, N0. 4, 1998.

15. Ueda, K., Tabata, H., and Kawai, T., "Magnetic and Electrical Properties of Transition-Metal-doped ZnO films", Appl. Phys. Lett., Vol-79, No. 7, pp 988-990, 2001.

16. Das, K., Ray, S., Chaudhuri, S. and Maity, A. B., "Structural and Luminescence Properties of Sol-gel Derived Cu doped ZnO flims", Indian Journal of Pure and Applied Physics, V-47, pp 377-382, 2009.

17. Jeon, J. H., Jeong, S. Y., and Cho, C. R., "Heteroepitaxial Relation and Optical Properties of Cu-Doped ZnO Films Grown by Using Pulsed Laser Deposition", J. Korean Phys. Soc., Vol-54, No. 2, pp 858-862, 2009.

18. Hou, D. L., Ye, X. J., Meng, H. J., Zhou, H. J., Li, X. L., Zhen, C.M. and Tang, G. D., "Magnetic Properties of n-type Cu-doped ZnO thin films", Appl. Phys. Lett., Vol. 90, N0. 142502, 2007.

CHAPTER-II
THEORETICAL BACKGROUND

Part A: Formation of Thin Films

2.1 Introduction

Thin film is prepared by deposition of the film materials (metals, semi-conductors, insulators, dielectric etc.) atom by atom on a substrate through a phase transformation. Sufficient time interval between the two successive deposition of atoms and also layers are required so that these can occupy the minimum potential energy configuration. In thermodynamically stable films, all atoms or molecules should be in their minimum potential energy sites and incoming atoms or molecules will take up positions and orientations energetically compatible with the neighboring atoms of the substrate or to the previously deposited layers, the effect of substrate or the initial layers will diminish gradually [1].

2.2 Different stages of film formation

There are three mechanism of thin film condensation which can be distinguished, depending on the strength of interaction between the atoms of the growing film and between the atoms of the film and substrate. These are

(i) In the Frank-van der Merwe or layer-by-layer growth mode, the adsorbate-substrate interaction dominates the adsorbate-adsorbate interaction and thus a new layer begins to grow only when the previous layer is completed.

2.1(i) Layer-by-layer growth mode

(ii) In the Vollmer-Weber or island growth mode, the adsorbate-adsorbate interaction dominates and thus deposition produces multilayer islands.

2.1(ii) Island growth mode

(iii) The Stranski-Krastanov or layer-plus-island growth mode is a particularly interesting case that has recently been exploited in the production of nanometre scale islands. After the formation of 1 or more complete monolayers, three dimensional islands nucleate and grow on top of the complete layer.

2.1(iii) Layer-plus-island growth mode

In most cases, mechanism (ii) takes place and we shall focus our attention on this mechanism in brief.

2.2.1 Condensation

Thin films are most commonly prepared by the condensation of atoms on a substrate from the vapor phase of the material. Condensation means the transformation of a gas in to a liquid or solid. Thermodynamically, the only requirement for condensation to occur is that partial pressure of the film material in the gas phase be equal or larger than its vapor pressure in the condensed phase at that temperature. Condensation of a vapor atom is determined by its interaction with the impinged surface. The impinging atom is attracted to the surface by the instantaneous dipole and quadruple moments of the surface atoms. Consequently the atoms losses its velocity component normal to its surface in a short time, provided the incident kinetic energy is not too high. The vapor atom is then physically absorbed (called ad atom) but it may or may not be completely thermally equilibrated [2]. It may move over the surface by jumping from one potential to the other because of the thermal activation from the surface and its own kinetic energy parallel to the surface. The ad atom has a finite stay or residence time on the

substrate during which it may interact with other ad atoms to form stable cluster and be chemically absorbed with the release of the heat of condensation. If is not absorbed the ad atom re-evaporates or desorbs into the vapor phase. Therefore, condensation is the net result of equilibrium between the absorption and desertion process.

The probability that an impinging atom will be incorporated into the substrate is called the "condensation" or "striking coefficient". It is measured by the ratio of the amount of material condensed on a surface to the total amount impinged. In fact, often the striking coefficient is so small that condensation is not observable by ordinary techniques. On the other hand, the striking coefficient is found to be strongly dependent on the total time during which the substrate was subjected to the impingement, and also on the substrate temperature. A non- unity striking coefficient is usually explained in terms of monomer re-evaporation form the areas on the substrate, which are outside, the capture zones around each stable nucleus [3].

2.2.2 Nucleation

Nucleation is the birth stage of a film. Condensation is initiated by the formation of small cluster through the combination of several absorbed atoms. These clusters are called nuclei and the process of formation is called nucleation.

There are two types of nucleation occur during the formation of a film. They are

a) **Homogeneous nucleation:** The total free energy is used in the formation of a cluster of ad-atoms.
b) **Heterogeneous nucleation:** Particular shapes of clusters are formed by collisions of atoms on the substrate surface, and in the vapor phase its super saturation is sufficiently high. They initially developed within increase in free energy until a critical size is reached above which growth continues with a decrease in free energy. In atomistic theory, in low substrate temperature or very high super saturations, the critical nucleus may be a single atom which will form a pair with another atom by random occurrence to become a stable cluster and grow spontaneously.

2.2.3 Growth

There are several stages in the growth process from the initial nucleation of the deposits to the final continuous three dimensional film formation states. These stages of film growth have been observed by many workers from their electron microscopic and other studies. These are valid not only for deposits condensing from the vapor phase but also for others, i.e. for solutions, by electro deposition, chemical reactions anodic oxidation, etc. There are four stages of the growth process based on the electron microscope observations [4]. They are

(i) The island stage/Nucleation growth stage
(ii) The coalescence stage
(iii) The channel stage
(iv) The continuous film stage

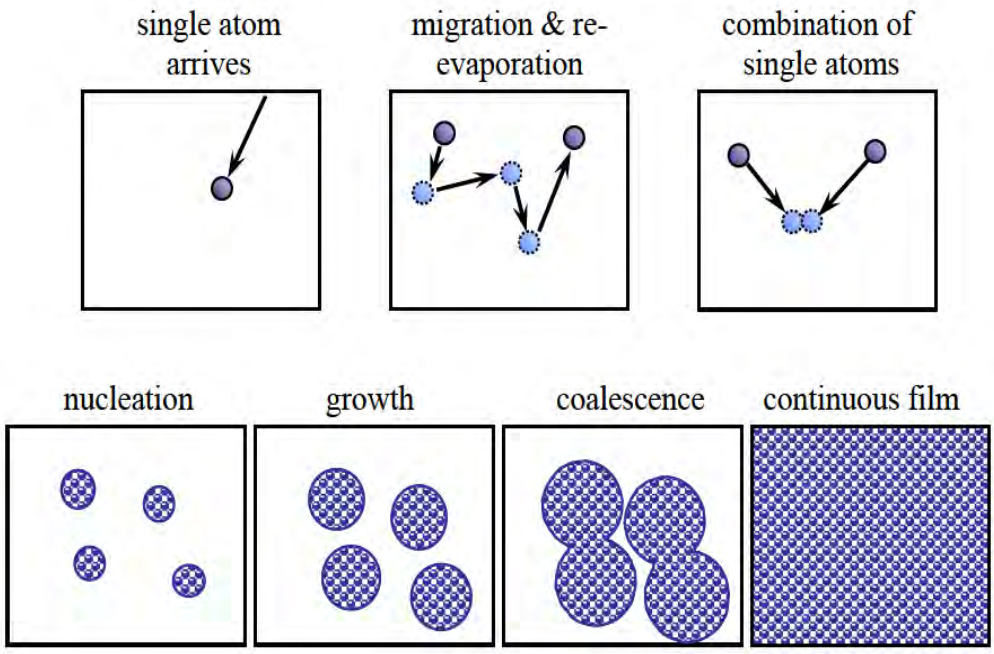

Fig.2.2: Different stages of the film growth

2.2.3 (i) The island stage

When a substrate under impingement of condenses monomers is observed in the electron microscope, the first evidence of condensation is a sudden burst of nuclei of fairly uniform size. The smallest nuclei detected have a size of 2.0 to 3.0 mm. Growth of nuclei is three dimensional, but the growth parallel to the substrate is greater than that normal to it. This is probably because growth occurs largely by the surface diffusion of monomers on the substrate, rather by direct impingement from the vapor phase. The tendency to form an island structure is increased by (a) at high substrate temperature, (b) at low boiling point film material, (c) at low deposition rate, (d) at weak binding energy between film material and substrate, (e) at high surface energy of the film material and (f) at low surface energy of the substrate.

2.2.3(ii) The Coalescence stage

As island increases their size by further deposition and come closer to each other, the larger ones appear to grow by coalescence of the smaller ones. The coalescence occurs in less than 0.ls for the small nuclei. In addition, nuclei having well-defined crystallographic shapes [5] before coalescence become rounded during the event. The composite island takes on a crystallographic shape again if left for a sufficiently long time before interacting with its neighbors.

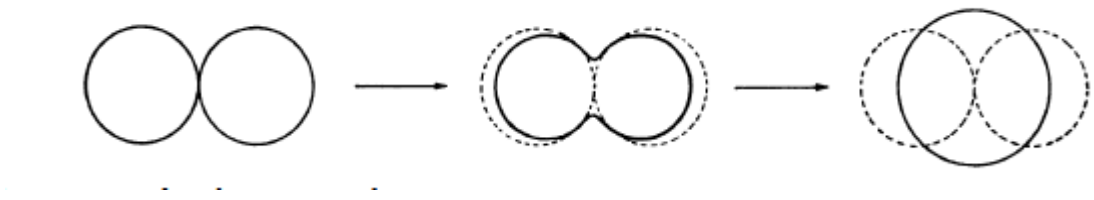

Fig.2.3: Coalescence of two supercritical nuclei and Shape change during coalescence

2.2.3 (iii) The Channel stage

When larger islands grow together they have channels of interconnected holes of exposed substrate in the form of a network structure on the substrate. As deposition continues, secondary nucleation occurs in these channels and forms the last stage of nucleation.

2.2.3 (iv) The continuous film stage

It is the final stage of the film growth. This process is slow and filling the empty channels which requires a considerable amount of deposits. These empty channels are filled by secondary nucleation, growth and coalescence and in this way of a continuous film is formed.

Part B: Theoretical Principles of Film Characterization

2.3 Introduction

The physical properties of thin films of a material are different from those of the bulk material. When the thin films are used in many practical purposes (like, solar cell electrode, antireflection coating, interference coating, etc.) it's electrical, optical and other properties must be known. Depending on its uses, transmitivity, reflectivity, optical absorption, band gap energy, extinction co-efficient, refractive index etc. are calculated within certain wavelength range of incident photon energy. It is also interesting to study the thin film resistivity and also on its dependence on film thickness, which is often referred to as size effect. The resistivity of metals at room temperature is of the order of 10^{-6} Ω-cm, in semiconductor 10^{2} ~ 10^{9} Ω-cm, and in insulator it ranges from 10^{14} ~ 10^{22} Ω-cm. Electrical resistivity of semiconductor strongly depends on temperature. At high temperature it may behave as conductor and at absolute zero a pure semiconductor will be an insulator.

2.4 Surface Morphology and Structural Characterization

2.4.1 Study of Scanning Electron Microscopy (SEM)

The scanning electron microscope (SEM) is a type of electron microscope that creates various images (surface morphology) by focusing a high energy beam of electrons onto the surface of a sample and detecting signals from the interaction of the incident electron with the sample's surface. The type of signals gathered in a SEM varies and can include secondary electrons, characteristic x-rays, and back scattered electrons. In a SEM, these signals come not only from the primary beam impinging upon the sample, but from other interactions within the sample near the surface. The SEM is capable of producing high resolution images of a sample surface in its primary use mode, secondary electron imaging. Due to the manner in which this image is created, SEM images have great depth of field yielding a characteristic three-dimensional appearance useful for understanding the surface structure of a sample. This great depth of field and the wide range of magnifications are the most familiar imaging mode for specimens in the SEM. Characteristic x-rays are emitted when the primary beam causes the ejection of inner shell

Fig.2.4: Photograph of Scanning Electron Microscopy (SEM)

electrons from the sample and are used to tell the elemental composition of the sample. The back-scattered electrons emitted from the sample may be used alone to form an image or in conjunction with the characteristic x-rays as atomic number contrast clues to the elemental composition of the sample.

2.4.2 Scanning process and image formation

In a typical SEM, an electron beam is thermionically emitted from an electron gun fitted with a tungsten filament cathode. Tungsten is normally used in thermo ionic electron guns because it has the highest melting point and lowest vapour pressure of all metals, thereby allowing it to be heated for electron emission, and because of its low cost. The electron beam, which typically has an energy ranging from a few hundred eV to 40 keV, is focused by one or two condenser lenses to a spot about 0.4 nm to 5 nm in diameter. The beam passes through pairs of scanning coils or pairs of deflector plates in the electron column, typically in the final lens, which deflect the beam in the *x* and *y* axes so that it scans in a raster fashion over a rectangular area of the sample surface.

When the primary electron beam interacts with the sample, the electrons lose energy by repeated random scattering and absorption within a teardrop-shaped volume of the specimen known as the interaction volume, which extends from less than 100 nm to

around 5 μm into the surface. The size of the interaction volume depends on the electron's landing energy, the atomic number of the specimen and the specimen's density. The energy exchange between the electron beam and the sample results in the reflection of high-energy electrons by elastic scattering, emission of secondary electrons by inelastic scattering and the emission of electromagnetic radiation, each of which can be detected by specialized detectors. The beam current absorbed by the specimen can also be detected and used to create images of the distribution of specimen current. Electronic amplifiers of various types are used to amplify the signals which are displayed as variations in brightness on a cathode ray tube. The raster scanning of the CRT display is synchronized with that of the beam on the specimen in the microscope, and the resulting image is therefore a distribution map of the intensity of the signal being emitted from the scanned area of the specimen. The image may be captured by photography from a high resolution cathode ray tube, but in modern machines is digitally captured and displayed on a computer monitor .

2.4.3 Study of Energy Dispersive Analysis of X-ray (EDAX)

Energy Dispersive X-ray Diffraction (EDX) is the elemental analysis of the thin film. It is an analytical technique used for the elemental analysis or chemical characterization of a sample. It is one of the variants of XRF. As a type of spectroscopy, it relies on the investigation of a sample through interactions between electromagnetic radiation and matter, analyzing x-rays emitted by the matter in response to being hit with charged particles. Its characterization capabilities are due in large part to the fundamental principle that each element has a unique atomic structure allowing x-rays that are characteristic of an element's atomic structure to be identified uniquely from each other.

To stimulate the emission of characteristic X-rays from a specimen, a high energy beam of charged particles such as electrons or protons (see PIXE), or a beam of X-rays, is focused into the sample being studied. At rest, an atom within the sample contains ground state (or unexcited) electrons in discrete energy levels or electron shells bound to the nucleus. The incident beam may excite an electron in an inner shell, ejecting it from the shell while creating an electron hole where the electron was. An electron from an outer, higher-energy shell then fills the hole, and the difference in energy between the higher-energy shell and the lower energy shell may be released in the form of an X-

ray. The number and energy of the X-rays emitted from a specimen can be measured by an energy dispersive spectrometer. As the energy of the X-rays are characteristic of the difference in energy between the two shells, and of the atomic structure of the element from which they were emitted, this allows the elemental composition of the specimen to be measured.

2.4.4 X-ray Diffraction (XRD) Study

The X-ray diffraction (XRD) provides substantial information on the crystal structure. XRD is one of the oldest and effective tools for the determination of the atomic arrangement in a crystal; X-rays are the electromagnetic waves and its wavelength ≈ 0.1nm. The wavelength of an X-ray is thus of the same order of magnitude as the lattice constant of crystals.

Bragg reflection is a coherent elastic scattering in which the energy of the X-ray is not changed on reflection. If a beam of monochromatic radiation of wavelength λ is incident on a periodic crystal plane at an angle θ and is diffracted at the same angle. The Bragg diffraction condition for X-rays is given by

$$2d\sin\theta = n\lambda \quad \ldots\ldots\ldots\ldots\ldots\ldots\ldots\ldots \quad (2.1)$$

Where, d is the distance between crystal planes; θ is the X-ray incident angle; λ is the wavelength of the X-ray and n is a positive integer which represents the order of reflection. Equation (2.1) is known as Bragg law. This Bragg law suggests that the diffraction is only possible when $\lambda < 2d$ [6]. For this reason we cannot use the visible light to determine the crystal structure of a material.

2.5 Measurement of Film Thickness

Thickness is the single most significant film parameter. It may be measured either by in-situ monitoring of the rate of deposition, or after the film is taken out of deposition chamber. Techniques of the first type often called as monitor method generally allow both monitoring and controlling of the deposition rate and film thickness. Other techniques are also used for thickness measurement. Any physical quantity related to film thickness can in principle be used to measure the film thickness. It may be measured either by several methods with varying degrees of accuracy. The methods are chosen on the basis of their convenience, simplicity and reliability. Since the film

thicknesses are generally of the order of a wavelength of light, various types of optical interference phenomena have been found to be most useful for measurement of film thicknesses.

Multiple-Beam Interferometry

During Evaporation, i) Multiple-Beam Interferometry, (Tolansky Fezeau fringes method, Fringes of equal chromatic order.) ii) Michelson interferometer iii) Using a Hysteresis graph relative and other methods used in film-thickness determination with particular reference to their merits and accuracies. Multiple-Beam Interferometry technique was employed for the measurement of thickness of the thin films. A brief description of the method is given below. This method utilizes the resulting interference effects when two silvered surfaces are brought close together and are subjected to optical radiation. This interference technique, which is of great value in studying surface topology in general, may be applied simply and directly to film-thickness determination. When a wedge of small angle is formed between unsilvered glass plates, which are illuminated by monochromatic light, broad fringes are seen arising from interference between the light beams reflected from the glass on the two sides of the air wedge. At points along the wedge where the path difference between these two beams are an integral and odd number of wavelengths, bright and dark fringes occur respectively. If the glass surfaces of the plates are coated with highly reflecting layers, one of which is partially transparent, then the reflected fringe system consists of very fine dark lines against a bright background. A schematic diagram of the multiple-beam interferometer along with a typical pattern of Fizeau fringes from a film step is shown in Fig 2.5. As shown in this figure, the film whose thickness is to be measured is over coated with a silver layer to give a good reflecting surface and a half-silvered microscope slide is laid on top of the film whose thickness is to be determined. A wedge is formed by the two microscope slides and light multiply reflected between the two silvered surfaces forms an interference pattern with a discontinuity at the film edge.

The thickness of the film "*d*" can then be determined by the relation, $d = \frac{\lambda}{2}\frac{b}{a}$ where, λ is the wavelength and *b/a* is the fractional discontinuity identified in the figure 2.5.

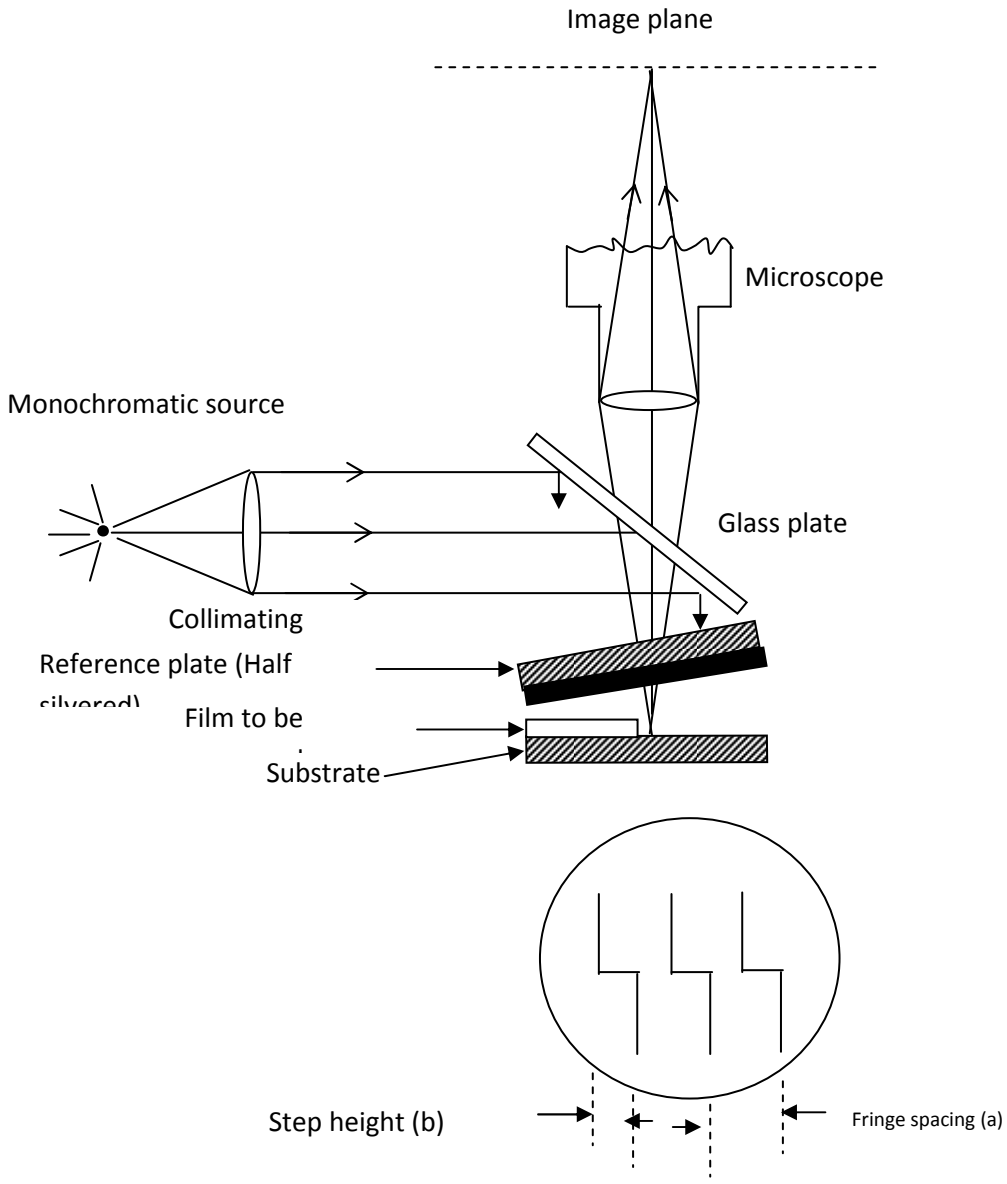

Fig.2.5: Interferometer arrangement for producing reflection Fizeau fringes of equal thickness

In general, the sodium light is used, for which λ = 5893 Å. In conclusion, it might be mentioned that the Tolansky method of film-thickness measurement is the most widely used and in many respects also the most accurate and satisfactory one [7].

The thickness of the films deposited on glass substrates was measured by using a multiple-beam interferometric method. For film thickness measurement separate glass slide has been used in addition to the sample substrates. The step generated on the surface of the glass slide was used to measure the film thickness.

2.6 Optical Characterization

2.6.1 Absorption Co-efficient

When a semiconductor is illuminated by light, photon strikes the surface, a fraction of photons are reflected, some of these are absorbed within the semiconductor and the remainder transmitted into the semiconductor. The absorption of radiation by any medium occurs through the excitation of electrons and photons.

For semiconductor, it is convenient to consider several types of absorption arising from

i) Electronic transitions between different energy bands.
ii) Electronic transitions within energy band.
iii) Electronic transitions to localized states of impurity atoms.
iv) Lattice vibrations.
v) Vibrations of impurity atoms.

In the fundamental absorption region the transmission T is given by

$$T = A \exp\left(-\frac{4\pi kt}{\lambda}\right) \quad \ldots \quad \ldots \quad \ldots \quad (2.2)$$

Where A is a constant, k is the extinction co-efficient and t is the thickness. For $K^2 << n^2$, the principle variation of T occurs in the exponential term and pre-exponential term A. Therefore,

$$T \sim \exp(-\alpha t) \quad \ldots \quad \ldots \quad .. \quad \ldots \quad \ldots \quad (2.3)$$

Where $\alpha = \frac{4\pi k}{t}$ is the absorption co-efficient of the film. Thus the value of absorption co-efficient may be calculated from the relation

$$\alpha = -\frac{\ln T}{t} \quad \ldots \quad \ldots \quad \ldots \quad \ldots \quad (2.4)$$

Otherwise from equation (2.2) plotting Eqn. 2.2 as $\ln(\frac{1}{T})$ vs t curve at a fixed wavelength, a straight line will be obtained. The slope of the straight line will give α and intercept will give A.

According to **Bardeen** [8], the relationships that exist for possible transition across the energy gap of a semiconductor show that the absorption co-efficient α may be written as

$$\alpha = \frac{A(h\nu - E_g)^n}{t} \quad \ldots \quad \ldots \quad \ldots \quad (2.5)$$

Where A is a constant, hν is the photon energy, n is a index related to the density of state (n= ½ for direct transition and n=2 for indirect transition) and E_g is the optical band gap of the semiconductor. By plotting $(\alpha h\upsilon)^n$ against hν for the several values of n it is possible to determine which of these conditions dominate and hence determine the appropriate energy gap of the sample.

2.6.2 Beer-Lambert Law

The Beer-Lambert law (or Beer's law) is the linear relationship between absorbance and concentration of an absorbing species. The general Beer-Lambert law is usually written as:

$$A = abc \quad \ldots \quad \ldots \quad \ldots \quad \ldots \quad (2.6)$$

where A is the measured absorbance, "a" is a wavelength-dependent absorptivity coefficient, b is the path length, and c is the analyte concentration. When working in concentration units of molarity, the Beer-Lambert law is written as:

$$A = \varepsilon bc \quad \ldots \quad \ldots \quad \ldots \quad \ldots \quad (2.7)$$

where *epsilon* is the wavelength-dependent molar absorptivity coefficient with units of $M^{-1}cm^{-1}$Experimental measurements are usually made in terms of transmittance (T), which is defined as:

$$T = I / I_o \quad \ldots \quad \ldots \quad \ldots \quad \ldots \quad (2.8)$$

where I is the light intensity after it passes through the sample and I_o is the initial light intensity. The relation between A and T is:

$$A = -\log T = -\log (I / I_o) = \log (I_0/I) \ldots \quad \ldots \quad \ldots \quad (2.9)$$

Modern absorption instruments can usually display the data as either transmittance, %-transmittance, or absorbance.

2.6.3 Derivation of the Beer-Lambert law

The Beer-Lambert law can be derived from an approximation for the absorption coefficient for a molecule by approximating the molecule by an opaque disk whose cross-sectional area, σ, represents the effective area seen by a photon of frequency υ. If the frequency of the light is far from resonance, the area is approximately 0, and if υ is close to resonance the area is a maximum. Taking an infinitesimal slab, dz, of sample**:**

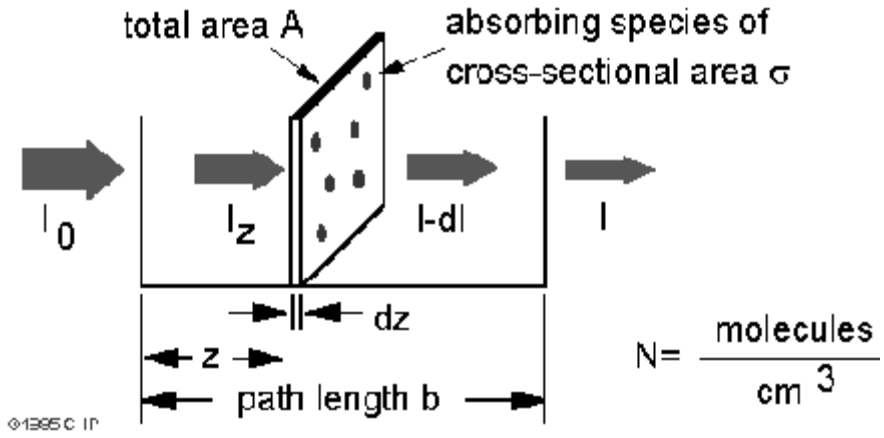

Fig.2.6: Absorption of light by a sample

I_o is the intensity entering the sample at z=0, I_z is the intensity entering the infinitesimal slab at z, dI is the intensity absorbed in the slab, and I is the intensity of light leaving the sample. Then, the total opaque area on the slab due to the absorbers is σNA dz. Then, the fraction of photons absorbed will be σNA dz / A so,

$$\frac{dI}{I_z} = -\sigma N\, dz$$

Integrating this equation from z = 0 to z = b gives:

$$\ln(I) - \ln(I_o) = -\sigma N b$$

or

$$-\ln(I / I_o) = -\sigma N b.$$

Since N (molecules/cm^3) (1 mole / $6.023x10^{23}$ molecules) 1000 cm^3 / liter = c (moles/liter) and 2.303 * log(x) = ln(x)

then $- \log(I / I_o) = \sigma(6.023x10^{20} / 2.303)\, cb$

or $$- \log(I / I_o) = A = \varepsilon\, bc$$

where $\varepsilon = \sigma\ (6.023x10^{20} / 2.303) = \sigma(\ 2.61x10^{20})$, and ε is called the molar absorptivity.

Thus the intensity of the transmitted light can be expressed as $I=I_0\, e^{-\alpha d}$ where d is the path length through the sample and α is the absorption coefficient. This equation

can be written as $$\alpha = \frac{2.303A}{d} \quad \ldots \quad \ldots \quad \ldots \quad \ldots \quad (2.10)$$

2.6.4 Direct Band Gap of Semiconductor

If the maximum of the valence band and the minimum of the conduction band energy exist for the same value of crystal momentum *p* in a semiconductor, then this type of semiconductor is called direct band gap semiconductor.

The form of the absorption process for a direct band gap semiconductor is shown in the energy momentum sketch of Fig. 2.7. Since the momentum of photons is small compared to the crystal momentum, the latter essentially is conserved in the transition. The energy difference between the initial and final state is equal to the energy of the original photon, i.e.,

$$E_f - E_i = h\nu \quad \ldots \quad \ldots \quad \ldots \quad \ldots \quad (2.11)$$

In terms of parabolic band

$$E_f - E_c = \frac{P^2}{2m_e^*} \quad \ldots \quad \ldots \quad \ldots \quad (2.12)$$

$$E_v - E_i = \frac{P^2}{2m_h^*} \quad \ldots \quad \ldots \quad . \quad (2.13)$$

Therefore, the specific value of crystal momentum at which the transition occurs is given by

$$(E_f - E_i) - (E_c - E_v) = \frac{P^2}{2}\left[\frac{1}{m_e^*} + \frac{1}{m_h^*}\right]$$

$$h\upsilon - E_g = \frac{P^2}{2}\left[\frac{1}{m_e^*} + \frac{1}{m_h^*}\right] \quad \ldots \quad \ldots \quad .. \quad \ldots \quad (2.14)$$

Where, $E_f - E_i = h\nu$ = Photon energy

and $E_C - E_V = h\nu$ = Energy gap

As the photon energy hν increases, so does the value of the crystal momentum at which the transition occurs (Fig 2.7) [6]. The energy from the band edge of both the initial and find states also increases. The probability of absorption depends on the density of the electron at the energy corresponding to the initial state as well as the density of empty states at the final energy. Since both these quantities increase with energy away from the band edge, the absorption co-efficient increase rapidly with increasing photon energy above E_g. A simple theoretical treatment gives the result, as

$$\alpha(h\nu) \approx \overset{*}{A}(h\nu - E_g)^{1/2} \quad . \quad \ldots \quad \ldots \quad \ldots \quad (2.15)$$

Where $\overset{*}{A}$ is a constant having the numerical value of 2×10^4 when α is expressed in cm^{-1} and hν and E_g are in electron volts (eV).

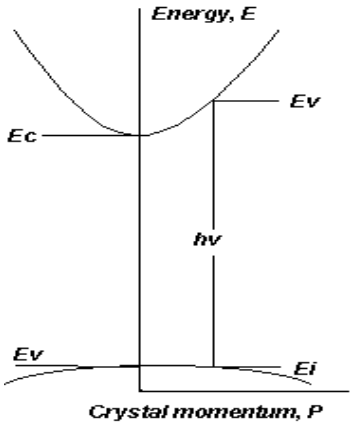

Fig.2.7: Energy-crystal momentum diagram of a direct band gap semiconductor

2.6.5 Indirect Band Gap of Semiconductor

In the case of indirect band gap semiconductor, the minimum energy in the valence band occurs at different values of crystal momentum (Fig. 2.8) [6]. Photon energies much larger than the forbidden gap is required to give transition of electrons from the valence band to conduction band.

As indicated in the energy momentum sketch of Fig.2.8, an electron can make a transition from the maximum energy in the valence band to the minimum energy in the conduction band in the presence of photons of suitable energy by the emission or absorption of photon. Hence the minimum photon energy required to excite an electron from the valence to conduction band is

$$h\nu = E_g - E_p \quad \ldots \quad \ldots \quad \ldots \quad \ldots \quad \ldots \qquad (2.16)$$

Where E_p is the energy of an absorbed photon with the required momentum.

An analysis of the theoretical value of the absorption co-efficient for the transition involving photon absorption gives the result

$$\alpha_a(h\nu) = \frac{A(h\nu - E_g + E_P)^2}{\exp(E_p / kT)^{-1}} \quad \ldots \quad \ldots \quad \ldots \quad (2.17)$$

For the transition involving photon emission

$$\alpha_e(h\nu) = \frac{A(h\nu - E_g - E_P)^2}{1 - \exp(E_p / kT)^{-1}} \quad \ldots\ldots \quad \ldots\ldots \quad \ldots\ldots \quad (2.18)$$

.Since both Photon emission and absorption are possible for $h\nu > E_g + E_p$, the absorption co-efficient is then

$$\alpha(h\nu) = \alpha_a(h\nu) + \alpha_e(h\nu) \quad \ldots \quad \ldots \quad \ldots \quad (2.19)$$

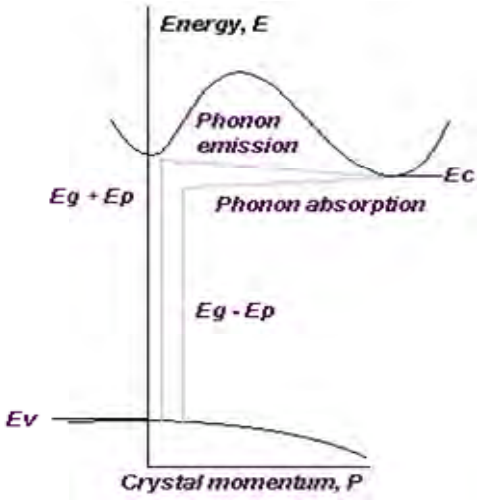

Fig.2.8: Energy-crystal momentum diagram of an indirect band gap semiconductor

2.6.6 Electronic Transitions

The absorption of UV or visible radiation corresponds to the excitation of outer electrons. There are three types of electronic transition which can be considered;

1. Transitions involving π, σ, and *n* electrons
2. Transitions involving charge-transfer electrons
3. Transitions involving *d* and *f* electrons (not covered in this Unit)

When an atom or molecule absorbs energy, electrons are promoted from their ground state to an excited state. In a molecule, the atoms can rotate and vibrate with respect to each other. These vibrations and rotations also have discrete energy levels, which can be considered as being packed on top of each electronic level.

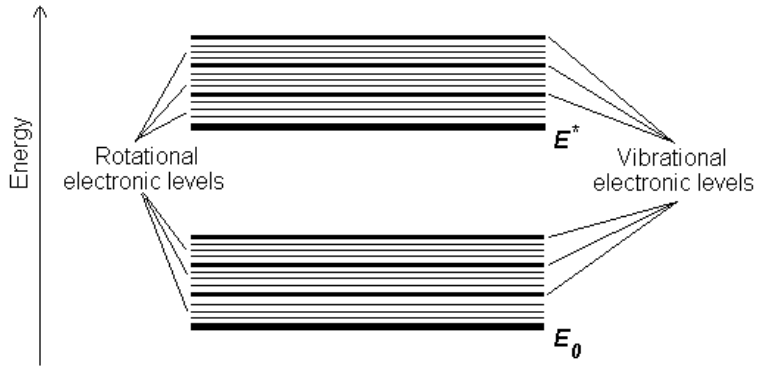

Absorbing species containing π, σ, and n electrons

Absorption of ultraviolet and visible radiation in organic molecules is restricted to certain functional groups (chromophores) that contain valence electrons of low excitation energy. The spectrum of a molecule containing these chromophores is complex. This is because the superposition of rotational and vibrational transitions on the electronic transitions gives a combination of overlapping lines. This appears as a continuous absorption band.

Possible electronic transitions of π, σ, and n electrons are;

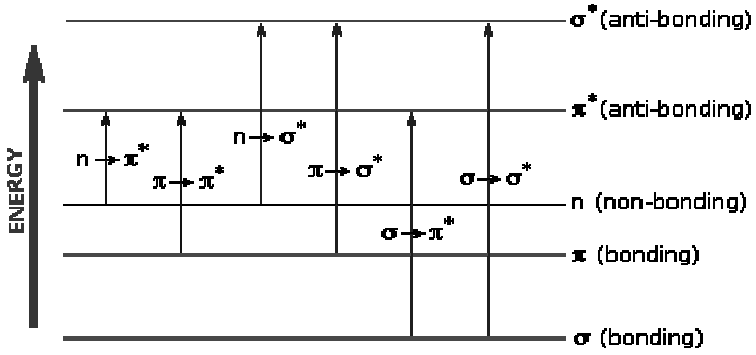

Fig.2.9: Possible electronic transitions

$\sigma \rightarrow \sigma^*$ Transitions

An electron in a bonding σ orbital is excited to the corresponding antibonding orbital. The energy required is large. For example, methane (which has only C-H bonds, and can only undergo $\sigma \rightarrow \sigma^*$ transitions) shows an absorbance maximum at 125 nm. Absorption maxima due to $\sigma \rightarrow \sigma^*$ transitions are not seen in typical UV-Vis. spectra (200 - 700 nm).

$n \rightarrow \sigma^*$ *Transitions*

Saturated compounds containing atoms with lone pairs (non-bonding electrons) are capable of $n \rightarrow \sigma^*$ transitions. These transitions usually need less energy than $\sigma \rightarrow \sigma^*$ transitions. They can be initiated by light whose wavelength is in the range 150 - 250 nm. The number of organic functional groups with $n \rightarrow \sigma^*$ peaks in the UV region is small.

n $\rightarrow \pi^*$ and $\pi \rightarrow \pi^*$ Transitions

Most absorption spectroscopy of organic compounds is based on transitions of *n* or π electrons to the π^* excited state. This is because the absorption peaks for these transitions fall in an experimentally convenient region of the spectrum (200 - 700 nm). These transitions need an unsaturated group in the molecule to provide the π electrons.

Molar absorbtivities from $n \rightarrow \pi^*$ transitions are relatively low, and range from 10 to100 L mol^{-1} cm^{-1} . $\pi \rightarrow \pi^*$ transitions normally give molar absorbtivities between 1000 and 10,000 L mol^{-1} cm^{-1} .

The solvent in which the absorbing species is dissolved also has an effect on the spectrum of the species. Peaks resulting from $n \rightarrow \pi^*$ transitions are shifted to shorter wavelengths (*blue shift*) with increasing solvent polarity. This arises from increased solvation of the lone pair, which lowers the energy of the *n* orbital. Often (but *not* always), the reverse (i.e. *red shift*) is seen for $\pi \rightarrow \pi^*$ transitions. This is caused by attractive polarisation forces between the solvent and the absorber, which lower the energy levels of both the excited and unexcited states. This effect is greater for the excited state, and so the energy difference between the excited and unexcited states is slightly reduced - resulting in a small red shift. This effect also influences $n \rightarrow \pi^*$ transitions but is overshadowed by the blue shift resulting from solvation of lone pairs.

2.6.7 Refractive index and Extinction coefficient

One of the most important optical constants of a material is its refractive index, which in general depends on the wavelength of the electromagnetic wave, through a relationship called dispersion. In materials where an electromagnetic wave can lose its energy during its propagation, the refractive index becomes complex. The real part is usually the refractive index, *n*, and the imaginary part is called the extinction coefficient, *K*. In this section, the refractive index and extinction coefficient will be presented in detail along with some common dispersion relations.

The refractive index of an optical or dielectric medium, is the ratio of the velocity c in vacuum to its velocity V in the medium; n=c/v. Using this and Maxwell's equations, one obtains the well known Maxwell's formula for the refractive index of substance as

$$n = \sqrt{\varepsilon_r \mu_r}$$

where ε_r is the static dielectric constant or relative permittivity and μ_r the relative permeability.

As μ_r = 1 for nonmagnetic substances, one gets, $n = \sqrt{\varepsilon_r}$, which is very useful in relating the dielectric properties to optical properties of materials at any particular frequency of interest. As ε_r depends on the wavelength of light, the refractive index also depends on the wavelength of light, and this dependence is called dispersion. In addition to dispersion, an electromagnetic wave propagating through a lossy medium experiences attenuation, which means it loses its energy, due to various loss mechanisms such as the generation of phonons (lattice waves), photogeneration, free carrier absorption, scattering, etc. In such materials, the refractive index becomes a complex function of the frequency of the light wave. The complex refractive index, denoted by *n**, with real part *n*, and imaginary part *K*, called the extinction coefficient, is related to the complex relative permittivity, $\varepsilon_r = \varepsilon_r' - j\varepsilon_r''$ by:

$$n* = n - jk = \sqrt{\varepsilon_r} = \sqrt{\varepsilon_r' - j\varepsilon_r''} \quad \text{... … …… … (2.20)}$$

where ε_r' and ε_r'' are, respectively, the real and imaginary parts of ε_r. Equation (4.17) gives:

$$n^2 - k^2 = \varepsilon_r'' \text{ and } 2nk = \varepsilon_r'' \quad \text{... … …… …… … (2.21)}$$

In explicit terms, *n* and *K* can be obtained as:

$$n = (1/2^{½})[(\varepsilon_r'^2 + \varepsilon_r''^2)^{1/2} + \varepsilon_r']^{1/2} \quad \text{... ... ... … …… … (2.22)}$$

$$k = (1/2^{1/2})[(\varepsilon_r'^2 + \varepsilon_r''^2)^{1/2} - \varepsilon_r']^{1/2} \quad \text{... … …… …… … (2.23)}$$

The optical constants *n* and *K* can be determined by measuring the reflectance from the surface of a material as a function of polarization and the angle of incidence. For normal

incidence, the reflection coefficient, *r*, is obtained as

$$r = \frac{1 - n^*}{1 + n^*} = \frac{1 - n + jk}{1 + n - jk} \quad \text{. ... … …… …… … (2.24)}$$

The reflectance *R* is then defined by:

$$R=|r|^2=\left|\frac{1-n+jk}{1+n-jk}\right|^2=\frac{(1-n)^2+k^2}{(1+n)^2+k^2} \quad \ldots \quad \ldots \quad \ldots \quad (2.25)$$

And we have calculated refractive index by using following equation

$$n=\left(\frac{1+R}{1-R}\right)+\sqrt{\left(\frac{4R}{(1-R)^2}-k^2\right)} \quad \ldots. \ldots. \ldots.. \ldots. \quad (2.26)$$

Notice that whenever *K* is large, for example over a range of wavelengths, the absorption is strong and the reflectance is almost unity. The light is then reflected and any light in the medium is highly attenuated.

2.7 Electrical Characterization

2.7.1 Resistivity and Conductivity Measurement

The tendency of a material is to resist the flow of an electrical current through it and to convert the electrical energy into heat energy is called resistance. According to Ohm's law,

$$R=\frac{V}{I} \quad \ldots \quad \ldots \quad \ldots \quad \ldots \quad \ldots \quad \ldots \quad (2.27)$$

Where R is the resistance of a material, V is the potential difference and I is the current flow through the material.

The resistance per unit length of unit cross section is called resistivity. It is denoted by ρ and mathematically defined as,

$$\rho=\frac{RA}{L} \quad \ldots \quad \ldots \quad \ldots. \quad \ldots \quad \ldots \quad \ldots \quad (2.28)$$

Where A is the cross-sectional area and L is the length.

Electrical conductivity of a material is reciprocal of resistivity of the material. It is denoted by σ and mathematically defined as

$$\sigma=\frac{1}{\rho} \quad \ldots \quad \ldots \quad \ldots \quad \ldots \quad \ldots \quad (2.29)$$

Resistivity is an intrinsic property of a material and depends only on the crystal structure of the material. The resistivity can be obtained by measuring the resistance

of a specimen of the material with well-defined regular geometric shape. There are many methods to measure resistivity. Some of them have been discussed below.

There are four methods commonly used for the measurement of resistivity.

A) Direct method

B) Two-probe method

C) Four probe method

D) Van-der Pauw's method

2.7.1A Direct Method

The resistivity of a thin film can be measured easily by direct method using the relation

$$\rho = R\frac{bt}{L} \qquad \ldots \quad \ldots \quad \ldots . \quad \ldots \quad (2.30)$$

Where, b and t are the breadth and thickness of the sample. For simplicity, if we consider, b = L, the above equation becomes

$$\rho = Rt \quad \ldots . \quad \ldots .. \quad \ldots .. \quad (2.31)$$

Measuring the resistance R and thickness, t one can easily determine the resistivity.

2.7.1 B Two-Probe Method

In this method a potential is applied between the two ends of the specimen and the voltage drop is measured between two points in the specimen. The method is generally used to determine the high resistivity i.e., low conductivity having order 10^{-14} to 10^{-18} mho-cm^{-1}. The voltage drop is measured between potential probe as shown is Fig. 2.10B.

2.7.1C Four-Probe Technique

Four-probe method is usually used for the determination of low resistivities. For this purpose four metal pins at an equal distance D are pressed by springs against the semiconductor sample as shown in Fig. 2.10C. If the outside pins carry a current of

intensity, I a voltage drop is measured between the inner probes of magnitude V. Assuming the sample to be much thicker than the pin distance, D the resistivity ρ is given by

$$\rho = \frac{2\pi DV}{I} \qquad \ldots\ldots \quad \ldots . \quad \ldots \quad \ldots \quad (2.32)$$

The effect of the contact resistance is avoided in Four-probe method.

2.7. 1D Van-der Pauw Method

The resistivity of a film having any arbitrary shape can be uniquely determined by **Van-der Pauw** [9] method. A brief account of this method is given below because in our measurement we have used Van-der Pauw method.

Fig.2.2 Direct method

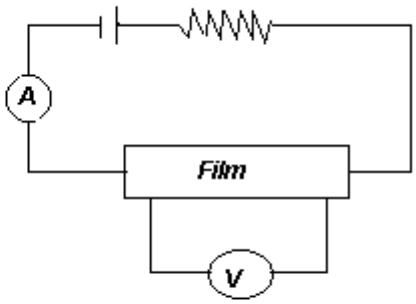

Fig.2.2B: Four probe method

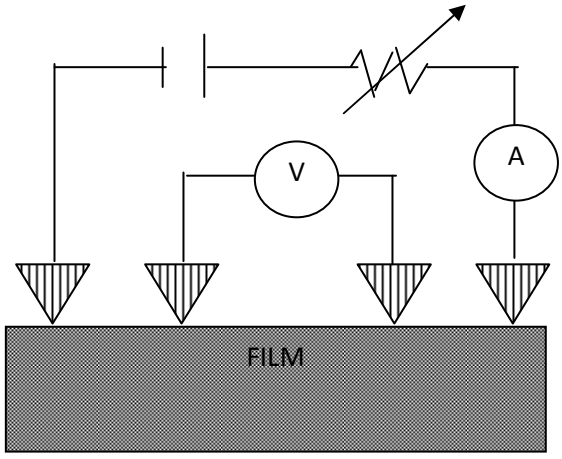

Figure 2.10C: Circuit arrangement of four-probe method

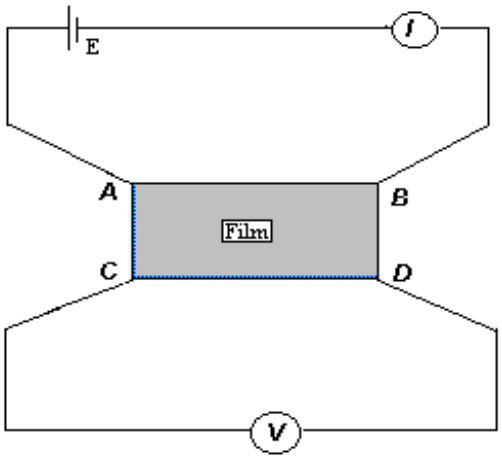

Figure 2.10 D: Circuit arrangement of Van der Pauw's technique

At first we select a region on the sample where four electrical contacts were made at four corners, say A, B, C, and D as shown in Fig. 2.10D. Silver paste or indium was used to the contact. If a current I_{AB} entering the specimen through the contact A and leaving through the contact, B produces a potential difference V_D-V_C between C and D then the resistance $R_{AB, CD}$ is defined as

$$R_{AB,CD} = \frac{V_D - V_C}{I_{AB}} = \frac{V_{CD}}{I_{AB}} \quad \ldots \quad \ldots \quad \ldots \quad \ldots \quad (2.33)$$

Similarly,

$$R_{BC,DA} = \frac{V_A - V_D}{I_{BC}} = \frac{V_{DA}}{I_{BC}} \quad \ldots \quad \ldots \quad \ldots \quad (2.34)$$

$$R_{CD,AB} = \frac{V_B - V_A}{I_{CD}} = \frac{V_{AB}}{I_{CD}} \quad \ldots \quad \ldots \quad \ldots \quad (2.35)$$

and $$R_{DA,BC} = \frac{V_C - V_B}{I_{DA}} = \frac{V_{BC}}{I_{DA}} \quad \ldots \quad \ldots \quad \ldots \quad (2.36)$$

The resistivity of a thin film can be expressed by the equation

$$\rho = \frac{\pi t}{\ln 2}\left[\frac{R_{AB.CD} + R_{BC,AD}}{2}\right] \times f\left[\frac{R_{AB.CD}}{R_{BC.DA}}\right] \quad .. \ldots\ldots \quad (2.37)$$

$$\rho = 4.53t \times \left[\frac{R_{AB.CD} + R_{BC,DA}}{2}\right] \times f\left[\frac{R_{AB.CD}}{R_{BC.AD}}\right] \quad \ldots \quad \ldots \quad (2.38)$$

Where t is the thickness of the film and the function f can be evaluated from the equation

$$\left[\frac{R_{AB.CD} - R_{BC.DA}}{R_{AB.CD} + R_{BC.DA}}\right] = \frac{f}{\ln 2} \, arc\cosh \frac{\exp(\ln 2 / f)}{2} \quad \ldots \quad \ldots \quad \ldots \quad (2.39)$$

If $R_{AB, CD}$ and $R_{BC, DA}$ is almost equal, f may be approximately equal to unity and then the equation (2.38) takes the form,

$$\rho = 2.265 \; t \; (R_{AB, CD} + R_{BC, DA}) \text{ ohm-cm} \ldots \ldots \ldots \ldots \ldots \quad (2.40)$$

It is very difficult to get f, so we have taken the value of f from the chart for different ratio greater than unity.

2.7.2 Factors Affecting Resistivity Measurement

The effects of the following factors are remarkable in the measurement of resistivity:

a) Length to breadth ratio, L/b of the film

b) Current electrodes

c) Current density

d) Microscopic inhomogenity of the film

e) Sensitivity of the measuring devices

f) Electrical contact resistivity

2.7.3 Activation Energy

The energy required to transfer charge from one neutral island to another is known as 'activation energy' and is denoted by ΔE. This is equivalent to the electrostatic binding energy of the charge to the island. When these charge carries are excited to at least this energy from the Fermi level, there will be tunneling from one island to another. These island or small particles are called crystallites. The activation energy is related with film conductivity and given by the relation

$$\sigma = \sigma_o \exp\left(\frac{-\Delta E}{2kT}\right) \quad \text{... .. ... …} \quad (2.41)$$

Where ΔE is the activation energy, K is the Boltzmann constant and T is the absolute temperature.

Eq. (2.15) can be written as,

$$\ln \sigma = \left(\frac{-\Delta E}{2kT}\right) + \ln \sigma_o \quad \text{... ... ... …} \quad (2.42)$$

Equation (2.42) is equivalent to straight line equation, y = mx+ c.

The activation energy ΔE is calculated from the slope of a curve ln σ vs. (1/T). Therefore the activation energy ΔE is given by

$$\Delta E = -\frac{\ln \sigma}{1/T} 2k \quad \text{… …… …..} \quad (2.43)$$

References:

1. Lampkin, C. M., "Aerodynamics of nozzles used in spray pyrolysis", Prog. Crystal Growth Chaact, pp 406-416, 1979.

2. Zhang, Z., and Lagally, M. G., "Atomistic Processes in the Early Stages of Thin-Film Growth" Science. Vol. 276, pp 377-383, 1997.

3. Chopra, K. L., ''Nucleation, Growth and Structure of Films" Thin Film Phenomena, McGraw-Hill book Company, New York, pp 110-137, 1969.

4. Jensen, P., Havlin, S. et al. "A Fractal Model for the first stage of thin films growth" Fractals, Vol. 4, No. 3, pp 321-329, 1996.

5. Ratsch, C., Venables, J. A. "Nucleation theory and the early stages of thin film growth" J. Vac. Sci. Technol, pp 0734-2101, 2003.

6. Kittel, C., "Introduction to Solid State Physics", 7th edition, Jhon wiley and Sons, Inc., New York, 1996.

7. Tolansky, S., "Multiple Beam Interferometry of Surface and Films", Oxford University Press, London, 1948.

8. Barden, J., Blatt, F. J., and Hall, L. H., Proc of Atlantic City Photoconductivity Conference, 1954.

9. Van-der Pauw, L. J., Philips Res. Rept., Vol-13, pp 1, 1958.

CHAPTER- III
THIN FILM DEPOSITION TECHNIQUES

3.1 Introduction

Thin films are defined as coatings of a thickness from about 5 Angstroms (Å) to a few micrometers (μm) [1, 2]. Several materials may be deposited as thin films on passive substrates such as glass or ceramic or on active substrates such as silicon. Modern thin film technology has evolved into a sophisticated set of techniques used to fabricate many products. Applications include very large scale integrated (VLSI) circuits; electronic packaging, sensors, and devices; optical films and devices; as well as protective and decorative coatings. Generally thin films are prepared by depositing the film material, atom by atom on to a substrate. One of the examples is the condensation of vapor to give a solid or liquid film. Thin-film deposition is any technique for depositing a thin film of material onto a substrate or onto previously deposited layers. Thin is a relative term, but most deposition techniques allow layer thickness to be controlled within a few tens of nanometers, and some allow single layers of atoms to be deposited at a time.

The process of deposition mainly depends on the means that are deployed which can be physical or chemical and thus the deposition techniques could be divided into two broad groups: Physical and chemical illustrates the classification of the techniques which are most commonly used in modern technology. A short description of each technique is given in the following sections.

Recent development and patents on Thin Film Technology

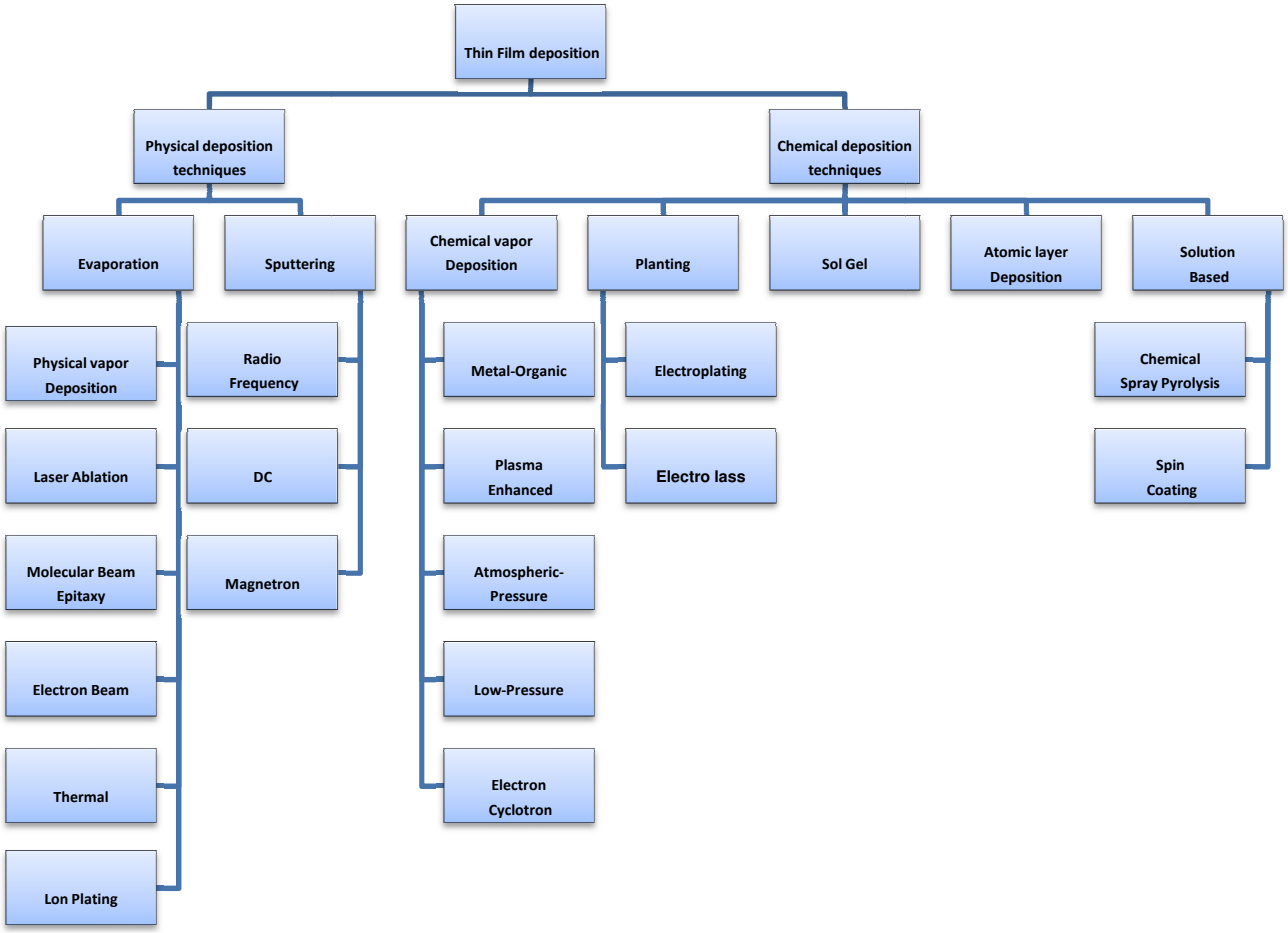

3.2 Physical Deposition Techniques

Several different kinds of thin films are deposited by evaporation and sputtering in modern technology e.g. micronanoelectronics [3]. In several applications sputtering is preferred over evaporation because of the wider choice of materials to work with, better adhesion to the substrate and better step coverage. Evaporation is mainly a laboratory technique whereas sputtering is employed in laboratories and industrial production of thin films. There are cases though where a combination of the two methods could be used such as in [4].

3.2.1 Evaporation

Among physical vapor deposition techniques evaporation is the one with the longest standing tradition. However, during the last 30 years of booming semiconductor industry which involves a great deal of thin film technology, deposition techniques like PVD (physical vapor deposition) or sputtering which often offer unquestionable advantages have been developed to perfection.

3 .2.1.1 Physical Vapor Deposition

PVD is a method to deposit thin films by the condensation of a vaporized material onto various surfaces (e.g., onto semiconductor wafers). The coating method involves purely physical processes such as high temperature vacuum evaporation rather than involving a chemical reaction at the surface to be coated as in chemical vapour deposition. One of the main industrial fields where PVD is extensively used is the fabrication of semiconductor devices. PVD covers a number of deposition technologies in which material is released from a source and transferred to the substrate. The most important technologies are evaporation, sputtering, painting and spray pyrolysis

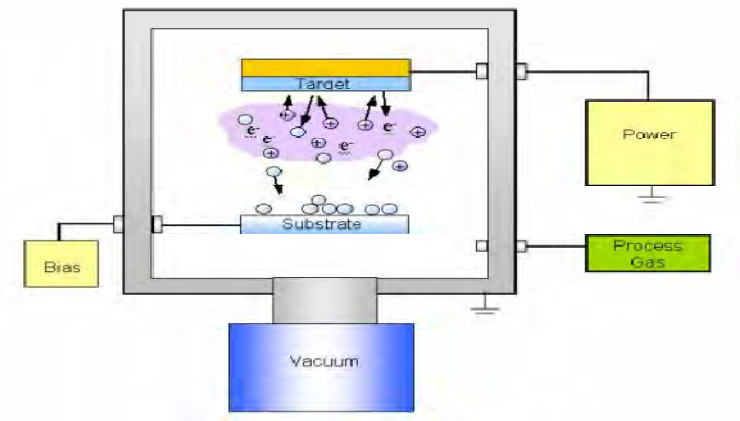

Fig 3.1: Physical vapor deposition method

PVD comprises the standard technologies for deposition of metals. It is far more common than CVD for metals since it can be performed at lower process risk and cheaper inregards to materials cost. The quality of the films is inferior to CVD, which for metals means higher resistivity and for insulators more defects and traps. The step coverage is also not as good as CVD.

Evaporation/sputtering of a target material onto a substrate

•Evaporation of a solid

•Transport of the gaseous species to the substrate

•Condensing gaseous species on the substrate, followed by nucleation and growth.

3.2.1.2 Laser Ablation

In principle, this technique is extremely simple as it uses pulses of laser energy to remove material from the surface of a target and deposit the eroded material onto a substrate. The vaporized material (ions, electrons, atoms, radicals or clusters) is known as a laser-produced plasma plume and travels away from the target in the vacuum chamber with velocities around 106cm/sec.

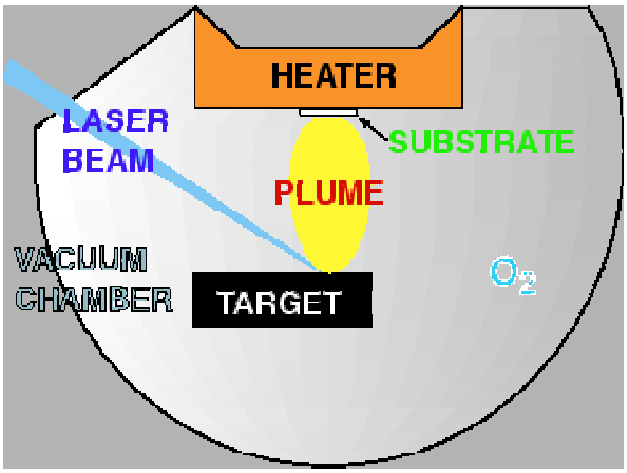

Fig 3.2: Principle of laser ablation. Energetic laser pulses hit the target and evaporate material from the surface. The emitted particles condense on the substrate surface.

When the ablated material hits the substrate surface at high impact energies (typically 100 eV) the particles stick to the surface with reasonably high adhesion, and are compressed, forming a continuous film [5-7]. Further laser pulses ablate more material and gradually the thickness of the film increases from a few atomic layers to microns.

In practice several variables are affecting the properties of the grown film such as laser fluency, background gas pressure and substrate temperature and therefore the optimization of the laser ablation can require a lot of time and effort. Applications of the technique range from the production of superconducting and insulating circuit components to biocompatible materials.

3.2.1.3 Molecular Beam Epitaxy

Molecular beam epitaxy (MBE) is a technique for epitaxial growth via the interaction of one or several molecular or atomic beams that occurs on a surface of a heated crystalline substrate. Angular distribution of atoms or molecules in a beam is provided by placing the solid sources of materials in evaporation cells.

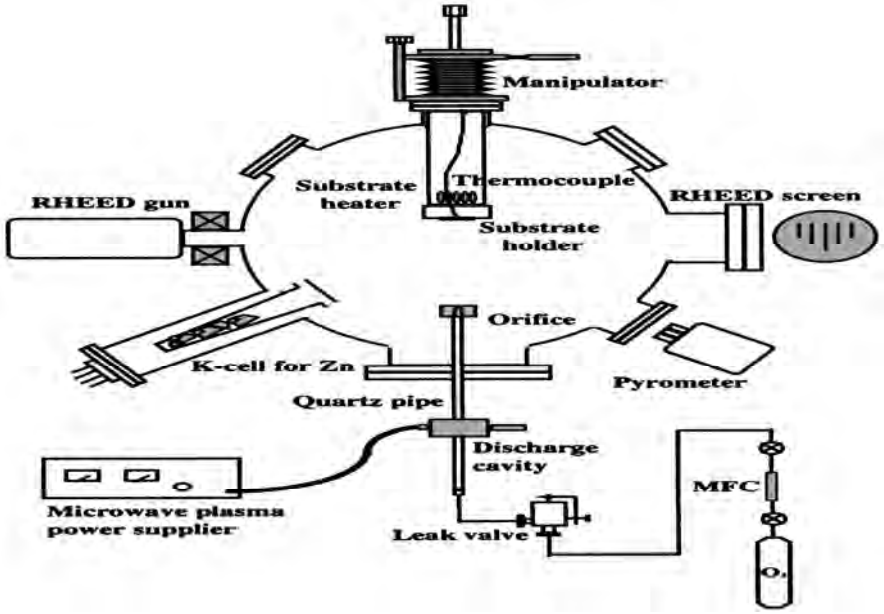

Fig 3.3: Schematic of the Molecular beam epitaxy system

The substrate is heated to the necessary of temperature and, when required, continuously rotated in order to improve the growth homogeneity. During the MBE technique the atoms are arranged in a single-crystal manner upon a crystalline substrate which acts as a seed crystal. Thus the lattice of the grown film is the same as that of the substrate. In MBE the heated, e.g between 400 - 800°C, single-crystal is placed in an ultrahigh vacuum, e.g 133x10-11 Pa, together with atomic streams from heated cells that contain the materials of interest. The most important aspect of MBE is the slow

deposition rate (typically less than 1000 nm per hour), which allows the films to grow epitaxial. The slow deposition rates require proportionally better vacuum to achieve the same impurity levels as other deposition techniques evaporation of elemental sources independently at a controlled rate. Molecular beams intercept at the substrate surface UHV conditions (10-10 bar), low growth rates, Line-of-sight. High purity, complex layer structures, good control of doping.

3.2.1.4 Electron Beam (EB-PVD)

EB-PVD is a technique suitable for the fabrication of nanometer scale structures. In EB-PVD a target anode is bombarded with an electron beam given off by a charged tungsten filament under high vacuum. The electron beam causes atoms from the target to transform into the gaseous phase. These atoms then precipitate into solid form, coating everything in the vacuum chamber with a thin layer of the anode material.

3.2.1.5 Thermal Evaporation for HTS Deposition

TE is the classical technique applied for metal - plating of glass or plastic surfaces, like e.g. aluminium coatings widely used for capacitors, plastic wrappings, and as barrier against water diffusion. It is evident that the deposition of quaternary metal – oxide compounds imposes quite different requirements to the technique and will go far beyond the rudimentary concept of evaporating a single metal in a vacuum chamber. The necessary features of a conventional HTS deposition system are depicted in figure 3.4. The metal species the superconductor is composed of are evaporated in high vacuum ambient. Usually, the chamber is pumped to 10-6 mbar background pressure. During deposition, the distance between the sources and the substrate which is in the range of several ten centimeters sets the scale for the required mean free path. Ballistic propagation of the vapor requires a residual gas background below 10-4 mbar, even when an oxygen flow is introduced .To control the film composition the evaporation rates have to be online monitored individually by some kind of sensor heads. Feedback loops to the sources serve to stabilize the evaporation rates.

The substrate is mounted in or on a heater element and kept at a temperature which promotes epitaxial film growth. Since HTS require elevated oxygen pressure for their

formation the introduction of oxygen is an essential but tricky task. To avoid flooding of the chamber with oxygen the main chamber is permanently pumped at, while the reactive gas has to be introduced close to the substrate. In the early days, housing as described by Baudenbacher (1990) served to confine the gas around the substrate. Its small opening towards the sources constitutes an enhanced gas flow resistance and allows differential pumping to a certain extent.

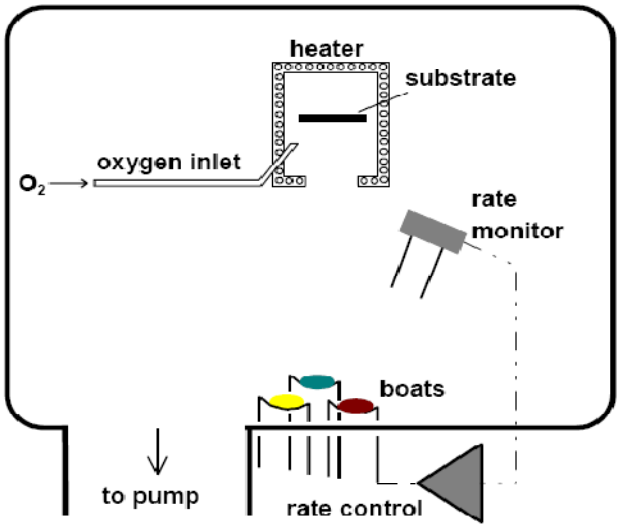

Fig 3.4: Main features of a conventional HTS evaporation system.

Since the height of the region with enhanced oxygen pressure is comparable to its lateral extension, i.e. the dimensions of the substrate, this concept can be applied only for small chips (typically in the order of 10 – 20 mm). Otherwise, with increasing thickness of this oxygen zone the metal vapors start scattering. Since the scattering cross section depends on the molecular weight, as a first consequence the composition gets extremely pressure dependent. If the gas pressure or the length of the path through the oxygen is further increased, the vapor does not penetrate this barrier and cannot reach the substrate any more.

3.2.1.6 Ion Plating

Ion plating could be described as discharge assisted evaporation [1]. It is a technique in which the evaporation of a material is combined with ionization of the atom flux by an electron filament or plasma. A glow discharge is maintained at a pressure from $133 \times 10^{-}$

^{1} to $133x10^{-2}$ Pa between the filament (anode) and the substrate (cathode) so that the evaporated atoms are ionized. The discharge potential is maintained at the highest possible value so that the ionized atoms are accelerated towards the substrate. Due to the high energy with which the ions are reaching the substrate the adhesion of the deposit is of high quality. By using an inert gas atmosphere in the chamber the discharge will keep the substrate clean. Yet the conditions have to be chosen with great care [8-10].

3.2.2 Sputtering

Sputtering is a method used to deposit both thin metal films and insulators onto a substrate. Unlike evaporation, the material to be sputtered does not have to be heated. During sputtering an atom or molecule is knocked out of a target material by accelerated ions which are produced from excited plasma. The atom or molecule is then condensed on a substrate either in its original or in a modified form [11]. Prior to the sputtering procedure a vacuum of less than one ten millionth of an atmosphere must be achieved. From this point a closely controlled flow of an inert gas such as argon is introduced. Specifically, a sputtering system consists of an evacuated chamber, a target (cathode) and a substrate table (anode). It is a process in which the chemically inert atoms, e.g. argon (Ar) as mentioned above, are ionized in a glow discharge which is called plasma [12]. The ions are accelerated into a target by the electric field at the boundary of the plasma. Atoms from the target are knocked out and these atoms are allowed to reach the substrate.

If the plasma ions are accelerated by a DC field then the sputtering technique is called DC [13]. If an RF field is used then the technique is called RF sputtering and Magnetron if magnets with alternating polarity are arranged behind or sometimes at the sides of the target to enable lower pressures to be used and thus a cleaner film to be created [14-17]. In particular, during sputtering secondary electrons can be captured close to the target from a magnetic field. The electrons follow helical paths around the magnetic field lines and undergo more ionizing collisions with neutral gaseous near the target than they would without the magnetic field. Therefore, a higher sputter rate is achieved trough this enhancement of the ionization. Additionally, with this method the

plasma can be sustained at a lower pressure. The magnetic trap does not affect the sputtered atoms since they are neutrally charged.

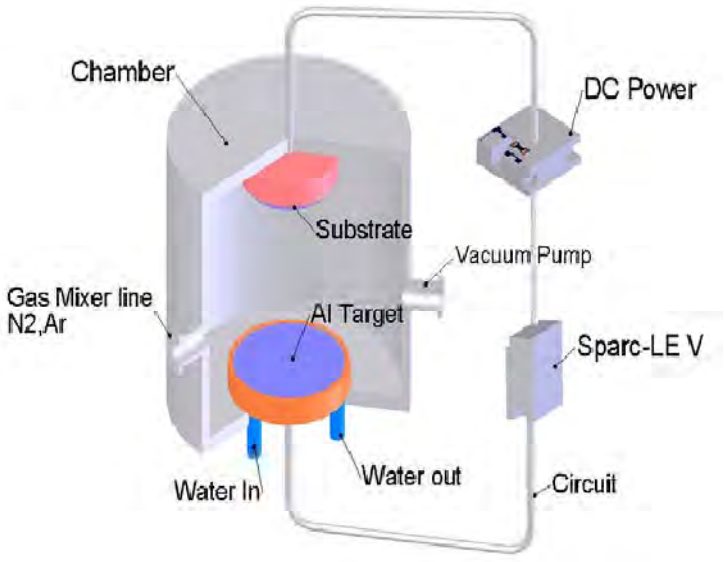

Fig 3.5: Schematic drawing of the magnetron sputtering system

Sputtering is a procedure that takes place in a low pressure gas environment and is less directional than electron beam evaporation and can typically achieve much higher deposition rates. It can be used with metallic targets but also dielectric films such as silicon dioxide (SiO_2) can be sputtered even though usually chemical vapour deposition methods. Yet, some specialty materials such as piezoelectric zinc oxide and aluminum nitride films are well suited to sputtering [12].

3.3 Chemical Deposition Techniques

Here, a fluid precursor under goes a chemical change at a solid surface, leaving a solid layer. An everyday example is the formation of soot on a cool object when it is placed inside a flame. Since the fluid surrounds the solid object, deposition happens on every surface, with little regard to direction; thin films from chemical deposition techniques tend to be conformal, rather than directional.

3.3.1 Chemical Vapour Deposition

During CVD thin films are developed on a substrate by using chemical reactions. Reactive gases are supplied into a vacuum chamber and these gases react on a substrate and form a thin film or a powder. The reactions though which form a solid material do

not always occur on or close to the heated substrate, heterogeneous reactions, but in the gas phase as well, homogeneous reactions [4]. Gaseous by-products are removed from the chamber [21].

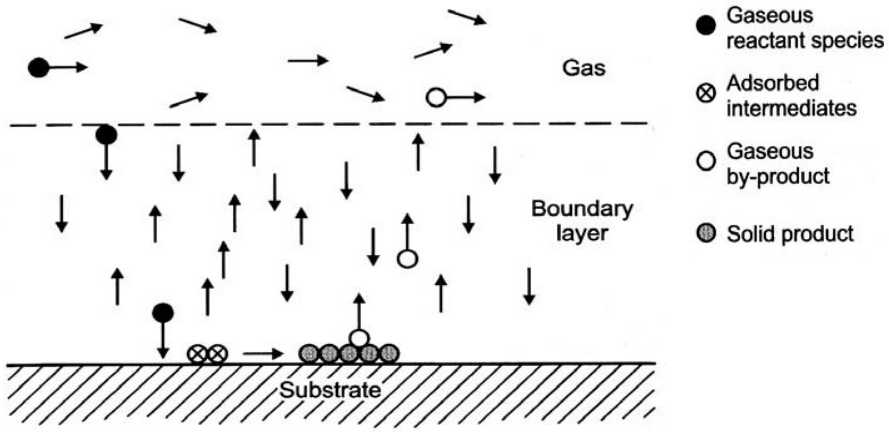

Fig 3.6 : Schematic representation of the steps in CVD processes

CVD is operated at low or atmospheric pressure. Epitaxial, amorphous, polycrystalline and uniaxially oriented polycrystalline layers can be deposited with good purity, control and economically [18]. The main application of CVD technology is in the semiconductor industry.

3.3.1.1 Metal-Organic Chemical Vapour Deposition

This is a technique for depositing thin layers of atoms onto a semiconductor wafer. Using MOCVD you can build up many layers, each of a precisely controlled thickness, to create a material which has specific optical and electrical properties. Atoms that will be incorporated in the crystal a recombined with complex organic gas molecules and passed over a hot semiconductor wafer. The heat breaks up the molecules and deposits the desired atoms on the surface, layer by layer. In contrast to molecular beam epitaxy (MBE) the growth of crystals is by chemical reaction and not by physical deposition. By varying the composition of the gas, we can change the properties of the crystal at an almost atomic scale. Using this method high quality semiconductor layers can be grown and the crystal structure of these layers is perfectly aligned with that of the substrate [19-23]. It has become the dominant process for the manufacture of laser diodes, solar cells, and LEDs.

3.3.1.2 Plasma-Enhanced Chemical Vapour Deposition

Deposition rates can be enhanced if the deposition occurs in glow-discharge plasma [12]. During PECVD thin films are deposited from a vapour (gas state) onto a substrate [24-26]. Plasma of the reacting gases is created and then several chemical reactions are taking place. In general the plasma is created by an RF frequency or by a DC discharge between two electrodes.

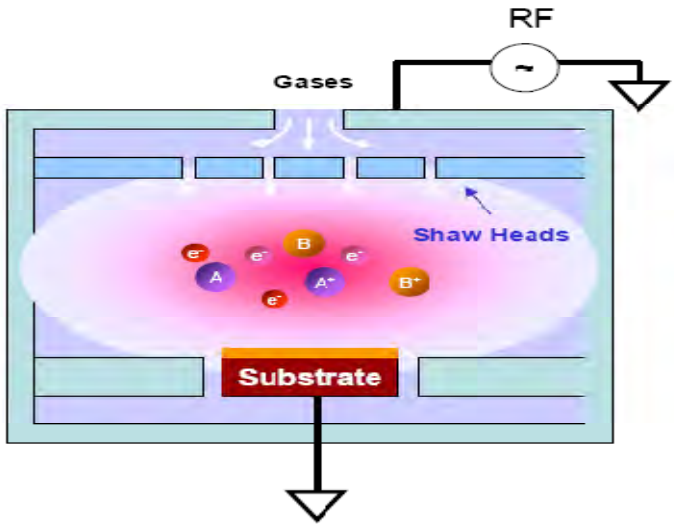

Fig 3.7: The Plasma –Enhanced Chemical Vapor Deposition Processes

The space between the two electrodes is filled with the reacting gases. PECVD is widely used in very large scale integration (VLSI) which is the process of fabricating integrated circuits by combining several transistor based circuits into a single chip. It enables the deposition of dielectric films such as oxides and nitrides on wafers with small feature sizes and line widths at low temperature and on devices which are not able to withstand the high temperatures of a thermally activated reaction [4]. PECVD is additionally used in amorphous silicon thin film deposition e.g. for photovoltaic panels.

3.3.1.3 Atmospheric-Pressure Chemical Vapour Deposition

This method is used to grow epitaxial for example single crystalline films of Si, compound semiconductors such as GaAs, InP and HgCdTe and to deposit at high rates SiO2, for example, from the reaction SiH4 and oxygen, at low temperatures of 300 to

450°C [4]. This method was also used to produce transition metal phospides which have found application as wear-and corrosion-resistant coatings [27-30]. The APCVD is susceptible to gas phase reactions and step coverage is often poor. High gas dilutions help avoid gas phase nucleation.

3.3.1.4 Low-Pressure Chemical Vapour Deposition

Films deposited by LPCVD are either amorphous, in the case of the inorganic dielectrics, or polycrystalline, in the case of polysilicon or metals [12].

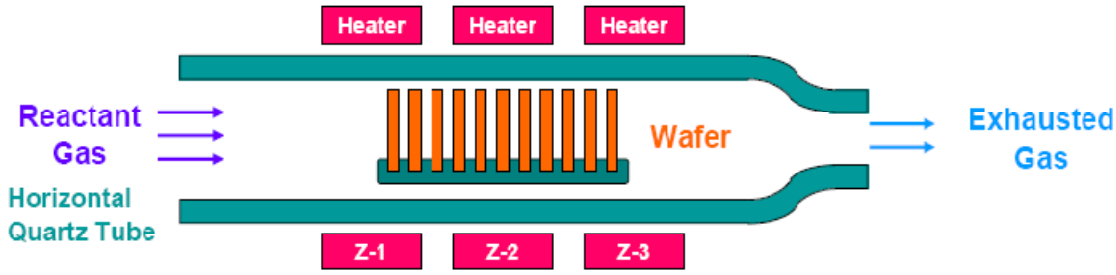

Fig 3.8: The Low – Pressure Chemical Vapour Deposition

The material properties can depend on the exact process, including the conditions such as temperature, gas flow rates, pressures, and the chemistry or morphology of the layer on which the film is deposited [31, 32]. The mass density of a deposited film, for example, depends on how many voids are present (regions where atoms could fit but due to the relatively low temperature of deposition do not get filled up). Thermally grown silicon dioxide has fewer voids than LPCVD silicon dioxide, which has fewer voids than PECVD silicon dioxide.

3.3.1.5 Electron-Cyclotron Resonance Chemical Vapour Deposition

In ECRCVD one uses electron cyclotron resonance (ECR) to generate a high-density plasma (HDP) that can deposit materials at high rates while pressures and temperatures remain low [4]. This technology provides a way to ensure durable ultra thin films. The equipment can be used for both enhanced etching and enhanced deposition and it provides high uniformity of deposition and etching across large area substrates.

3.3.2 Plating

Plating relies on liquid precursors, often a solution of water with a salt of the metal to be deposited. Some plating processes are driven entirely by reagents in the solution (usually for noble metals), but by far the most commercially important process is electroplating. It was not commonly used in semiconductor processing for many years, but has seen resurgence with more widespread use of chemical-mechanical polishing techniques.

3.3.2.1 Electroplating

During electroplating an electrical current is applied in order to reduce cations of the material to be deposited from an aqueous solution. The cations then coat a conductive substrate with a thin layer of the material. The substrate is the cathode of the circuit and the anode is the material e.g metal, to be plated on the substrate. Both components are immersed in a solution called an electrolyte containing one or more dissolved metal salts as well as other ions that permit the flow of electricity. Plating uniformity depends on maintaining a uniform current density there where the plating is taking place [12]. Features of different areas and regions at the corners of features may plate at different rates. Electroplating is used in microelectronics to deposit copper interconnect on silicon integrated circuits and it is widely used in creating copper and magnetic material microstructures in magnetic MEMS sensors and actuators. It is also used in making high-aspect-ratio microstructures, called HARM when using molds made with standard optical Lithography [33] and called LIGA when the molds are made using X-ray lithography with highly collimated synchrotron sources [34].

3.3.2.2 Electro less plating

The electro less depositing process is a coating method that plates the films on substrates by an autocatalytic reaction of coated materials without the use of external electrical powers. This process can provide a uniform deposit regardless of substrate geometry. It is also known as chemical or autocatalytic plating [35]. Specifically, the deposition of a metallic coating on a component is achieved as several chemical reactions are taking place within an aqueous solution without the application of an electrical current. The aqueous solution (bath) supplies the electrons for the deposition

reaction. These baths are extremely complex using a variety of chelating and/or complex agents that hold the metals in solution. The plating thickness tends to be uniform compared to electroplating due to the absence of electric fields. It is most commonly used for nickel, copper, cobalt, and gold plating.

Electroplating and Electroless deposition are the most economical processes for applying metallic coatings of thickness between 10 and 500μm on many engineering components. This is mainly because their rates of deposition can provide the required product quality in acceptable process times at relatively low capital and operating costs [35].

3.3.3 Atomic Layer Deposition

Atomic layer deposition allows ultra-thin films (of a few nanometers) to be deposited in a controlled manner with high precision. It is a gas phase chemical process and it utilizes sequential precursor gas pulses to deposit a film, one layer at a time. In most cases 2 chemicals (precursors) are used and the first one produces a monolayer of gas on the wafer surface and the second is then introduced in the chamber and reacts with the first one so as to produce a monolayer film on the wafer surface. The main advantages of ALD are that complete control over the deposition process is obtained at the nanometer scale because by this method precisely one atomic layer in each cycle is deposited. Moreover, conformal coating can be achieved even in high aspect ratio and complex structures and pin-hole and particle free deposition is achieved. ALD finds applications in semiconductors, MEMS (e.g. coatings for microfluidics), coatings of nanoporous structures, fuel cells (e.g. single metal coating for catalyst layers), flat panel display, magnetic and optical storage, solar cell, nanotechnology and nanomaterials.

3.3.4 Sol-Gel

Sol-gel method is a wet chemical route for the synthesis of colloidal dispersions of oxides which can be altered to powders, fibers, thin films and monoliths. In general, sol-gel method consists of hydrolysis and condensation reactions. Sol-gel coating is a process of preparation of single or multicomponent oxide coating which may be glass, glass ceramic or crystalline ceramic depending on the process. Also, the nanomaterials used in modern ceramic and device technology require high purity and facilitate to

control over composition and structure. The solgel coating is one of the interesting methods because it has many advantages. Examples are as the followings:

1. The chemical reactants for sol-gel process can be conveniently purified by distillation and crystallization.
2. All starting materials are mixed at the molecular level in the solution so that a high degree of homogeneity of films can be expected.
3. Organic or inorganic salts can be added to adjust the microstructure or to improve the structural, optical and electrical properties of oxide films.
4. The sol-gel coating is almost exclusively applied for fabrication of transparent layers with a high degree of planarity and surface quality.

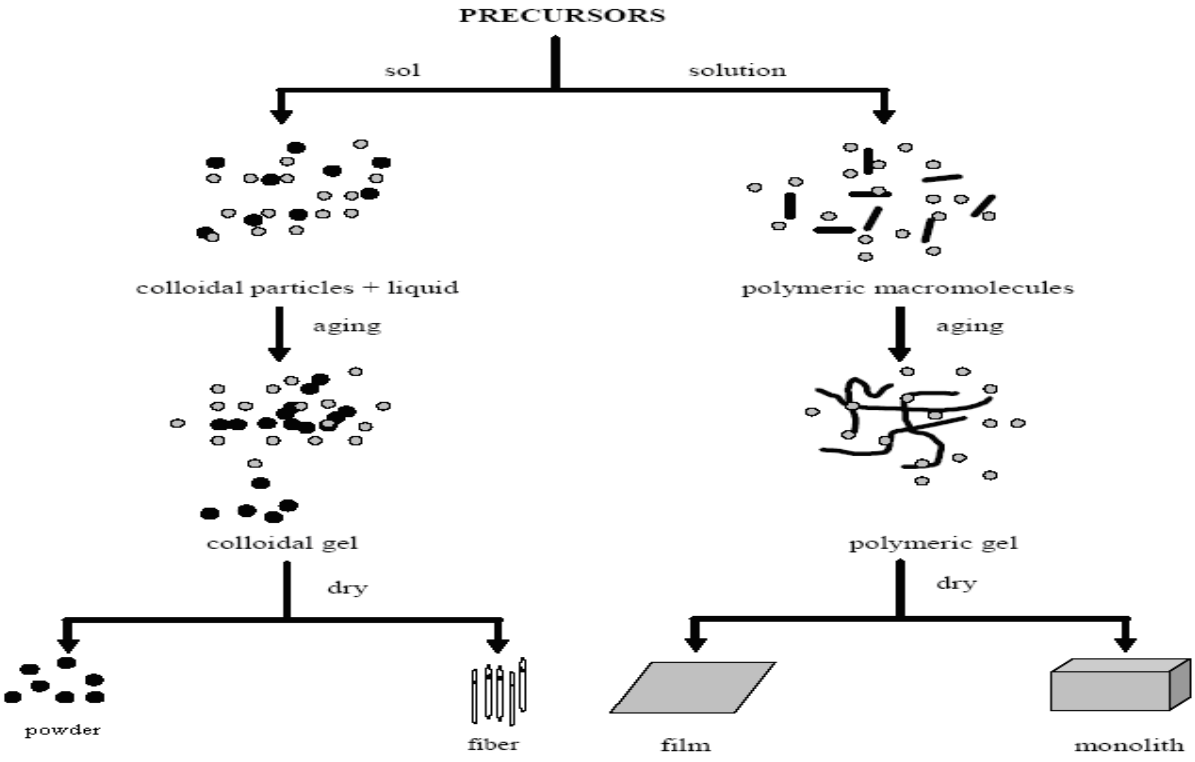

Fig 3.9: Generalized scheme of sol-gel synthesis

3.3.5 Solution-Based Deposition

Solution-based deposition uses a liquid precursor, usually a solution of organmetallic powders dissolved in an organic solvent. This is a relatively inexpensive, simple thin film process that is able to produce stoichiometrically accurate crystalline phases.

3.3.5. Spin Coating

Spin coating has been used for several decades for the application of thin films. It is a procedure used to apply uniform thin films to flat substrates Spin Coating involves the acceleration of a liquid puddle on a rotating substrate [36].

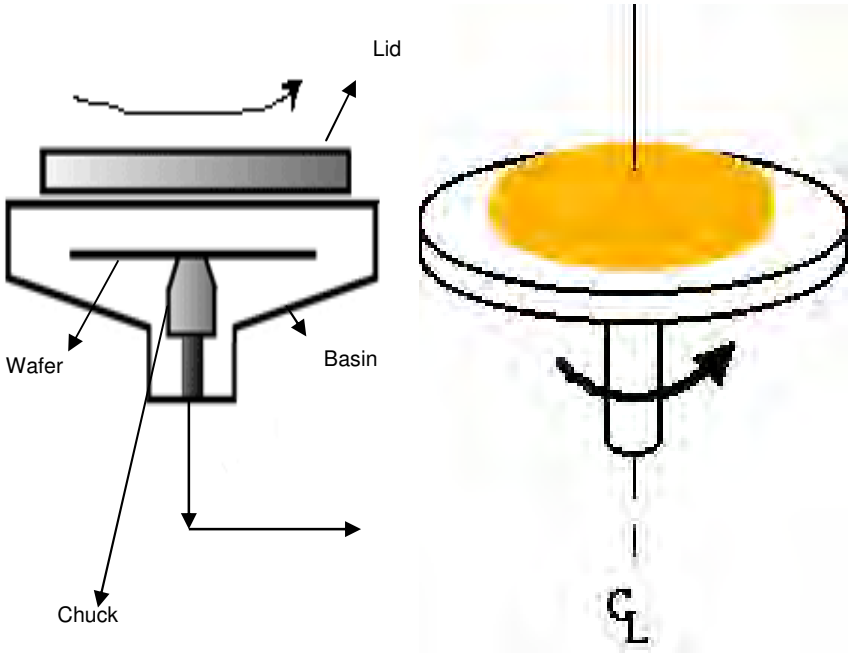

Fig 3.10: Spin Coating

A typical process involves depositing a small puddle of a fluid resin onto the center of the substrate and then spinning the substrate at high speed. The film-forming process is primarily driven by two independent parameters – viscosity and spin speed. The range of film thicknesses easily achieved by spin coating is 1-200 mm. For thicker films, high material viscosity, low spin speed, and a short spin time are needed. However, these parameters can affect the uniformity of the coat. Multiple coatings are preferred for a film thickness greater than 15mm.

3.3.5.2 Chemical spray pyrolysis (CSP)

It is a process where a precursor solution, containing the constituent elements of the compound, is pulverized in the form of tiny droplets onto the preheated substrate, where upon the thermal decomposition of the precursor an adherent film of thermally more stable compound forms. Spray pyrolysis involves several stages:

(a) generation microsized droplets of precursor solution

(b) evaporation of solvent

(c) condensation of solute

(d) decomposition of the precursor or solute and

(e) sintering of the solid particles.

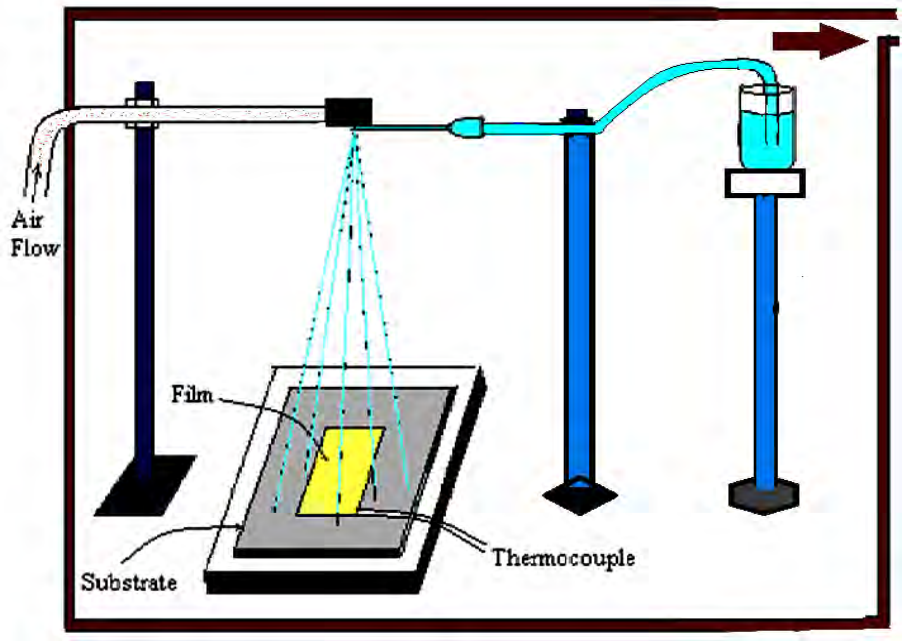

Fig 3.11: Experimental setup of spray pyrolysis technique

CSP is a convenient, simple and low-cost method for the deposition of large-area thin films, and it has been used for a long time. Additionally it is a low cost method (the device does not require high quality targets or vacuum) the composition and microstructure can easily be controlled (facile way to dope material by merely adding doping element to the spray solution) and the deposition takes place at moderate temperatures of 100-500ºC. Furthermore it offers the possibility of mass production. However as every other method, CSP has some disadvantages such as the possibility of

oxidation of sulfides when processed in air atmosphere, difficulties regarding the growth temperature determination. Apart from that after a long processing time the spray nozzle may become cluttered. Finally the films quality may depend on the droplet size and spray nozzle [37].This method is useful for the deposition of oxides and is also a powerful method to synthesize a wide variety of high purity, chemically homogeneous ceramic powders.

Advantages of Spray Pyrolysis Technique:

1. Inexpensive technique.
2. Possibility to produce large area film.
3. Ability to form crystalline or amorphous deposition.
4. Ability to control deposition parameters such as deposition temperature, deposition rate, thickness etc.
5. Particles are more uniform in size.
6. Simple and continous operation.
7. Easy fabrication.
8. Easy to control.
9. Vacuum less.

3.4 Current & Future Developments

Thin film technologies and their applications are constantly evolving. In fact, with the growing need for component and assembly miniaturization, well established thick film processes are rapidly approaching their technological limits. As a result, more and more manufacturers of electronic, mechanical, chemical, optical and energy supply devices are replacing the conventional thick film processes with thin film technologies in order to manufacture smaller components and parts.

In recent years several deposition devices have been developed in order to fabricate complex multilayers and structures and to optimize the thin film deposition conditions and the quality and homogeneity of the obtained thin films. These devices utilize either physical vapour deposition technique or chemical vapour deposition techniques and a few of the recent patents in thin film deposition.

Applications of thin film technology include very large scale integrated circuits (VLSI), electronic packaging, magneto-optical recording media, sensor technology etc. One of the most promising applications concerns photovoltaic systems in order to reduce their cost. Thin-film modules are expected to be cheaper to manufacture due to their reduced material costs, energy costs, handling costs and capital costs. According to thin film photovoltaic (TFPV) systems will be generating 26GW of power worldwide and represent a market worth $20bn. The prediction about TFPV is based on the rapid growth of all types of photovoltaics but also on the low cost of manufacturing and flexibility of deployment associated with TFPV - especially in residential applications – compared with currently dominant crystalline silicon photovoltaic technologies. “NanoMarkets” expects TFPV to account for more than half the world's production of photovoltaic systems by 2015. In the automotive industry surface and thin film techniques are also extensively used mainly in sensors, optics, electronics and surface modification assuring the production of safer and more comfortable automobiles. additionally, the 2007 German Future Prize winning thin film technology of Dr. Klaus Streubel, Dr. Stefan Illek (both of OSRAM) and Dr. Andreas Bräuer (of the Fraunhofer-Institute for Applied Optics and Precision Engineering) is the key to producing LED chips of extremely high brightness and also enables them to be packed tightly together to create a large illuminating surface. High-efficiency light emitting diodes from OSRAM that are based on this innovative technology will open up new applications ranging from mini projectors and rear projection televisions to night vision systems in vehicles and general room lighting.

References:

1. Maissel, L. I., Glang, R., " Handbook of Thin Film Technology. Mc Graw-Hill Company", 1970.

2. Smith, D. L., "Thin Film Deposition, Principles & Practice. McGraw- Hill Professional", 1995.

3. Tan, T., Li, Y., Liu, Y., *et al.* , " Two-step preparation of Ag/tetrapod-like ZnO with photocatalytic activity by thermal evaporation and sputtering", Mater Chem Phys Vol. 111, pp 305-308, 2008.

4. Madou, M. J., Fundamentals of Microfabrication, the Science of Miniaturization. 2nd Ed., CRC Press, 2002.

5. Khandelwal, R., Singh, A. P., Kapoor, A., *et al.*, " Effects of deposition temperature on the structural and morphological properties of SnO2 films fabricated by pulsed laser deposition", Opt. Laser Tech., Vol. 41, pp 89-93, 2009

6. Mahmoud, M. H., Ahmed, M. A., "Mössbauer study of the pulsed laser deposition of polycrystalline magnetic films", J. Magnetism Magnetic Mater, Vol. 320, pp 2647- 2649, 2008.

7. Camacho, J. M., Castro-Rodríguez, R., and Peña, J. L., "Transparent conductive oxide thin films of CdTe-doped indium oxide prepared by pulsed-laser deposition", Vol. 40, pp 895- 900, 2008.

8. Zhao, S. S., Du, H., Zheng, J. D., *et al.*, " Deposition of thick TiAlN coatings on 2024 Al/SiCp substrate by Arc ion plating", Surf. Coat. Tech., Vol. 202, pp 5170-5174, 2008.

9. Huang, J. H., Tsai, Z. E., and Yu, G. P., " Mechanical properties and corrosion resistance of nanocrystalline ZrNxOy coatings on AISI 304 stainless steel by ion plating", Surf. Coat Tech., Vol. 202, pp 4992- 5000, 2008.

10.Miyake, A., Yamada, T., Makino, H., *et al*., " Effect of substrate temperature on structural, electrical and optical properties of Ga doped ZnO films on cycroolefin polymer substrate by ion plating deposition", Thin Solid Films Article in Press, 2008.

11.Bashar, S. A., "Study of Indium Tin Oxide (ITO) for Novel Optoelectronic Devices", PhD Thesis, King's College London, University of London, Department of Electronic Engineering, 1998.

12. Solanski, R., Moore, C. A., and Collins, G. J., "Laser-Induced CVD", Solid State Technol., Vol. 28, No. 6, pp 220-227, 1985.

13. Chawla, V., Jayagantan, R., Chawla, A. K., Chandra, R., " Morphological study of magnetron sputtered Ti thin films on silicone substrate", Mater Chem. Phys., Vol. 111, pp 414-418, 2008.

14. Dunlap, R. A., Gaudet, J. M., Hatchard, T. D., " A Mössbauer effect and Xray diffraction study of Fe- Ga- Al thin films prepared by combinatorial sputtering", J. Magnetism Magnetic Mater, Vol. 320, pp 2730-2736, 2008.

15. Zhao, Q. X., Bian, F., Zhou, Y., Gao, Y. F., *et al*., "Optical emission, electron temperature and microstructure of Cu film prepared by magnetron sputtering", Mater Lett., Vol. 62, pp 4140-4142, 2008.

16. Zhang, B., Dong, X., Xu, X., Zhao, P., Wu, J., " Characteristics of zirconium-doped indium tin oxide thin films deposited by magnetron sputtering", Solar Energy Mater Solar Cells, Vol. 92, pp 1224-1229, 2008.

17. Shiung, H. C., Houng, B., Yi, H. B., Ju, C. G., Li, F. S., "Effect of Ru addition on the properties of Al-doped ZnO thin films prepared by radio frequency magnetron sputtering on polyethylene terephthalate substrate", J. Alloys Comp., Vol. 464, pp 89-94, 2008.

18. Jensen, K. F., Chemical Vapour Deposition. Microelectronics Processing: Chemical Engineering Aspects, D. W. Hess, K. F. Jensen, Eds. Washington, D.C.: Amer Chemical Society, 1989.

19. Chatterjee, S., Samanta, S. K., Banerjee, H. D., Maiti, C. K., **"**Metalloorganic compound- based plasma enhanced CVD of ZrO2 films for microelectronic applications", Bull Mater Sci., Vol. 24, pp 579-582, 2001.

20. Yang, P. F., Jian, S. R., Lai, Y. S., *et al*., **"** Morphological, structural, and mechanical characterizations of InGaN thin films deposited by MOCVD", J. Alloys Comp., Vol. 463, pp 533-538, 2008.

21. Luo, W., Wang, X., Xiao, H., Wang, C., *et al*., **"** Growth and fabrication of AlGaN/GaN HEMT based on Si(111) substrates by MOCVD", Microelectronics J., Vol. 39, pp 1108-1111, 2008.

22. Malandrino, G., Lipani, Z., Toro, R. G., Fragalà, M. E., **"**Metal-organic chemical vapor deposition of $Bi_2Mn_4O_{10}$ films on $SrTiO_3$ <100>", Inorganica Chimica Acta., Vol. 361, pp 4118-4121, 2008.

23. Ishikawa, H., Shimanaka, K., Tokura, F., *et al*., **"** MOCVD growth of GaN on porous silicon substrates", J. Crystal Growth, Vol.8, pp 30, 2008.

24. von Rohr, P. R., Borer, B., " Plasma-Enhanced CVD for Particle Synthesis Using Circulating Fluidized Bed Technology", Chem. Vap. Deposition, Vol. 13, pp 499-506, 2007.

25. Wright, D. N., Marstein, E. S., Rognmo, A., Holt, A., " Plasma-enhanced chemical vapour-deposited silicon nitride films; the effect of annealing on optical properties and etch rates", Solar Energy Mater Solar Cells, Vol. 92, pp 1091-1098, 2008.

26. Dupuis, J., Fourmond, E., Lelièvre, J. F., Ballutaud, D., Lemiti, M., " Impact of PECVD SiON stoichiometry and post-annealing on the silicon surface passivation"., Thin Solid Films, Vol. 516, pp 6954-6958, 2008.

27. Blackman, C. S., Carmalt, C. J., O'Neill, S. A., *et al*., " Atmospheric- Pressure CVD of Vanadium Phosphide Thin Films from Reaction of Tetrakisdimethylamidovanadium and Cyclohexylphosphine", Chem. Vap. Deposition, Vol. 10, pp 253-255, 2004.

28. Zhou, J., Xu, H., Mab, Q., Zhang, L., Dai, Y., Peng, B., " Mechanical and thermal properties of SiO2/S composite coating prepared by APCVD", Mater Sci. Eng., Vol. 491, pp 147-153, 2008.

29. Zhang, J., Li, J., Luo, L., Wo, Y., " Microstructure and morphology of SiOx film deposited by APCVD", J. Alloys Comp., Vol. 2, pp 14, 2008.

30. Morales, C., Juarez, H., Diaz, T., *et al*., " Low temperature SnO_2 films deposited by APCVD", J. Microelect., Vol. 39, pp 586-588, 2008.

31. Zheng, H., Su, J., Fu, Z., Li, G., Li, X., " Heteroepitaxial growth and characterization of 3C-SiC films on on-axis Si (110) substrates by LPCVD", Ceramics Int., Vol. 34, pp 657-660, 2008.

32. Endler, I., Höhn, M., Herrmann, M., Pitonak, R., *et al*., " Novel aluminumrich $Ti_{1-x}Al_xN$ coatings by LPCVD", Surface Coatings Technol., Vol. 4, pp 98, 2008.

33. Frazier, A. B., Allen, M. G., " Metallic microstructures fabricated using photosensitive polyimide electroplating molds", Microelectromech Syst, Vol. 2,pp 87-94, 1993.

34. Guckel, H., " High-aspect-ratio micromachining via deep X-ray lithography", Proc IEEE, Vol. 86, pp 1586-1593, 1998.

35. Tang, J., Zuo, Y., " Study on Corrosion Resistance of Palladium Films on 316L Stainless Steel by Electroplating and Electroless Plating", Corrosion Science, Vol. 7., pp 14, 2008.

36. Dana A., Schwartz, Kevin R., Kittilstved and Daniel R., "Above-room-temperature ferromagnetic Ni^{2+}-doped ZnO thin films prepared from colloidal diluted magnetic semiconductor quantum dots" Applied Physics Letters, Vol. 85, 2004.

37. Dedova, T., " Chemical Spray Pyrolysis Deposition of Zinc Sulfide Thin Films and Zinc Oxide Nanostructured Layers", PhD Thesis, Tallinn University of Technology, Faculty of Chemistry and Materials Technology, Department of Materials Science, Chair of Semiconductor Materials Technology, 2007.

CHAPTER-IV
EXPERIMENTAL DETAILS

Part-A: Film Preparation

4.1 Introduction

Spray pyrolysis is a processing technique being considered in research to prepare thin and thick films, ceramic coatings, and powders. Unlike many other film deposition techniques, spray pyrolysis represents a very simple and relatively cost-effective processing method (especially with regard to equipment costs). It offers an extremely easy technique for preparing films of any composition. Spray pyrolysis does not require high-quality substrates or chemicals. The method has been employed for the deposition of dense films, porous films, and for powder production. Even multilayered films can be easily prepared using this versatile technique. Spray pyrolysis has been used for several decades in the glass industry [1] and in solar cell production [2].

Typical spray pyrolysis equipment consists of an atomizer, precursor solution, substrate heater, and temperature controller. The following atomizers are usually used in spray pyrolysis technique: air blast (the liquid is exposed to a stream of air) [3], ultrasonic (ultrasonic frequencies produce the short wavelengths necessary for fine atomization) [4] and electrostatic (the liquid is exposed to a high electric field) [5].

4.2 Experimental Equipments

4.2.1 Preparation of Masks

In order to study the various properties of thin film, it is necessary that they must be properly patterned. The direct deposition of thin film pattern requires a suitably shaped aperture, commonly referred to as a mask. For the purpose of various experimental studies, film of specific size and shape are required. Mask was made from stainless steel plate with the desired pattern cut into it. The aperture was made in a bath machine. The most commonly used method of patterning thin film is the physical masking, which is accomplished by placing the mask of desired shape on the substrate. In the

present work, thin mica sheet was used for the preparation of masks as shown in figure 4.1.

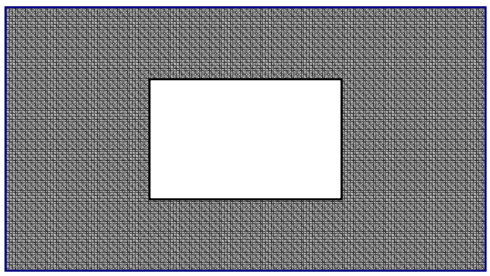

Fig.4.1: Mask for the sample

Regardless of mask material and fabrication process all masks should be thoroughly cleaned and inspected before use. Surface contaminants, particularly oil, grease or other organic materials may become volatile when the mask is heated and then be absorbed by the substrate and this may be a cause of weak film adhesion. The mask is placed in proximity to the substrate, there by allowing condensation of evaporate only in the exposed substrate areas. The mask was prepared in such away that the edge of the mask is smooth so that it is helpful for determining the film thickness accurately.

4.2.2 Heater

The heater 'H' is an ordinary hot plate, 3 K watt nichrome wire heater which is put in spherical shape holder. An electronic power supply (voltage variance) unit is connected with the heater power line to supply proper heat to the substrate. A thick stainless steel plate 'G' is placed on heater. Substrate with mica sheet is placed on this suspected plate.

4.2.3 The Design of the Reactor

The design of the reactor is shown is Fig.4.2. It is a vertical batch type reactor composed of a galvanized iron enclosure 'E', heater 'H' and heat susceptor 'G',

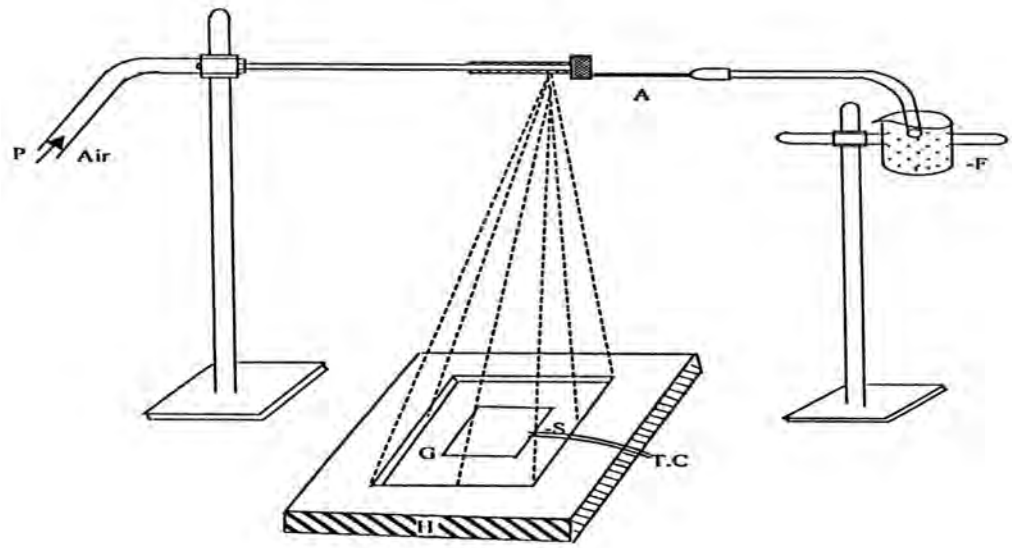

F = Beaker. H= Heater.

G = Graphite block. P = Upper tube.

A = Lower tube. T.C.= Thermocouple

Fig. 4.2: Experimental setup of spray pyrolysis technique

Fig 4.3: The schematic diagram of a locally developed spray pyrolysis system (BUET)

thermocouple 'T.C', lower tube "A", upper tube "P".For the rapid expulsion of the by product gases there are opening at the side and at the top of the reactor. It helps

focusing the incoming sprayed solution towards the substrate 'S' and also provides a chimney action to the exhaust gas upwards.

4.2.4 The Fume chamber

It is a large type chamber with a slanting top and is provided with a chimney. There is an exhaust fan with regulated power supply fitted at the top of the chimney [6]. The slanting top and the sidewalls are made of glass and wood. There are airtight doors in the front side. The chamber has purging facilities. The whole spray system and the reactor are kept inside this fume chamber at the time of film deposition because of the safety grounds and to check air current disturbances at the deposition site. These two points just stated are very important for the spray process when deposition is carried out in open- air atmosphere.

4.2.5 Air Compressor

It is reservoir type electrical air compressor. A rotary pump in this section mode draws atmospheric air and keeps it reserved in a large capacity air tank. At the outlet of the tank a pressure gauge is attached which records the pressure of the air at the time of supplying it from the tank. There is a by pass control valve which can keep the output pressure constant.

4.2.6 Spray Head/ Nozzle

The single spray nozzle consists of capillary tubes (stainless steels) fitted perpendicular to the other tube as shown in Fig. 4.2. When compressed air is passed rapidly through the upper tube 'P' in direction tangential to the mouth of the lower tube 'A', a partial vacuum is created at the front part of the tube 'A' whose other end is kept immersed in the spray liquid. Due to this partial vacuum the liquid rises up through the tube 'A' and the compressed air drives it away in the form of fine spray particles. The thinner spray nozzle would give the finer spray particles. A very fine needle shaped capillary tube was used for the spray nozzle and it may vary from nozzle to nozzle.

4.3 Substrate and substrate cleaning

The most commonly available microscope glass slides were used as substrates in the present work. The cleanliness of substrate surface exerts a decisive influence on film growth and adhesion. A thoroughly cleaned substrate is a pre-requisite for the preparation of films with reproducible properties. The choice of cleaning techniques depends on the nature of the substrate, the type of contaminants and the degree of cleanliness required. Since our glass substrates were ordinary soda lime microscope slides and over slides and therefore residue from manufacturing and packaging, fingerprints, oils and air borne particulate maters were supposed to be contaminations. The following procedure was found adequate for substrate cleaning in our laboratory. The gross contaminations of each of the substrates are first removed by warm aqueous solution of sodium carbonate.

After washing in a stream of cold water they are dipped at first into nitric acid for some time and then washed in de-ionized water several times and finally made dry by blowing hot air [7]. They are then preserved in desiccators. During the whole process slide, holding forceps always held the substrates.

4.4 Working solution

The solution was prepared by taking zinc acetate [$Zn(CH_3.COO)_2.2H_2O$] as a source compound. The most commonly used solvents are water and ethanol. As [$Zn(CH_3.COO)_3.2H_2O$] dissolves in water at room temperature, water was taken as solvent. Since the spray system used in the present experiment operates via a partial vacuum path at the mouth of the spray nozzle, the concentration of the solution prepared by the solvent should be such that the nozzle could at least draw it. The higher the solution concentration, the lower the spray rate. A typical value of solution concentration 0.1M was used in this work.

Also, in order to prepare the $Zn_{1-x}Cu_xO$ thin film the aqueous solution of zinc acetate [$Zn(CH_3.COO)_2.2H_2O$] and copper acetate [$Cu(CH_3.COO)_2.H_2O$] as the precursor were taken. To enhance the solubility of zinc acetate, 0.4ml of acetic acid was also added to the solution. In the work the concentration of the solution was kept 0.1M. Copper was

added in the form of copper acetate in the working liquid. In this work, 5%, 9%, 15%, 20% and 25% (at%) of copper was used for the purpose of doping.

4.5 Film Deposition Parameters

In the chemical spray deposition technique the structure, composition and other characteristics of the deposited films depend on a number of process variables [deposition parameters]. The variable quantities such the substrate temperature, solution and gas flow rate, deposition time, quality of the substrate material, size of atomized particles, solution concentration, and substrate to spray outlet distance, etc. are affected on the film properties. It is obvious that the substrate temperature is the most important deposition parameter and it is control with grate care.

For the deposition of $Zn_{1-x}Cu_xO$ thin film, all the above mentioned parameters except

- Substrate temperature (T_s)
- Deposition time (t_d)
- Solution concentration (C)
- Spray rate (S_r)
- Spray outlet to substrate distance (d_s) and
- Carrier air pressure (P_a),

were kept at their optimum values. To study the effect of any one of these six parameters on the film properties the remaining other were kept constant.

Air current disturbances become another parameter, which creates problem to get uniformity of thickness and homogeneity of the film.

4.6 Sample deposition

It has been stated earlier that spray pyrolysis method for preparing ZnO thin film is an economically attractive method [8-10], which consist basically of spraying solution on a heated glass substrate. The apparatus needed to carry out the chemical spray process consists of a device to atomize the spray solution and a substrate heater. Figure 4.2 shows a typical experimental setup of spray pyrolysis technique.

A considerable amount of (100ml) solution taken in the container 'F' fitted with the spray nozzle 'A'. The clean substrate with a suitable mask was put on the susceptor of the heater 'H'. The distance between the tip of the nozzle and the surface of the glass substrate was kept 25 cm. Before supplying the compressed air the substrate temperature 'T_s' was to be kept at a level slightly higher than the required substrate temperature because at the onset of spraying a slight fall of temperature is likely. The temperature of a substrate was controlled by controlling the heater power using a variac. The substrate temperature was measured by placing a copper constantant thermocouple on the substrate.

When compressed air is passed through 'P' at constant pressure (0.5 bar), a fine $Zn_{1-x}Cu_xO$ was produced and was automatically carried to the reactor zone where film was deposited on the heated substrate. A situation have been adjusted such that 6 minutes of spray produces $Zn_{1-x}Cu_xO$ thin film, thickness thickness of the range 200nm keeping substrate temperature at 623K.

The possible chemical reaction that takes places on the heated substrate to produce $Zn_{1-x}Cu_xO$ thin film may be as follows:

$$[Zn(CH_3COO)_2.2H_2O] + [Cu(CH_3COO)_2.H_2O] \xrightarrow[\text{Decomposes to}]{350^{\circ}C} Zn_{1-x}Cu_xO + CO_2\uparrow + CH_4\uparrow + \text{steam}$$

4.7 Rate of deposition

The rate of flow of the working solution can be controlled to a better accuracy by suitably designing the nozzle A and adjusting the air flow rate. In preparing ZnO films, the solution flow rate of 0.5ml/min to 0.7ml /min was used for the present experiment.

4.8 Film thickness and control

Thickness plays an important role in the film properties unlike a bulk material and almost all film properties are thickness dependent at least for thin films. Reproducible properties are achieved only when the film thickness and the deposition parameters are kept constant [11-13].

In the present spray deposition process, the deposition time is the main thickness-controlling factor, provided the other parameters remain constant. Since the deposition is carried out in normal atmosphere a direct control of thickness is not so easy. To control the film thickness therefore calibration chart may be used. The charts are generally plots of deposition time versus thickness, and can be prepared at different constant substrates temperatures prior to the preparation of particular experimental samples using the different solution and deposition variables. Since the rate of deposition in present set up is rather small, the thickness control is therefore not difficult.

4.9 Optimization of the Deposition Process

To obtain the optimum condition of the film deposition process, it is essential to select at first the requirements with respect to which the process should be optimized. The optimization process is very lengthy because there are a number of process variables. The basic requirement was to get a film of high transparency as well as high electrical conductivity.

For the process of optimization following set of films have been deposited:

- The first set of films was deposited at various substrate temperatures, keeping all other deposition parameters constant at an arbitrary level. From the set of

films the optimum substrate temperature T_s was selected with respect to the best conducting and transparent films.

- After obtaining the optimum value of T_s, second set of films were deposited by varying the substrate to spray outlet distance, d_s using the optimized T_s and other parameters were kept constant to the arbitrary level as they were in the first set. From this second set of films the optimum distance d_s was selected corresponding to the best film.

- Fixing the distance d_s and substrate temperature T_s, a third set of films were deposited by varying the pressure of the carrier gas P_a. From this set, optimum carrier air pressure P_a was selected.

- Keeping T_s, d_s and P_a as fixed fourth set of films were deposited by taking spray rate S_r as variable parameters. From this set, optimum spray rate S_r was selected.

- The fifth set of films were deposited keeping T_s, d_s, P_a and S_r at their optimum values. In this case, the solution concentration C was varied for selecting the optimum concentration of the working solution.

- Thus in all cases the optimum values of the parameters (T_s, d_s, P_a, S_r and C) were selected for deposition of films that exhibit good conductivity and high transparency.

The resulting optimization is undoubtedly a tentative one because the process variables are in some degree mutually interdependent.

Part-B: Measurement Details

4.10 Apparatus for optical characterization

4.10.1 Apparatus for spectrophotometer measurements

The optical behaviors of a semiconductor are investigated in term of the three phenomena namely transmission, reflection and absorption. When a semiconductor is illuminated by light, photon strikes the surface, a fraction of photons are reflected, some of these are absorbed within the semiconductor and the remainder transmitted into the semiconductor. For optical property studies of $Zn_{1-x}Cu_xO$ thin films, transmittance and absorbance were measured by using a double beam UV spectrophotometer. Measurements were made by placing the sample in the incident beam and another empty glass substrate in the reference beam of the instrument. The optical transmission and reflection spectra of the film with respect to glass substrate were than taken for wavelength range 300 to1100 nm using UV-1601 PC SHIMADZU VISIBLE SPECTROMETER in BCSIR, Dhaka.

Fig.4.4: Photograph of a recording Spectrophotometer

4.11 Apparatus for film thickness measurements

The film thicknesses of $Zn_{1-x}Cu_xO$ thin films were measured by the Fizeau fringes method in the department of Physics, BUET. The thickness of the film "*d*" can then be determined by the relation,

$$d = \frac{\lambda}{2}\frac{b}{a}$$

where λ is the wavelength and *b* is the step height and a is the fringe spacing.

4.12 Apparatus for structural characterization

4.12.1 Apparatus for SEM and EDX

The scanning electron microscope (SEM) is a type of electron microscope that creates various images (surface morphology) by focusing a high energy beam of electrons onto the surface of a sample and detecting signals from the interaction of the incident electron with the sample's surface.

Scanning Electron Microscopy (SEM) measurement was performed at Magnetic Material Division (MMD) of Atomic Energy Center (AECD), Dhaka. SEI quanta inspect, Model-S50 apparatus is used to carry out the SEM measurement. This apparatus operates in 25 KV. It has 100 to 100000 magnification capacity. This apparatus has two imaging system, secondary electron imaging (SE imaging) and back scattered imaging (BS imaging).

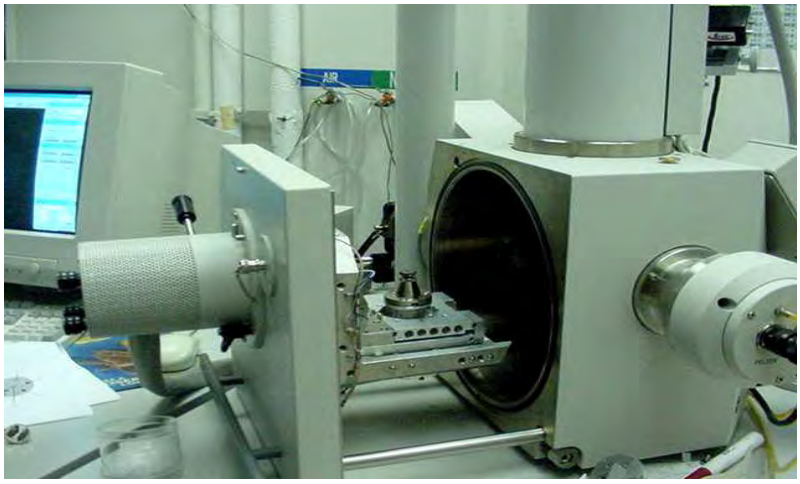

Fig.4.5: Photograph of Scanning Electron Microscopy (SEM)

EDAX describes the compositional analysis of the thin films. This is done by the scanning electron microscopy (SEM) by focusing the X-ray beam on the full frame or a particular spot of the thin films. The analysis represents the individual weight (%) of the element that is present in the thin films.

4.12.2 XRD Apparatus

The X-ray diffraction (XRD) provides substantial information on the crystal structure. XRD is one of the oldest and effective tools for the determination of the atomic arrangement in a crystal.

Attempts were made to study the structure of the films by X-ray diffraction. X-ray diffractometer system PW3040 X'Pert PRO X-ray Philips Company was used at Magnetic Material Division (MMD) of Atomic Energy Center, Dhaka (AECD). The monochromatic (using Ni filter) CuK_{α} radiation was used and the accelerating potential was 40 KV constituting a current of 30 mA. All the samples were irradiated over 2θ range from 20° to 60° to get possible fundamental peaks of the sample with the sampling pitch of 0.02° and time for each step data collection was 1.0 sec. All the data of the samples were analyzed by using computer software "X'PERT HIGHSCORE" from which structural parameters was determined.

4.13 Apparatus For Electrical Characterization

4.13.1 Lead Attachment to Thin Films

Generally two methods are used to attach lead to thin films, namely solid phase bonding and alloying bonding. The solid phase bonds are formed by thermo compression and ultrasonic means, whereas the alloy bonds are formed by soldering.

Soldering is the simplest and most commonly used process in joining leads to thin films and in the present work indium was used as soldering material to make electrical contact shown in Fig.4.6.

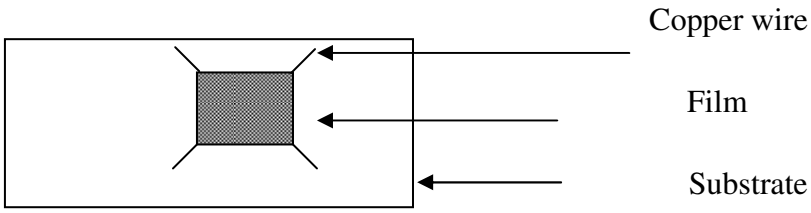

Fig.4.6: Diagram of film with lead attachment.

4.13.2 Measurements of Resistivity and Conductivity

Electrical resistivity and conductivity of $Zn_{1-x}Cu_xO$ thin films may be measured by different methods. In the present work, the resistivity and conductivity of thin films were measured by using Vander Pauws technique shown in Fig.4.7.

Van-der Pauw Method [14] is one of the standard and widely used techniques for the measurement of resistivity of thin film. The Van-der Pauw method is a technique for doing 4-probe resistivity and Hall effect measurements. The advantages of this method include low cost and simplicity. The Van-der Pauw technique can be used on any thin sample of material and the four contacts can be placed anywhere on the perimeter/boundary, provided certain conditions are met:

- The contacts are on the boundary of the sample (or as close to the boundary as possible)
- The contacts are infinitely small (or as close as possible)
- The sample is thin relative to the other dimensions

A brief account of this method is given bellow because in our measurement we have used Van-der Pauw Method.

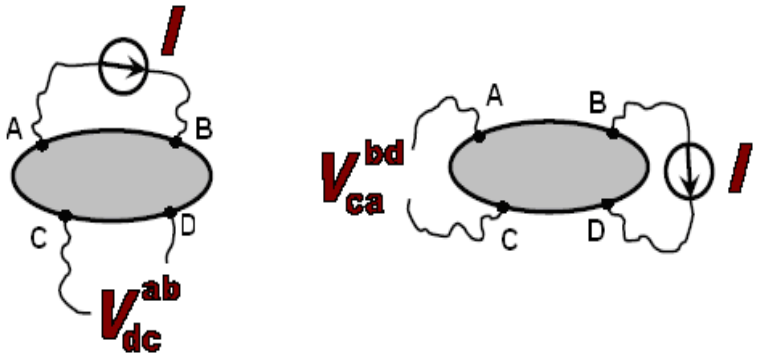

Figure 4.7: Van-der Pauw method for resistivity measurements of a thin film of arbitrary shape

At first we select a region on the sample where four electrical contacts were made at four corners, say A, B, C, and D as shown in figure 4.6. Silver past was used to the contact. The sample should not need to be of the shape as shown in figure. This method is applicable for any arbitrary shape of uniform sheet of material with four contacts applied to the periphery. Through commutative switches the connections are made between the film and the meter terminal.

The resistivity was calculated using equation (4.1) and conductivity by equation (4.2).

$$\rho = 2.265\ t\ (R_{AB,\,CD} + R_{BC,\,DA})\ \text{ohm-cm} \qquad \ldots\ldots\ldots\ldots\ldots\ldots (4.1)$$

$$\sigma = \frac{1}{\rho} \qquad \ldots\ldots\ldots\ldots\ldots\ldots\ldots\ldots (4.2)$$

References:

1. Mochel, J. M., US Patent, Vol. 2, pp 564,707, 1951.
2. Hill, J. E., and Chamberlin, R. R., US Patent, Vol. 3, pp 148,084, 1964.
3. Balkenende, A. R., Bogaerts, A., Scholtz, J. J., Tijburg, R. R. M., and Willems, H. X., Philips Journal of Research, Vol. 50(3–4), pp 365, 1996.
4. Arya, S. P. S., and Hintermann, H. E., Thin Solid Films, Vol. 193(1–2), pp 841, 1990.
5. Chen, C. H., Kelder, E. M., van der Put, P. J. J. M., and Schoonman, J., J. Mater. Chem, Vol.6, pp 765, 1996.
6. R Patil P. S., Kadam L. D., Lokhande C. D.,"Preparation and characterization of spray pyrolysed cobalt oxide thin films" Thin Solid Films, Vol. 272, pp 29-32, 1996.
7. Choudhury C., and Sehgal H. K., "Properties of Spray deposited Cobalt Oxide Selective Coating on Aluminium and Galvanised Iron Substrate" Applied Energy, Vol. 10, pp 313-324, 1982.
8. Jachon J., Varghes M., and Abraham K. E., "Studies on Cu, Fe, and Mn Doped SnO_2 Sem Conducting Transparent Films Prepared by a Vapor Deposition Technique" Chinise Journal of Physics, Vol. 45, No.1, pp 84-97, 2007.
9. Hong N. H., Sakai J., Prellier W., Hassini A., "Transparent Cr-doped SnO_2 thin films ferromagnetism beyond room temperature with a giant magnetic moment" J. Phys. Condens. Matter, Vol. 17, pp 1697–1702, 2005.
10. Korotcenkov G., Macsanov V., Tolstoy V., Brinzari V., Schwank J. and Faglia G., "Structural and gas response characterization of nano-size SnO_2 films deposited by SILD method", Sensors and Actuators B: Chemical, Vol. 96, 3, pp 602-609, 2003.
11. Kadam L. D., Patil P. S., "Thickness-Dependent Properties of Sprayed Cobalt Oxide Thin Films" Materials Chemistry and Physics, Vol. 68, pp 225–232, 2001.
12. Kadam L. D., Pawar S. H., and Patil P.S., "Studies on ionic intercalation properties of cobalt oxide thin films prepared by spray pyrolysis technique" Materials Science Communication, Materials Chemistry and Physics Vol. 68, pp 280–282, 2001.
13. Korotcenkov G., Brinzari V., Boris I., "(Cu, Fe, Co, or Ni)-doped tindioxide films deposited by spray pyrolysis: doping influence on film morphology" J Mater Sci, 43, p. 2761–2770, 2008.
14. van-der Pauw, L. J., Philips Res.Rept., Vol. 13, pp-1, 1958.

CHAPTER- V

RESULTS AND DISCUSSION

5.1 Introduction

The objectives of this study are to synthesis and characterize $Zn_{1-x}Cu_xO$ (x=0.00, 0.05, 0.09, 0.15, 0.20 and 0.25) thin films by spray pyrolysis method. In this chapter the results and discussion of the various experimental studies namely surface morphology, structural, optical and electrical properties of $Zn_{1-x}Cu_xO$ thin films have been presented and discussed step by step.

5.2 Surface morphology and Structural Investigations

5.2.1 SEM Study

Scanning electron microscopy is a convenient technique widely used to obtain the surface morphological information of thin films. Surface morphology of $Zn_{1-x}Cu_xO$ thin films was observed using Scanning electron microscopy (SEM) under 10000 magnification. Fig. 5.1 (a-e) is shown that all the films are found well covered on the glass substrate. SEM micrograph shows that films are uniform and nanofiber structure appear around the nucleation center of the as-deposited ZnO thin film is shown in fig. 5.1 (a). Similar feature was also reported by other researchers [1-2]. Due to interstitial holes of ZnO are filled with copper, most of the fiber has broken and transform into grain in 5% doping concentration fig 5.1 (b). There exist both grain and fiber in the film. But after 5% doping all the fiber has broken and transform into grain fig 5.1 (c). The size of grain decreases with the increase of Cu in 15% doping concentration fig 5.1 (d) [3]. Interestingly at 20% Cu, a combination of large and small grains is observed fig 5.1 (e) [4].

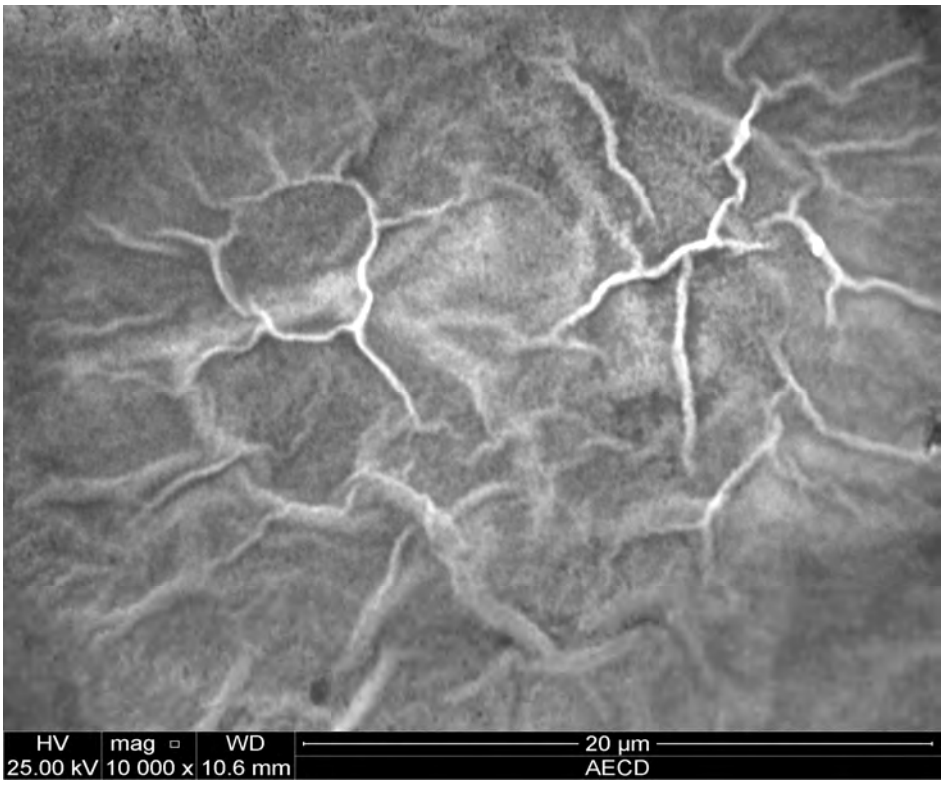

Fig. 5.1a: SEM image (10000 magnification) of pure ZnO thin film

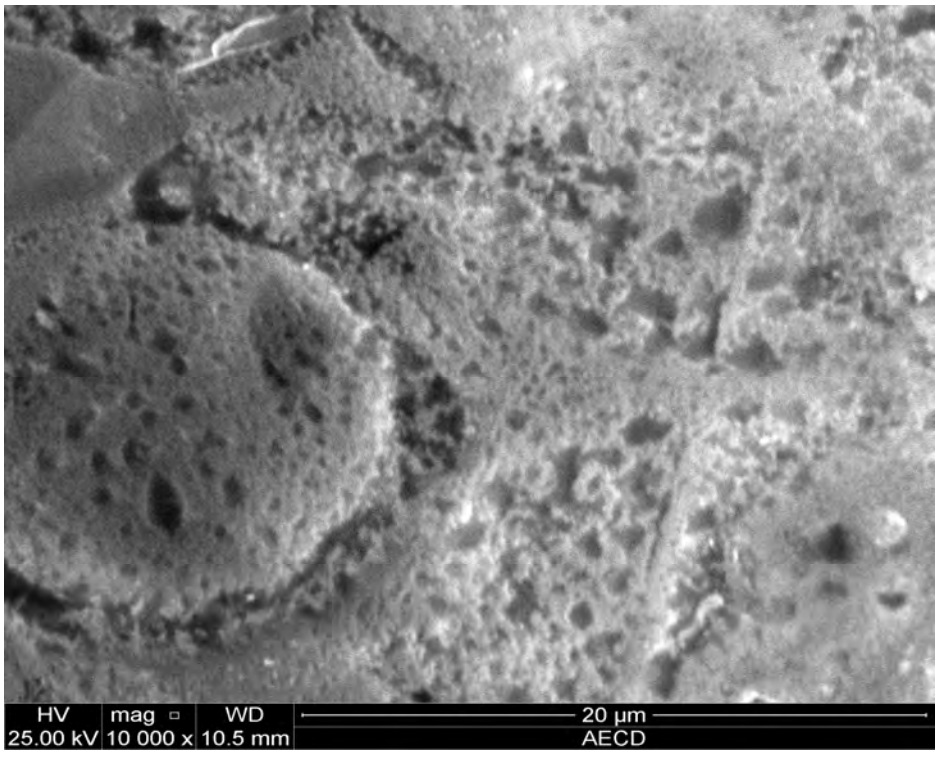

Fig. 5.1b: SEM image (10000 magnification) of 5% Cu doped ZnO thin film

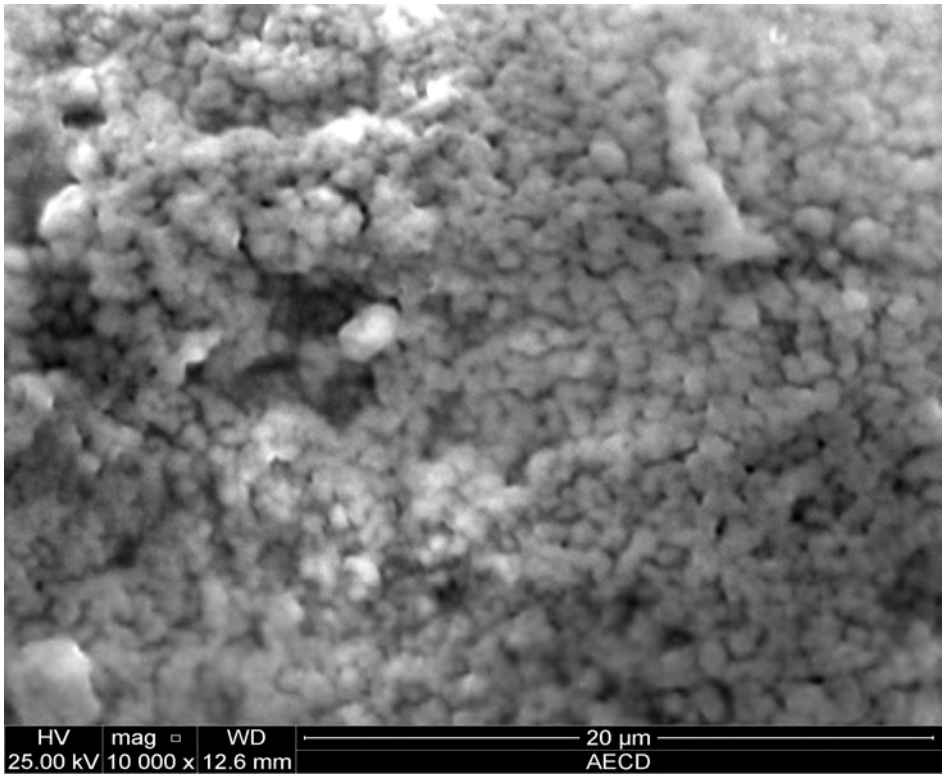

Fig. 5.1c: SEM image (10000 magnification) of 9% Cu doped ZnO thin film

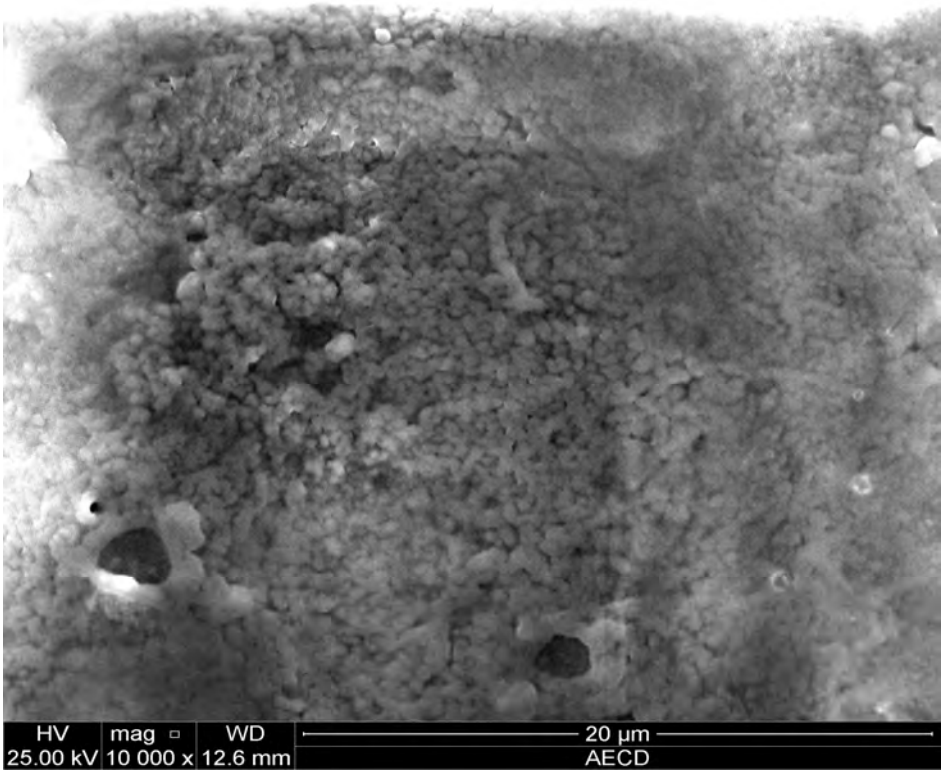

Fig. 5.1d: SEM image (10000 magnification) of 15% Cu doped ZnO thin film

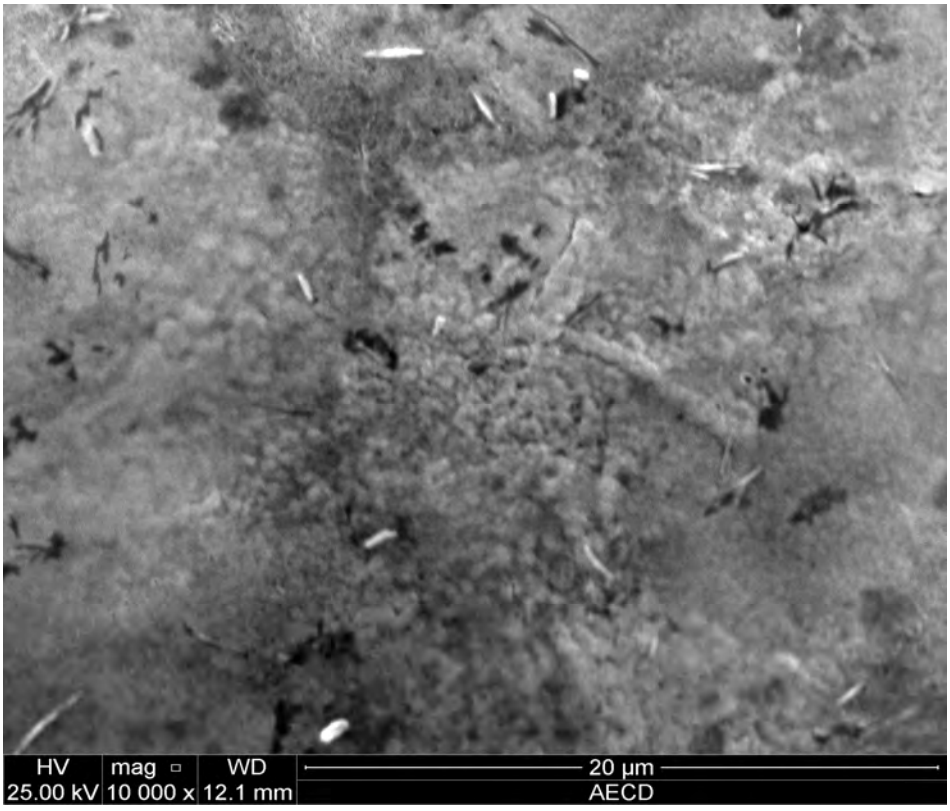

Fig. 5.1e: SEM image (10000 magnification) of 20% Cu doped ZnO thin film

5.2.2 EDX Study

The quantitative analysis of the as-deposited ZnO thin films carried out by EDX is shown in Figure 5.2(a). Two strong peaks corresponding to Zn and O were found in the spectrum, which confirms the high purity of the ZnO thin film. At high operating voltage the electron beam penetrates the film and reaches the glass surface, which results the Si peak. Figure (5.2a, 5.2b, 5.2c & 5.2d) are shown the EDX analysis spectrum for $Zn_{1-x}Cu_xO$ (x=0%, 5%, 15% and 25%) thin films.

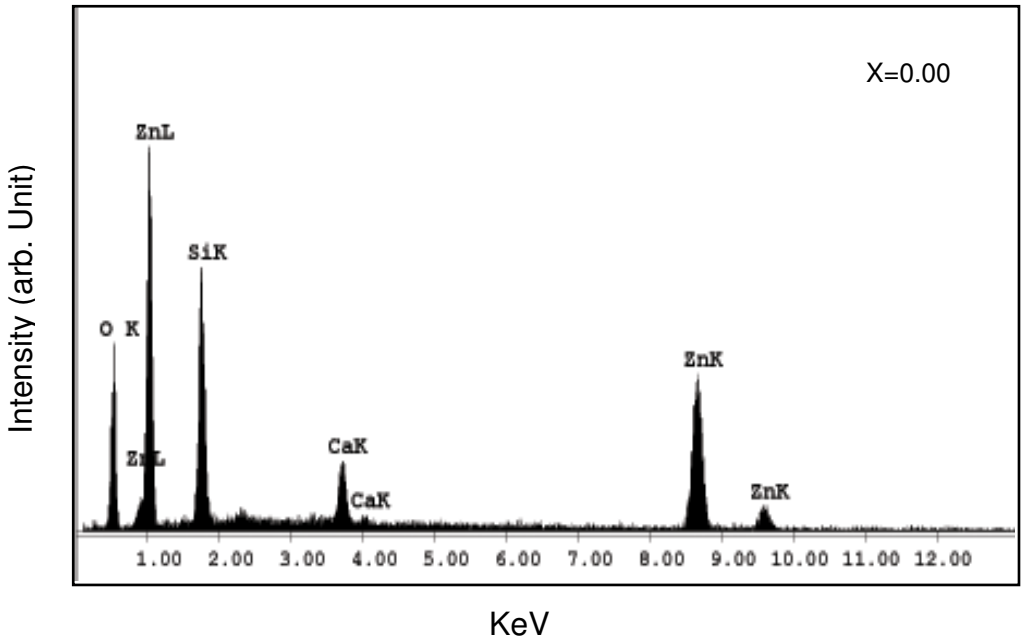

Fig. 5.2(a): EDX spectrum of pure ZnO thin film

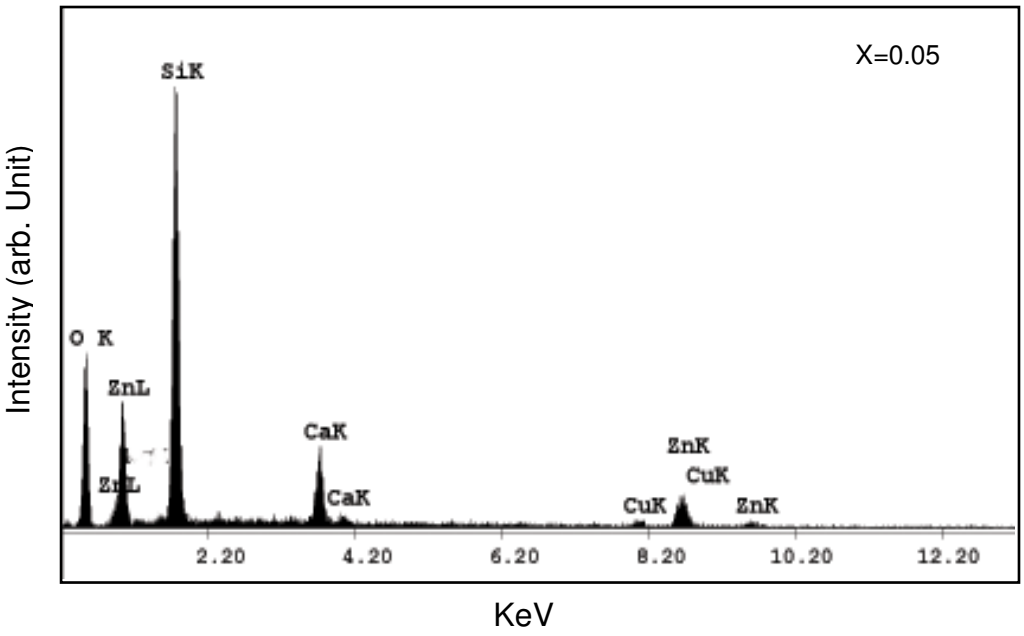

Fig. 5.2(b): EDX spectrum of 5% Cu doped ZnO thin film

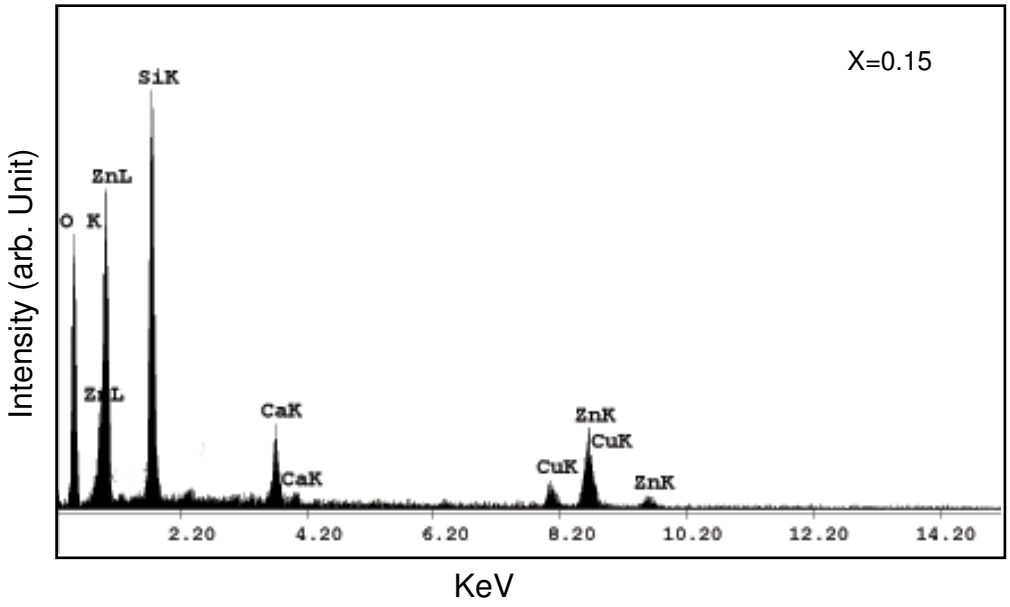

Fig. 5.2(c): EDX spectrum of 15% Cu doped ZnO thin film

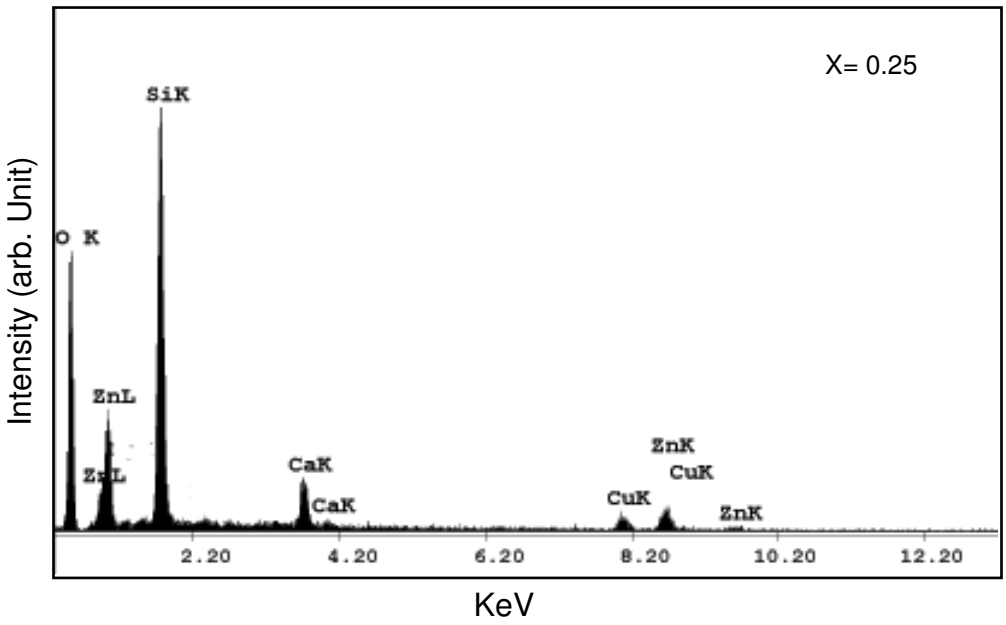

Fig. 5.2(d): EDX spectrum of 25% Cu doped ZnO thin film

Table 5.1: EDX analysis data for $Zn_{1-x}Cu_xO$ thin films.

Concentration (%)	Elements	Wt%	At%
0	Zn	81.68	60.98
	O	6.68	20.37
	Si	8.60	14.95
	Ca	3.04	3.70
5	Zn	46.06	24.58
	Cu	4.74	2.60
	O	15.23	33.20
	Si	27.03	33.58
	Ca	6.94	6.04
15	Zn	59.18	37.19
	Cu	10.20	6.60
	O	11.80	30.28
	Si	15.12	22.14
	Ca	3.70	3.79
25	Zn	37.69	18.50
	Cu	12.32	5.74
	O	21.20	44.52
	Si	23.93	27.34
	Ca	4.86	3.90

The compositional analysis data shows the good controllability of $Zn_{1-x}Cu_xO$ composition thin films by locally made low cost Spray Pyrolysis deposition technique. All peaks for Zn, Cu, and O are obtained for 5%, 15% and 25% doping concentration. From the EDX pattern it is observed that the height of the peak for Zn decreases and Cu increases with the increase of doping concentration. The percent of Zn, Cu and O present in different values of Cu are shown in the table 5.1.

5.2.3 XRD Study

The structural properties of annealed ZnO and Cu-doped ZnO films on glass substrates are investigated by X-ray diffraction patterns. The XRD patterns of the films were taken using CuK_{α} (λ = 1.54178 Å) source. XRD patterns of as-deposited ZnO and Cu doped ZnO films at various concentrations are shown in fig.(5.3) and (5.4). All peaks in this figure could be identified as a ZnO phase with a hexagonal wurtzite crystal structure. From the figures it is observed that the films are polycrystalline nature in all cases. The characteristic peaks were identified at 2θ = 31.69°, 34.33°, 36.17°, 47.49°, 56.55° , 62.80° and , 67.88° having (*hkl*) value (100), (002), (101), (102), (110), (103) and (112) respectively [4].

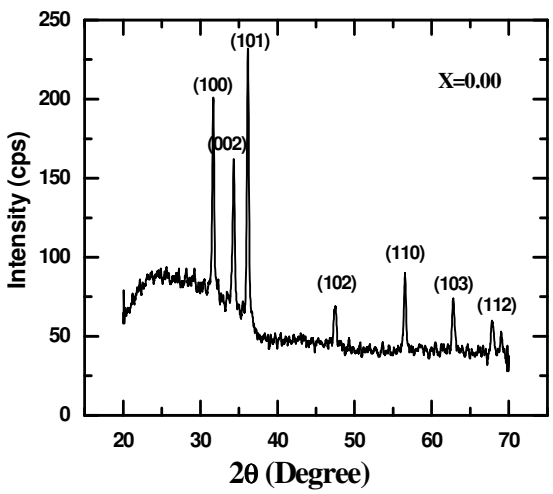

(a)

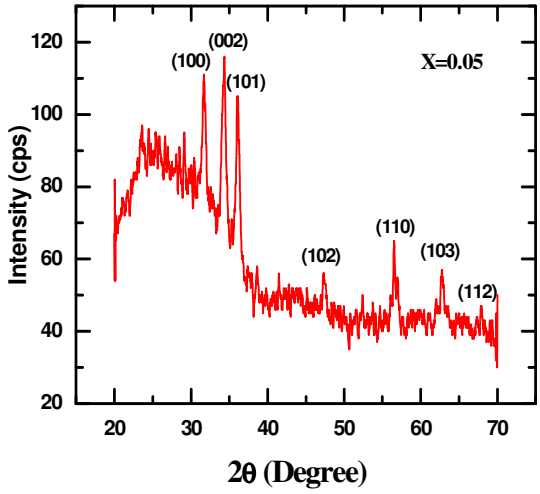

(b)

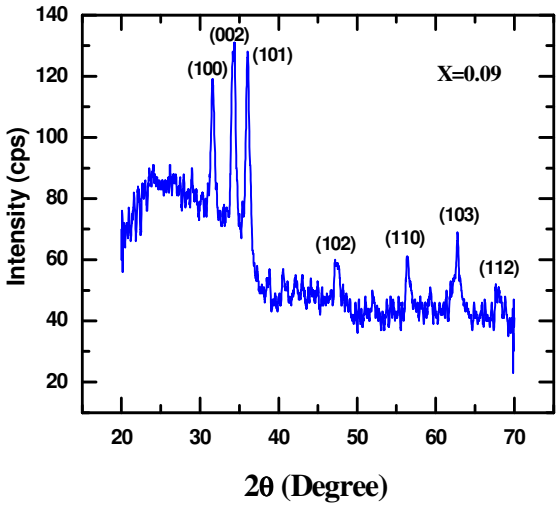

(c)

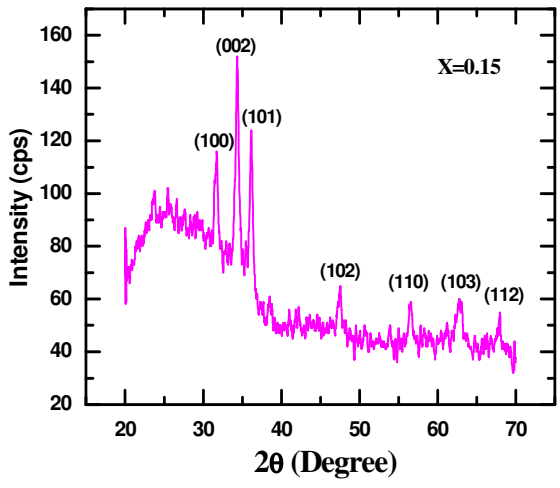

(d)

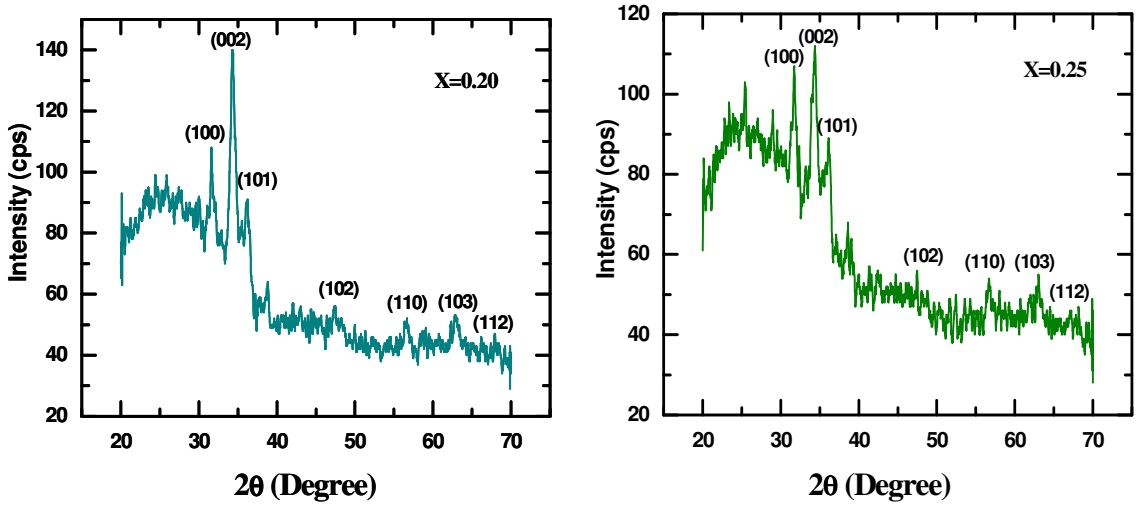

(e) (f)

Fig. 5.3: XRD patterns for as-deposited ZnO and Cu doped ZnO thin films for different Cu concentrations (a) x=0.00, (b) x=0.05, (c) x=0.09, (d) x=0.15, (e) x=0.20 and (f) x=0.25

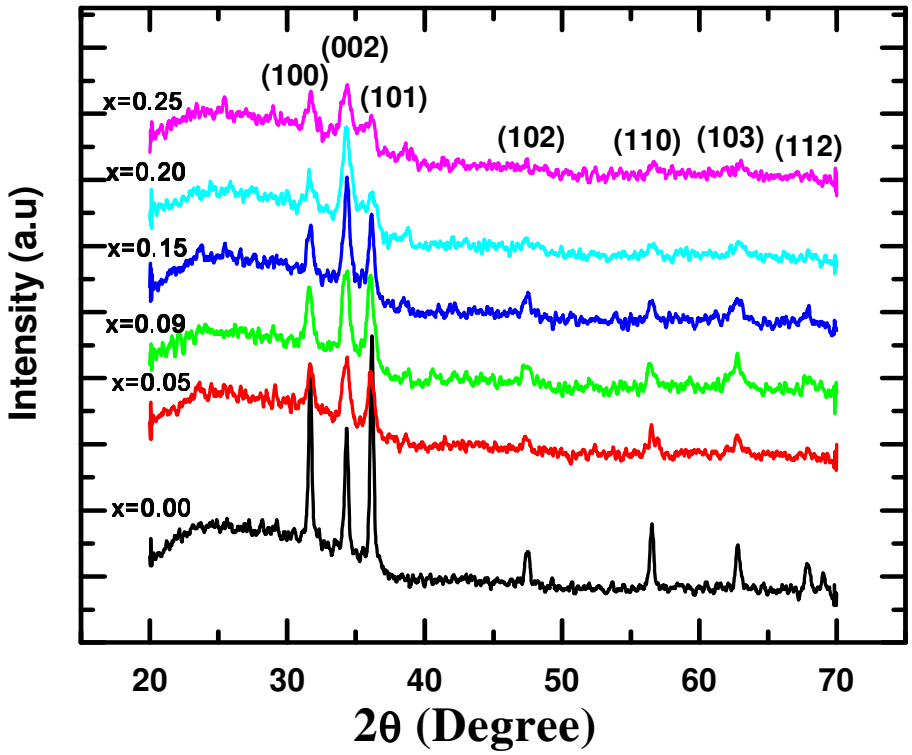

Fig. 5.4: XRD patterns of as-deposited $Zn_{1-x}Cu_xO$ thin films

The intense peaks in the XRD pattern of all samples clearly show the information of the hexagonal wurtzite phase of ZnO having prominent (002) plane in all samples, which is the most stable phase of ZnO. The shift in the (002) peak for higher Cu concentrations might be the substitution of Zn by Cu in the hexagonal lattice.

Crystallite size of the structure was calculated using the following relation [5].

$$D = 0.94\lambda/B\cos\theta \quad \ldots \ldots \ldots \ldots (5.1)$$

Where D is the crystallite size, λ is the wavelength of the X-ray used, θ is the diffraction angle and β is the full width at half maximum (FWHM).

Crystallite sizes of the deposited films have been calculated using (002) plane. The values of crystallite sizes are obtained 7.01 nm for pure ZnO and 3.21 nm, 2.75 nm, 4.82 nm, 3.86 nm and 2.41 nm for ZnO:Cu samples with Cu concentrations 5%, 9%, 15%, 20% and 25%, respectively. The grain size values and lattice parameters with different Cu concentrations are given in the following Table-5.2. Lattice constant slightly vary with doping concentration of Cu but no linear relation with Cu concentration. The shift in the lattice parameter is mainly due to the dopant occupying interstitial positions in the lattice. It is observed that the crystalline size in the doped films does not vary in any regular pattern with Cu dopant concentration, which is attributed to the lattice disorder produced in the films at higher dopant concentration due to difference in the ionic radii of Zn^{2+} amd Cu^{2+} ions and the combination of two different structures, hexagonal and cubic.

Table 5.2: Lattice parameters and grain size of undoped and Cu-doped ZnO thin films deposited on glass substrates.

Zn_{1-x} Cu_xO (X%)	**a (Å)**	**c (Å)**	**c/a ratio**	**Grain size (nm)**
0%	3.2604	5.2244	1.6024	7.01
5%	3.2602	5.2277	1.6035	3.21
9%	3.2678	5.2293	1.6002	2.75
15%	3.2620	5.2210	1.6006	4.82
20%	3.2674	5.2272	1.5998	3.86
25%	3.2611	5.2305	1.6039	2.41

5.3 Optical Properties

5.3.1 Transmission

The optical transmission spectra are shown in fig. 5.5 with wavelength range 300 nm - 1100 nm. The figures show the variation of transmittance with the doping concentration of copper. It is seen that transmittance increases with higher percentage of Cu at UV-VIS region. From the graph it is seen that the values of transmittance is high in the visible and IR region and it is minimum in the UV region. These spectra show high transmittance near about 75%-85% in the wavelength range from 400-1100 nm.

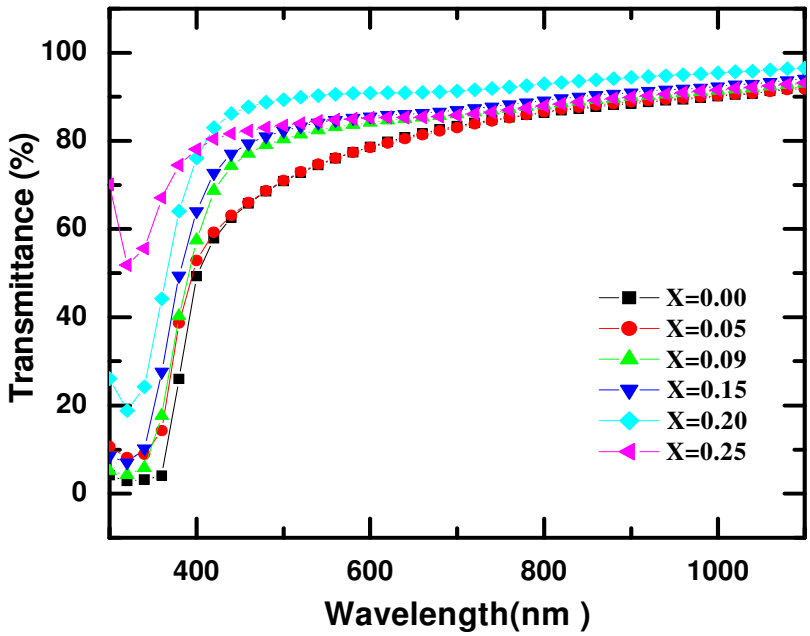

Fig. 5.5: Variation of optical transmittance with wavelength of $Zn_{1-x}Cu_xO$ thin films for different concentrations

5.3.2 Absorbance

The optical absorption spectra are shown in fig. 5.6 with wavelength range 300 nm - 1100 nm. The figures show the variation of absorbance with the doping concentration of copper. From the figure it is seen that the optical absorption decreases with the doping concentration of copper of the $Zn_{1-x}Cu_xO$ thin films [6]. These spectra shows high absorbance in the wavelength range from 300-400 nm.

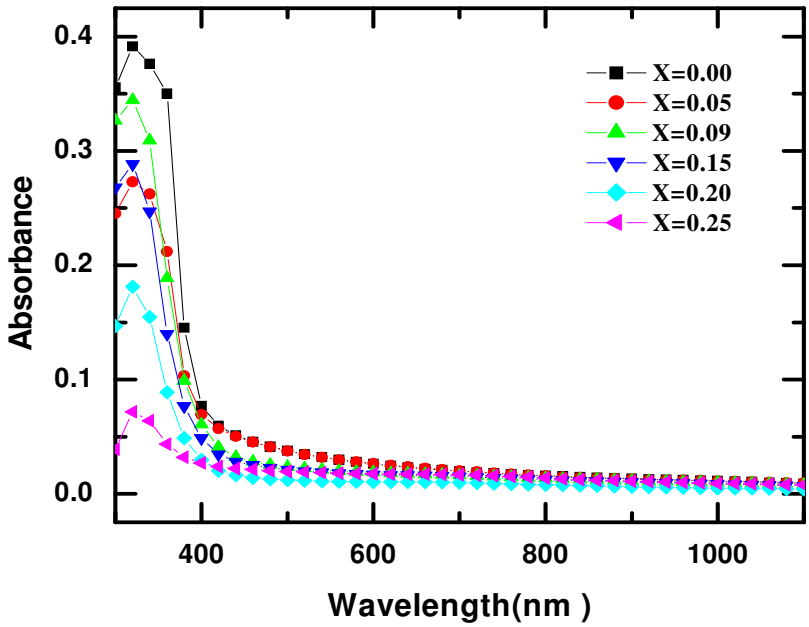

Fig. 5.6: Variation of optical absorbance with wavelength of $Zn_{1-x}Cu_xO$ thin films for different concentrations

5.3.3 Optical band gap

The optical band gap can be determined by analyzing the transmission data using the classical relation [7],

$$\alpha h\nu = A\,(h\nu - E_g)^n \qquad \ldots\ldots \quad \ldots\ldots \quad \ldots\ldots \ldots\ldots \quad (5.2)$$

where, A is a constant, "hν" is the photon energy and "E_g" is the optical band gap of the semiconductor and "n" is index related to the density of states for the energy band and is determined by the nature of optical transition involved in the absorption process.

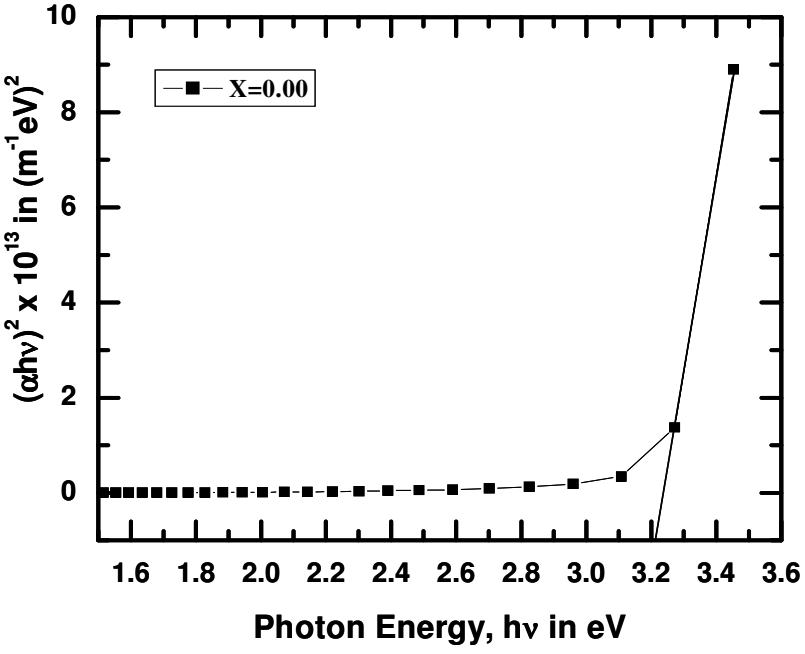

Fig. 5.7: Variation of $(\alpha h\nu)^2$ with photon energy for pure ZnO thin film

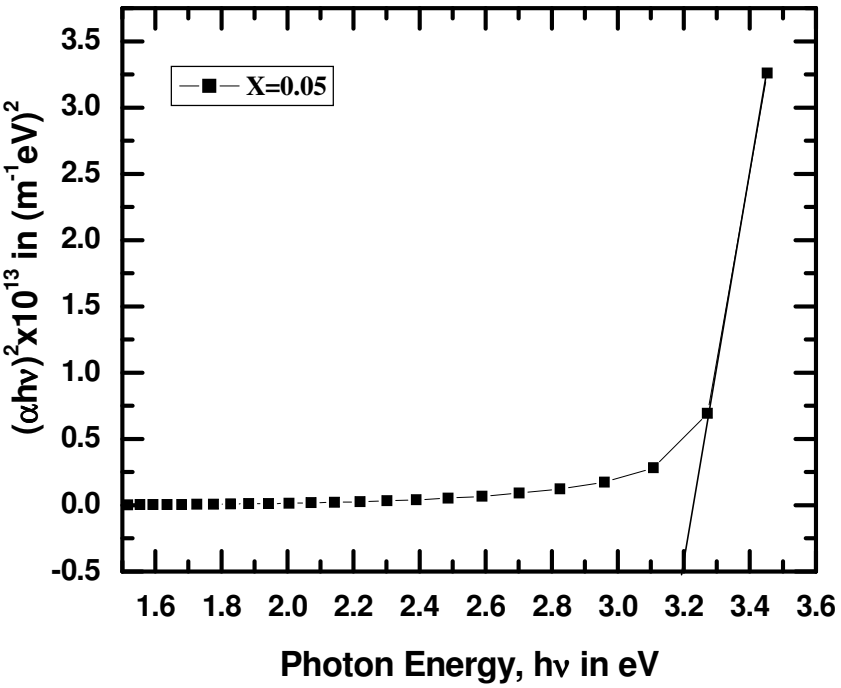

Fig. 5.8: Variation of $(\alpha h\nu)^2$ with photon energy for 5% Cu doped ZnO thin film

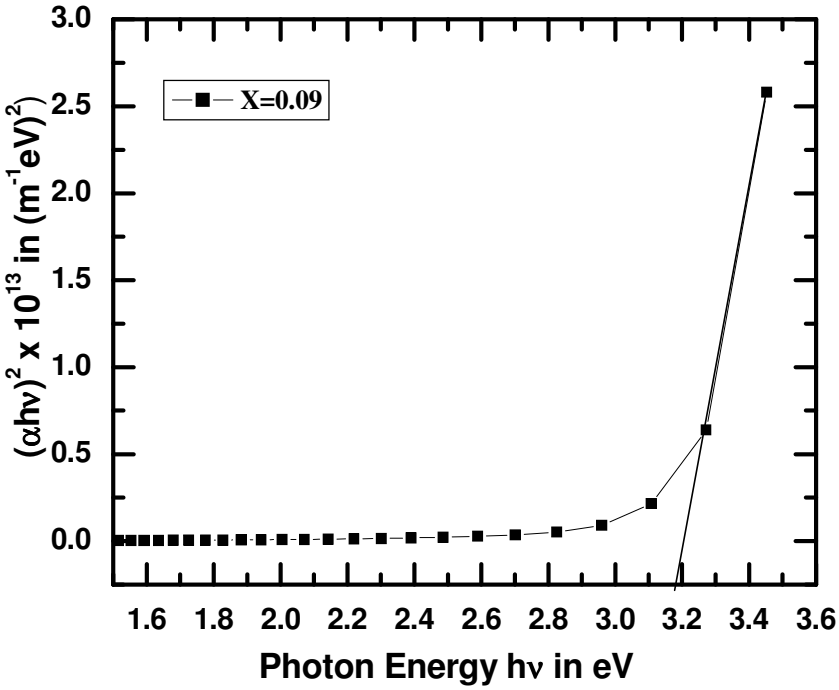

Fig. 5.9: Variation of $(\alpha h\nu)^2$ with photon energy for 9% Cu doped ZnO thin film

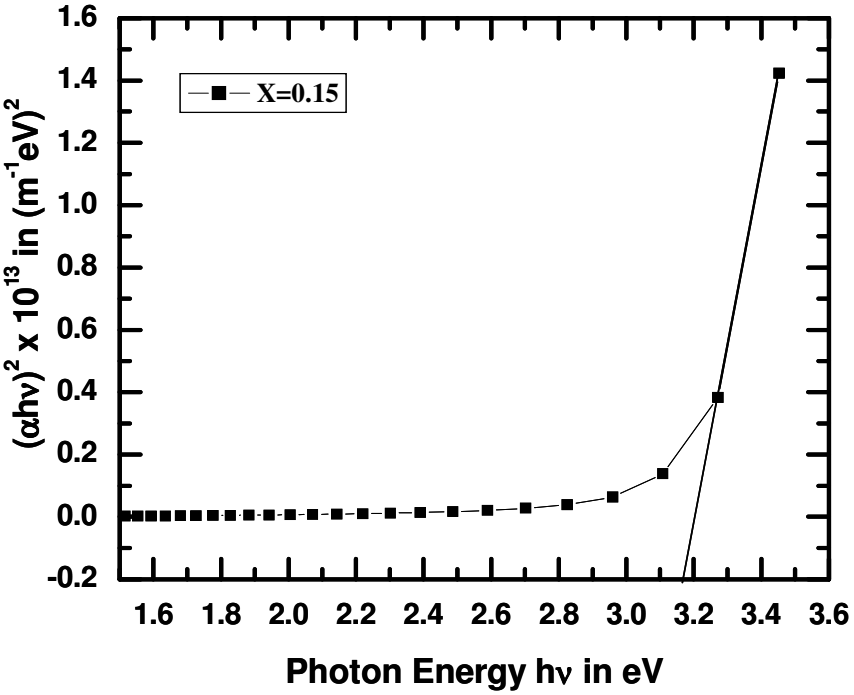

Fig. 5.10: Variation of $(\alpha h\nu)^2$ with photon energy for 15% Cu doped ZnO thin film

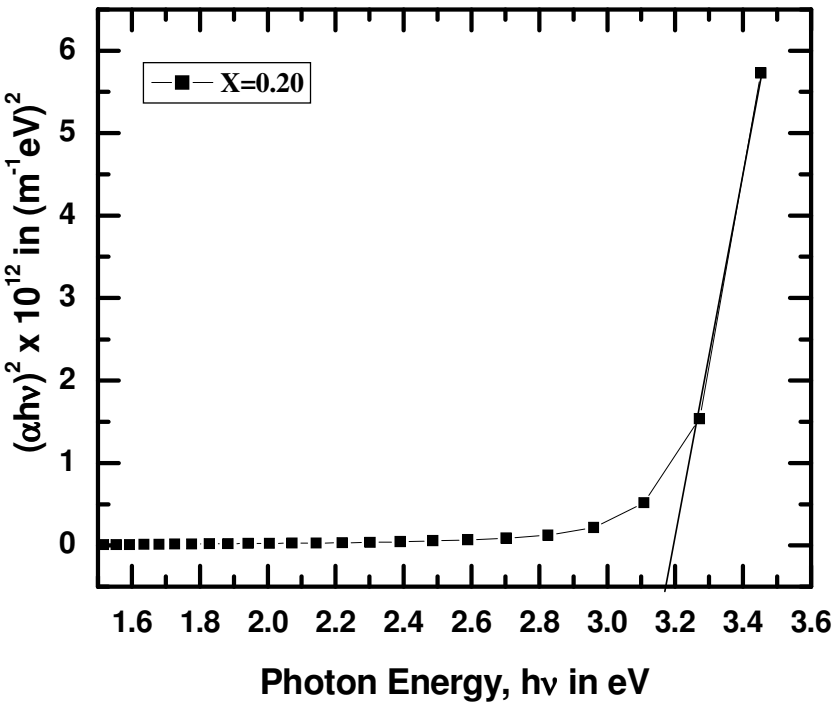

Fig. 5.11: Variation of $(\alpha h\nu)^2$ with photon energy for 20% Cu doped ZnO thin film

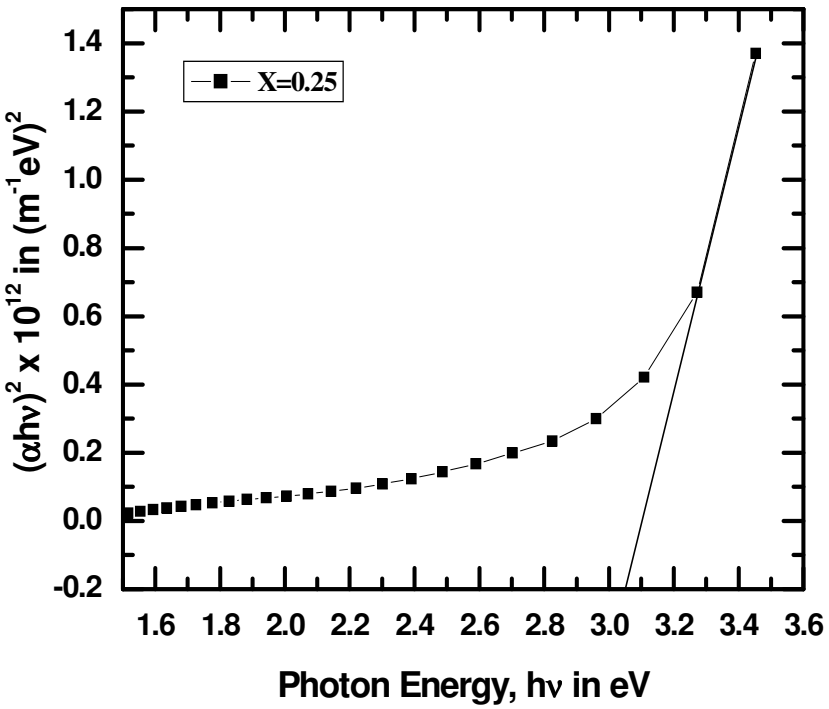

Fig. 5.12: Variation of $(\alpha h\nu)^2$ with photon energy for 25% Cu doped ZnO thin film

For the determination of band gap we have considered the direct (n = 2) transitions. Variation of $(\alpha h\nu)^2$ (direct allowed transition) with hν for different doping concentration of Cu doped ZnO thin films are shown in fig. (5.7) - (5.12). The band gap of the sample were obtained from intercept on energy axis after extrapolation of the straight-line section in the high-energy region of $(\alpha h\nu)^2$ vs. hν curve [8]. For direct transition the observed optical band gap depends on the doping concentration and varies from 3.21 eV to 3.05 eV which is shown in table 5.3. Similar result was also reported by Lee, H. J. et al [9].

Yan et al. [10] have reported that the Cu 3d orbital is much shallower than the Zn 3d orbital. When a Cu atom occupies a Zinc site in ZnO, it introduces two main effects: (1) the strong d-p coupling between Cu and O moves O 2p up, which narrows the direct fundamental band gap and (2) the Cu 3d orbital creates impurity bands above the ZnO valance band. As a result, for heavily doped ZnO:Cu thin films, the optical band gap contains two parts--- one produced by the direct fundamental band gap and the other originated from mixed impurity band gap.

Table 5.3: Variation of band gap of $Zn_{1-x}Cu_xO$ thin films with different doping concentration of Cu.

Sample	Concentration of Cu (%)	Direct band gap E_g in eV
$Zn_{1-x}Cu_xO$	0	3.21
	5	3.20
	9	3.19
	15	3.17
	20	3.16
	25	3.05

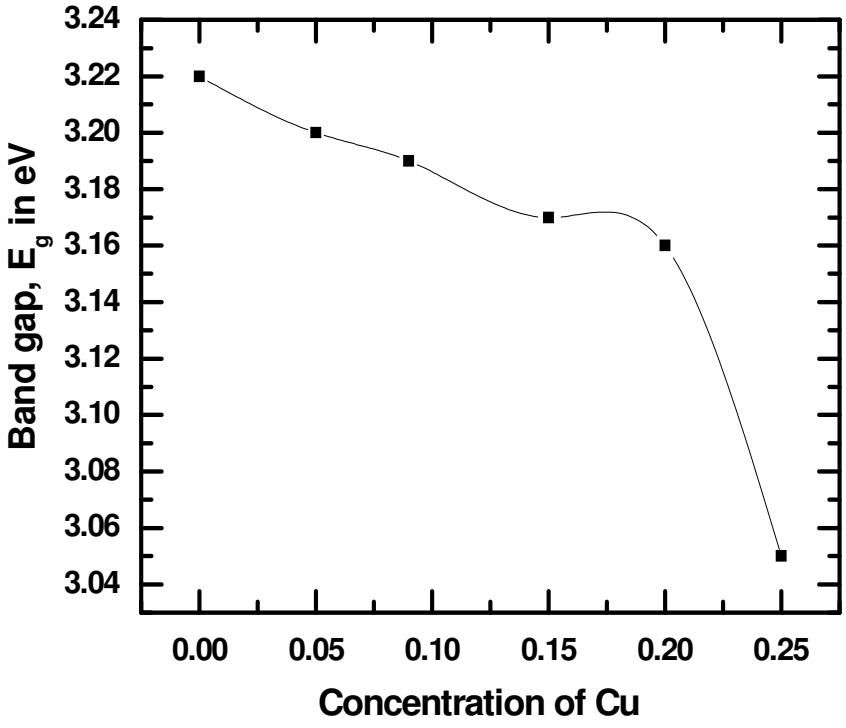

Fig. 5.13: Variation of direct band gap energies with concentration of Cu for $Zn_{1-x}Cu_xO$ thin films

It is observed that small amount of Cu present in the films greatly affects the optical band gap of ZnO. The band gap decreases as the Cu concentration increases. We think that this shift of the band gap with the Cu incorporation interpreted as mainly due to the sp-d exchange interactions between the band electrons and localized d electrons of the Cu^{2+} ions substituting Zn ions. The s-p and p-d exchange interactions give rise to a negative and a positive correction to conduction and valance band edges, leading to narrowing the band gap [11]. The nature of this variation in the band gap energy may be useful to design a suitable window material in fabrication of solar cells. The variation of direct band gap energies with different doping concentration of Cu is shown in fig 5.13.

5.3.4 Refractive index and extinction coefficient

The refractive index and extinction coefficient are determined by computing the transmission and reflection data. The variation of refractive index and extinction coefficient with wavelength for $Zn_{1-x}Cu_xO$ thin films are shown in fig. (5.14) and (5.15). The refractive index of the film significantly changes with the deposition parameter. From fig.(5.14) it is seen that the refractive index decreases with wavelength and also decreases with the doping concentration of Cu.

The refractive index has been calculated using the relation [12]

$$n = \left(\frac{1+R}{1-R}\right) + \sqrt{\left(\frac{4R}{(1-R)^2} - k^2\right)} \qquad \text{…. …. …. ….. (5.3)}$$

Where k is the extinction coefficient and R is the optical reflectance. The refractive index (n) values provide the optical properties of the films. From figure it is clear that n decreases rapidly with increasing wavelength from 400 to 550 nm and after that the value of ‘n’ remains constant. The gradual decrease of refractive index with wavelength implies that the normal dispersion occurred before the absorption edge followed by anomalous dispersion.

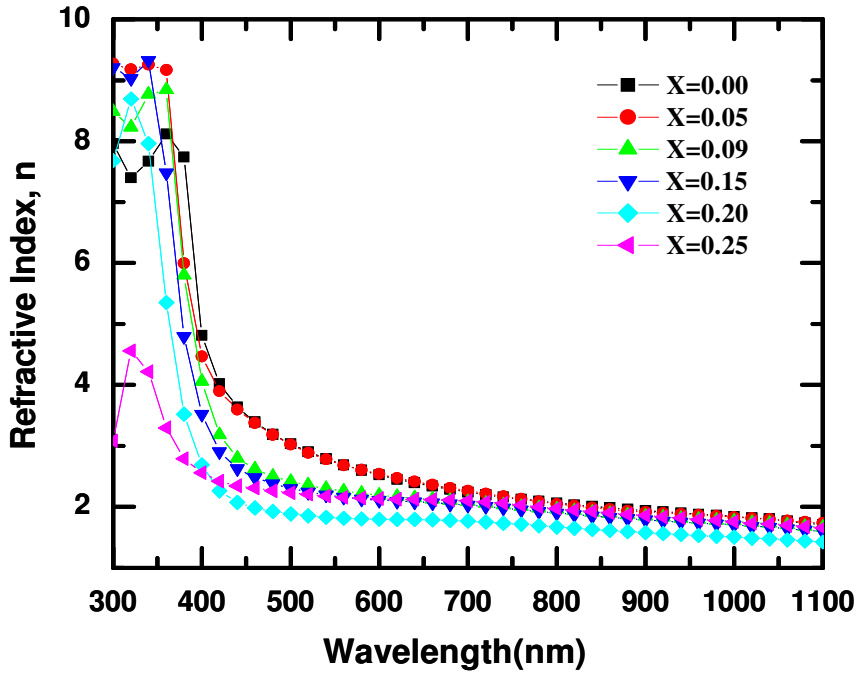

Fig.5.14: Variation of refractive index with wavelength of $Zn_{1-x}Cu_xO$ thin films for different concentrations

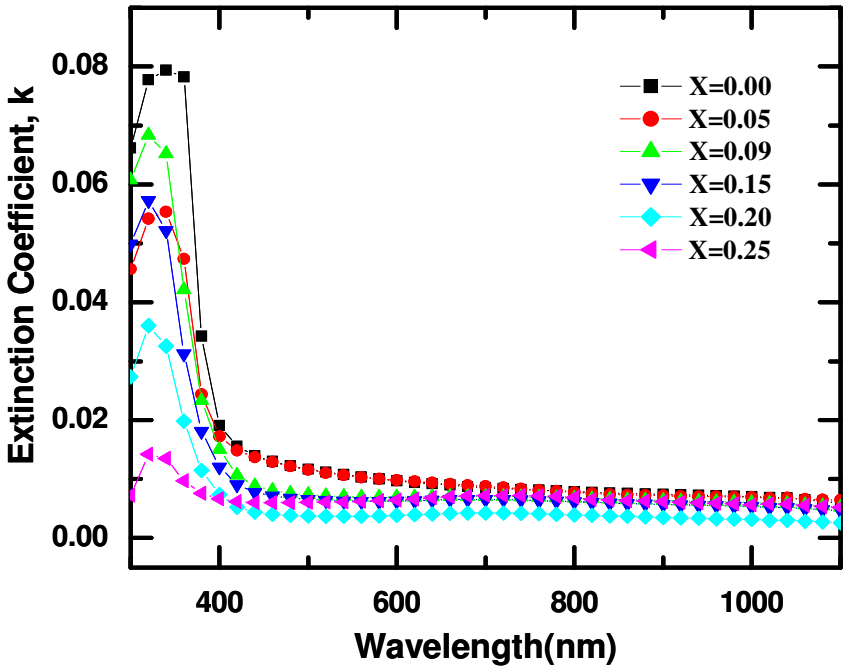

Fig.5.15: Variation of extinction coefficient with wavelength of $Zn_{1-x}Cu_xO$ thin films for different concentrations

From fig.(5.15) it is seen that the extinction coefficient decreases with wavelength and also decreases with the concentration of copper in $Zn_{1-x}Cu_xO$ thin films.

5.3.5 Optical conductivity

Figure (5.16) shows the variation of optical conductivity with photon energy. Optical conductivity of the thin films have been calculated using the equation [13]

$$\sigma = \alpha nc /4\pi \qquad \text{…. ….. ……. ….. (5.4)}$$

where α is the absorption coefficient, n is the refractive index and c is the velocity of light.

Optical conductivity of the $Zn_{1-x}Cu_xO$ thin films decrease with Cu concentration and increases with photon energy. The increased optical conductivity at high photon energies is due to the high absorbance of thin films in that region.

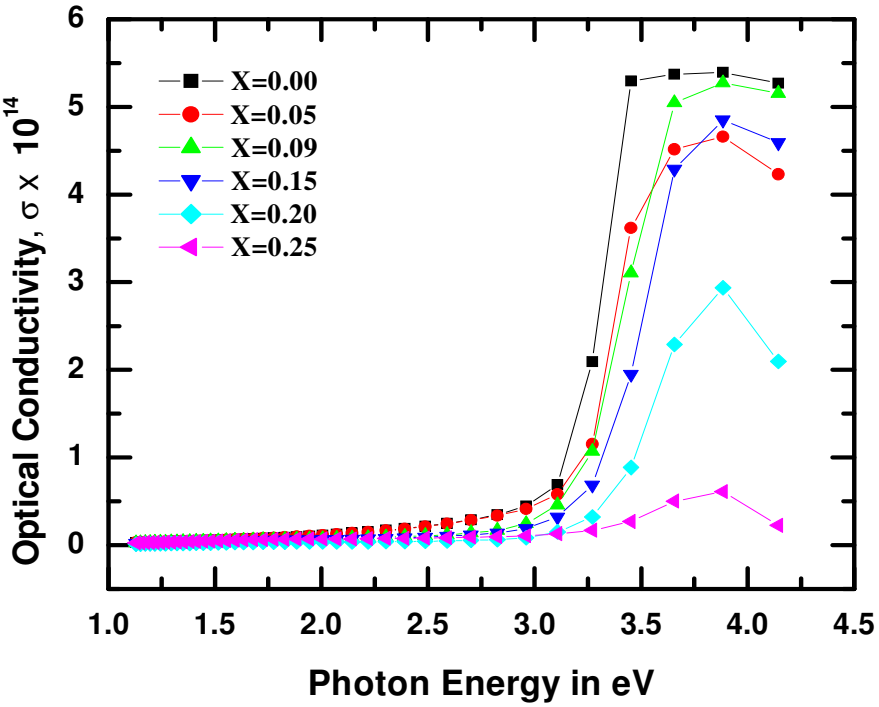

Fig.5.16: Variation of optical conductivity with photon energy of $Zn_{1-x}Cu_xO$ thin films for different concentrations

5.3.6 Dielectric constants

The real ε_r and imaginary ε_i parts of the complex dielectric constant were determined using the formula $\varepsilon_r = n^2 - k^2$ and $\varepsilon_i = 2nk$ [14]. Variation of the real (ε_r) and imaginary (ε_i) parts of the complex dielectric constant for different film thickness illustrate in Figure 5.17 (a, b). The complex dielectric constant is fundamental intrinsic material property. The real part of it is associated with the term that how much it will slow down the speed of light in the material and imaginary part gives that how a dielectric absorb energy from electric field due to dipole motion. The real part ε_r is the normal dielectric constant and imaginary part ε_i represents the absorption associated of radiation by free energy. It is seen that both ε_r and ε_i decrease with increasing wavelength. The figures revealed that the values of the real part are higher than that of the imaginary part and follow the same pattern.

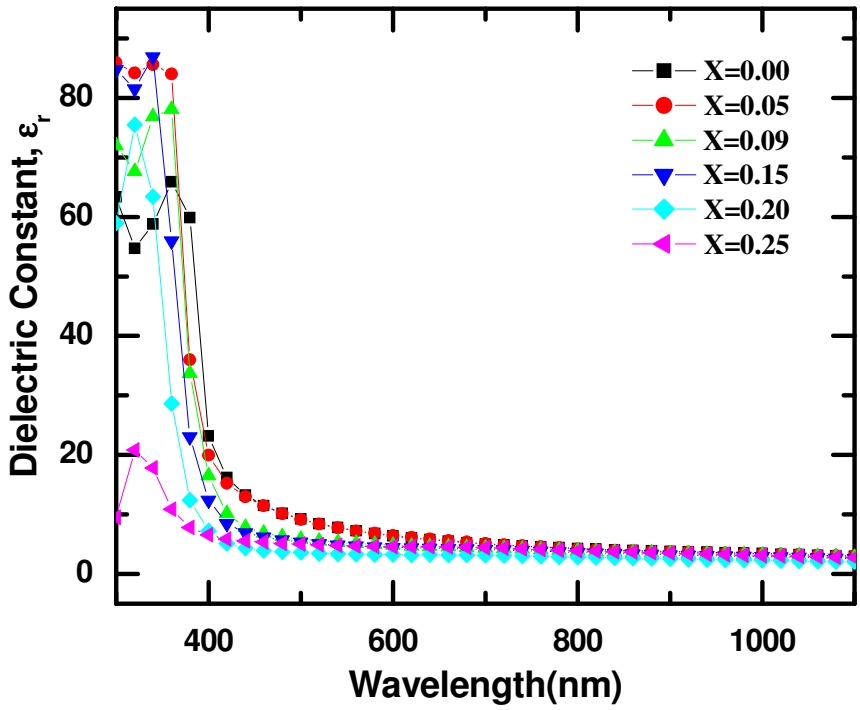

Fig.5.17(a): Variation of real part of dielectric constants with wavelength of $Zn_{1-x}Cu_xO$ thin films for different concentrations

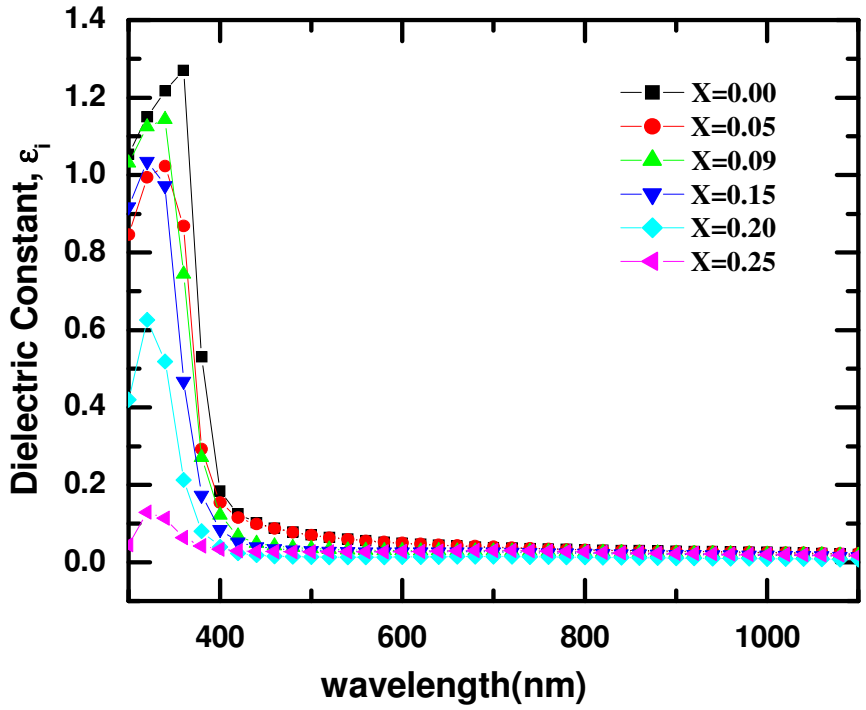

Fig.5.17(b): Variation of imaginary part of dielectric constants with wavelength of $Zn_{1-x}Cu_xO$ thin films for different concentrations

5.4 Electrical Properties

5.4.1 Variation of resistivity with temperature

Resistivity of the prepared ZnO and Cu doped ZnO thin films have been measured by van-der Pauw method [15]. The resistivity measurement has been performed over a range from room temperature to 440 K. During the measurement, the temperature increased slowly as a result the whole film is heated with uniform temperature. The variation of resistivity with temperature for films is shown in fig. (5.18). The figure shows that the resistivity gradually decreases with the increase of temperature, which indicates the semiconducting nature of the materials. Figure (5.18) also shows that the resistivity increases with the increase of Cu concentration [9]. The electrical resistivity of ZnO was increased by doping Cu indicating the acceptor like behavior of the Cu dopant. The four co-ordinated Zn, Cu and Cu cations have ionic radii of 0.06, 0.06 and 0.057 nm respectively, with stable electronic configuration, Zn^{2+} ($3d^{10}$), Cu^{2+} ($3d^{9}$) and Cu^{+} ($3d^{10}$). Diffusion at high firing temperature may lead defect reactions in which Cu^{2+} cations substitute Zn^{2+} cations in the wurtzite unit cell of ZnO. The stability of the coulomb forces of the interactions between the acceptor defect (Cu^{1+} Zn) and intrinsic ZnO donors may occur by capture of an electron from the lattice.

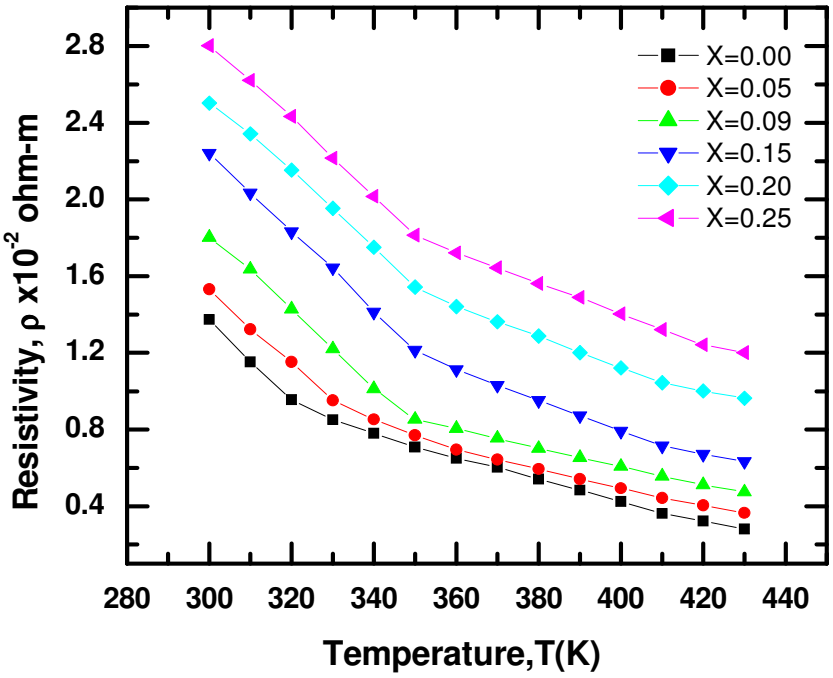

Fig.5.18: Variation of electrical resistivity with temperature for as deposited $Zn_{1-x}Cu_xO$ thin films

5.4.2 Variation of conductivity with temperature

The variations of electrical conductivity with temperature for as deposited $Zn_{1-x}Cu_xO$ thin films are shown in fig.(5.19). From the figure it is seen that the conductivity increases with the increase of temperature. This type of variation indicates the semiconducting behavior of the films. The conductivity decreases with the increasing of Cu concentration [9]. Incorporation of Cu into ZnO reduces its conductivity as Cu introduces deep acceptor level and it traps electrons from the conduction band.

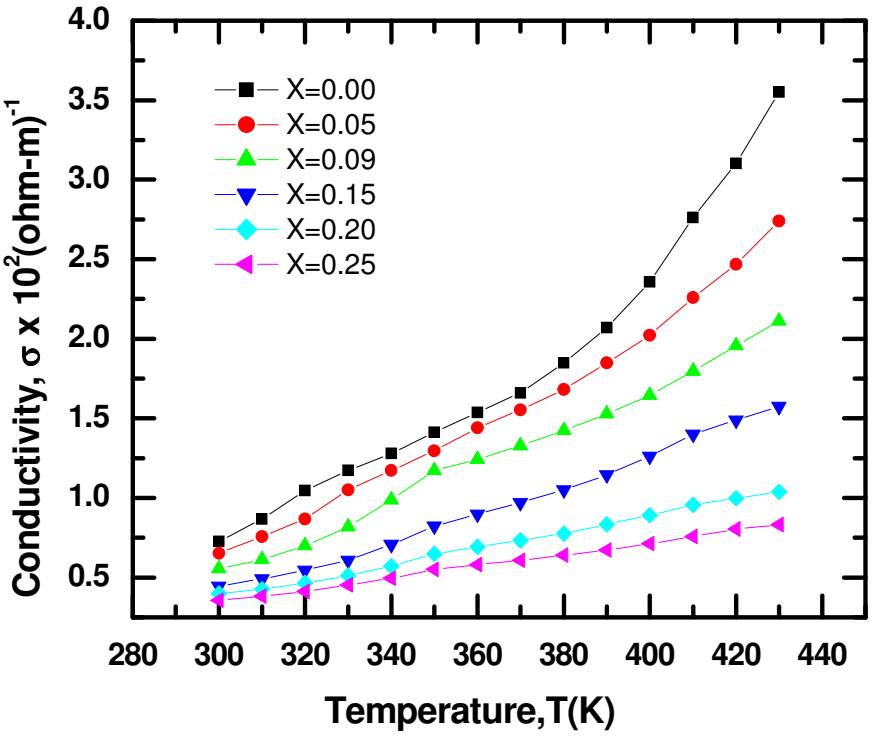

Fig.5.19: Variation of electrical conductivity with temperature for as deposited $Zn_{1-x}Cu_xO$ thin films

5.4.3 Activation Energy Measurement

The variation of lnσ with inverse temperature of $Zn_{1-x}Cu_xO$ thin films is shown in fig. (5.20). The activation energy may be obtained by the relation

$$\sigma = \sigma_o \exp\left(\frac{-\Delta E}{2kT}\right) \qquad \ldots\ldots\ldots\ldots\ldots\ldots (5.5)$$

Where ΔE is the activation energy, k is the Boltzmann constant and σ_o is the pre-exponential factor.

Eq. (5.5) can be written as,

$$\ln \sigma = \left(\frac{-\Delta E}{2kT}\right) + \ln\sigma_o \qquad \ldots\ldots\ldots\ldots\ldots\ldots (5.6)$$

Equation (5.6) is equivalent to straight line equation, y = mx+ c.

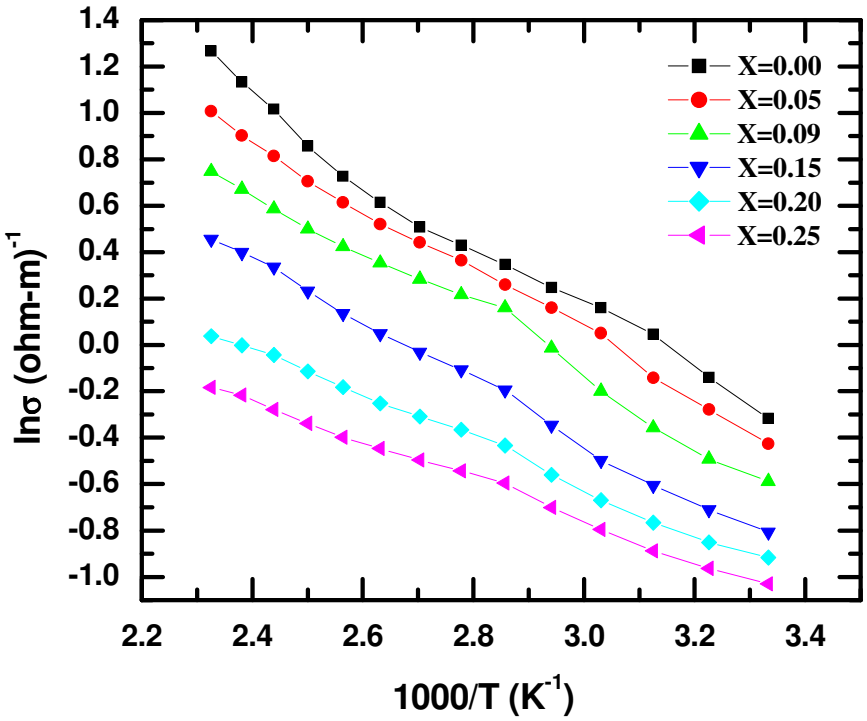

Fig.5.20: Variation of lnσ with 1/T for for as deposited $Zn_{1-x}Cu_xO$ thin films

From the slope of lnσ vs 1/T plot, the activation energy in the high temperature region was calculated. Following this relation the activation energy of the films were calculated from the slope of the plots [16].

Therefore the activation energy ΔE is given by

$$\Delta E = -\frac{\ln \sigma}{1/T} 2k \qquad \ldots\ldots \ldots\ldots \ldots\ldots \ldots\ldots \quad (5.7)$$

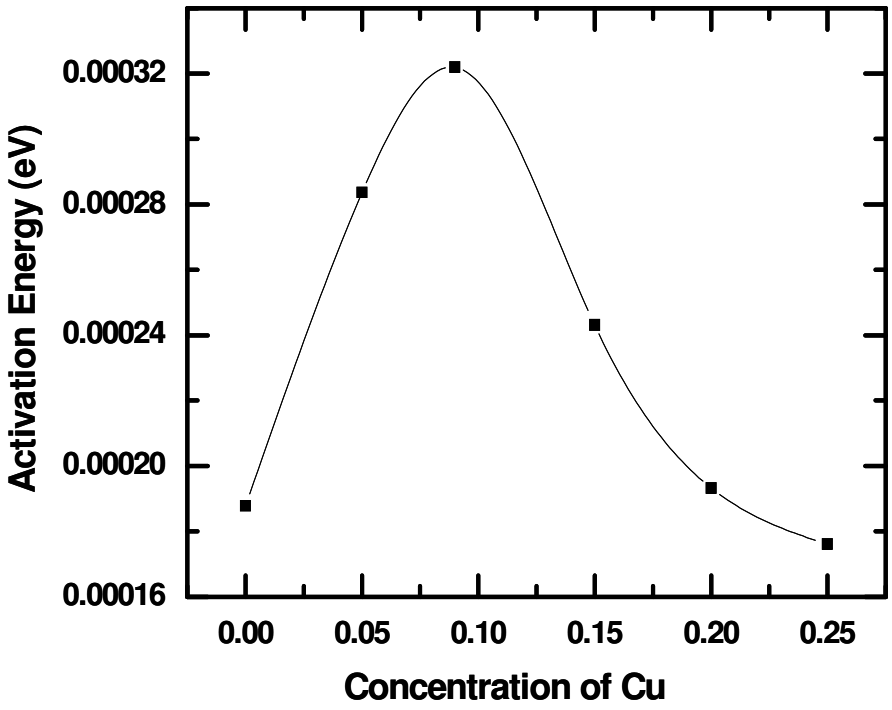

Fig.5.21: Variation of activation energy of Cu doped ZnO thin films

Figure 5.21 represents the variation of activation energy of different concentration for the as-deposited thin films. It is seen from the graph that the activation energy is increasing up to 9% and then it decreases with the higher percentage of copper concentration.

References

1. Islam, M. R., and Podder, J., "Optical Properties Of ZnO nano fiber thin films grows by spray pyrolysis of zince acetate precursor" Cryst. Res.Techno.Vol. 44, No.3, pp 286-292, 2009.

2. Llicana, S., Caglara, M., and Yakuphanoglu, F., "Electrical Conductivity, Optical and Structural Properties of Indium-doped ZnO nanofiber Thin Film Deposited by Spray Pyrolysis Method", Physica E., Vol-35, N0. 131, 2006.

3. Das, K., Ray, S., Chaudhuri, S. and Maity, A. B., "Structural and Luminescence Properties of Sol-gel Derived Cu doped ZnO flims", Indian Journal of Pure and Applied Physics, V-47, pp 377-382, 2009.

4. Rahmani, M. B., Keshmiri, S. H., Shafiei1, M., Latham, K., Wlodarski1, W., Plessis, J.and Zadeh, K. K., "Transition from n- to p-Type of Spray Pyrolysis Deposited Cu Doped ZnO Thin Films for NO_2 Sensing", American Scientific Publishers, Sensor Letters, Vol-7, pp 1–8, 2009.

5. Kang S. J., Joung Y. H., Shin H. H., Yoon Y. S., "Effect of substrate temperature on structural, optical and electrical properties of ZnO thin films deposited by pulsed laser deposition" J Mater Sci: Mater Electron, Vol. 1, P. 1073–1078, 2008.

6. Long, Z., Fei, L. P., Yuan, Y. Z., Min, L. Y., Lin, W. D. and Han, Y., "First-principles Study of Electronic and Optical Properties in Wurtzite $Zn_{1-x}Cu_xO$", Chin. Phys. B, Vol-19, No. 5, pp 56104, 2010.

7. Chauhan, Kumar A., and Chaudhary R. P., "Structure And Optical Properties of $Zn_{1-X}Ni_xo$ Nanoparticles By Coprecipitation Methodruby" Journal of Optoelectronics and Biomedical Materials Vol. 3, Issue 1, P. 17-23 , 2011.

8. Maiti U. N., Ghosh P. K., Ahmed S. F., Mitra M. K., and Chattopadhyay K. K., "Structural, optical and photoelectron spectroscopic studies of nano/micro ZnO:Cd rods synthesized via sol-gel route" J Sol-Gel Sci Techn, Vol. 41, P. 87–92, 2007.

9. Lee, H. J., Kim, B. S., Cho, C. R., and Jeong, S. Y., "A Study of Magnetic and Optical Properties of Cu doped ZnO", Phys. Stat. Sol., Vol-241, No. 7, pp 1533-1536, 2004.

10. Ahn, K. S., Deutsch, T., Yan, Y., Jiang, C. S., Perkins, C. L., Turner, J., and Al-Jassim, M., J. Appl. Phys., Vol-6, pp 102/2, 2007.

11. Furdyna, J. K., "Diluted Magnetic Semiconductors", Appl. Phys., Vol-64, No. 4, 1988.

12. Buba A. D. A., and Adelabu J. S. A., "Optical and Electrical Properties of Chemically Deposited ZnO Thin Films". The Pacific Journal of Science and Technology, Vol. 11, Num. 2, 2010.

13. Sharm, P., Sharma, V., and Katyal, S. C., "Variation of Optical Constant in GE10SE60TE30 Thin Film", Chalcogenide Lett, Vol-3, No. 10, pp 73-79, 2006.

14. Okoli, D. N., Ekpunobi, A. J., and Okeke, C. E., "Growth and Characterization of ZnCdS Thin Films by Chemical Bath Deposition Technique", Academic Open Internet Journal, Vol-18, pp 1-12, 2006.

15. Van-der Pauw, L. J., Philips Res. Rept., Vol-13, pp-1, 1958.

16. Tewari S., and Bhattacharjee A., "Structural, Electrical and Optical studies on Spray-deposited Aluminium-doped ZnO Thin films", Pramana – J. Phys., Vol. 76, No. 1, pp 153–163, 2011.

CHAPTER- VI

CONCLUSIONS AND SUGGESTIONS FOR FUTURE WORK

6.1 Conclusions

In the present work, Zinc oxide and Cu-doped ZnO thin films were prepared by spray pyrolysis method. Films of different doping concentration of Cu were deposited on glass substrate keeping the substrate temperature at 350^0C. Different physical properties such as structural, optical and electrical properties have been studied. The results of the present work are summarized and the following noteworthy conclusions as follows:

1. Spray pyrolysis is a suitable and noble technique for the production of good quality ZnO thin films. The substrate temperature is the most important parameter that should be controlled when spraying. Before spraying, the temperature distribution contributes to the non-uniformity of deposition on the substrate. The structural, optical and electrical property of ZnO thin films depend on the concentration of the dopant, which are optimized in the present work.

2. The thickness of the as-deposited films was estimated by Fizeau fringes interference method which varied from 195 to 198 nm.

3. Surface morphology of $Zn_{1-x}Cu_xO$ thin films was observed using SEM. SEM micrograph shows that all the films are found well covered on the glass substrate and sprayed particles (atoms) are absorbed onto glass substrate. Nanofibers are observed in the pure ZnO thin film. Due to interstitial holes of ZnO are filled with copper, most of the fiber has broken and transform into grain in 5% doping concentration. There exist both grain and fiber in the film. But after 5% doping all the fiber has broken and transform into grain. The size of grain decreases with the increase of Cu in 15% doping concentration. Interestingly at 20% Cu, a combination of large and small grains is observed.

4. X-ray diffraction studies show that as-deposited films are amorphous with crystalline nature. The characteristic peaks were identified at 2θ = 31.69^{o}, 34.33^{o}, 36.17^{o}, 47.49^{0}, 56.55^{0} , 62.80^{0} and , 67.88^{0} having (*hkl*) value (100), (002), (101), (102), (110), (103) and (112) respectively. The intense peaks in the XRD pattern of samples clearly show the formation of the hexagonal wurtzite phase of ZnO having prominent (002) plane in all samples, which is the most stable phase of ZnO. It was also observed that with increasing the concentration of Cu, the intensity of the ZnO peaks decreased and hence the crystallinity of ZnO decreased. The shift in the (002) peak for higher Cu concentrations might be due to the substitution of Zn by Cu in the hexagonal lattice. The values of crystallite sizes are obtained 7.01 nm for pure ZnO and 3.21 nm, 2.75 nm, 4.82 nm, 3.86 nm and 2.41 nm for ZnO:Cu samples with Cu concentrations 5%, 9%, 15%, 20% and 25%, respectively. The shifting in the lattice parameter values is mainly due to the Cu dopant occupying at the interstitial positions in the lattice.

5. Various optical constants such as absorbance, transmittance, refractive index and dielectric constant of the films have been studied for the as-deposited films are recorded in the wavelength ranges from 300 to 1100 nm. Absorbance decreases with higher percentage of Cu concentration. These spectra show high absorbance in the wavelength range from 300-400 nm. The values of transmittance is high in the visible and IR region and it is minimum in the UV region. These spectra show high transmittance near about 75%-85% in the wavelength range from 400-1100 nm. The band gap of the films varied 3.21 to 3.05 eV. The increase in the Cu incorporation in the film results in the overall decrease in the refractive index. The gradual decrease of refractive index with wavelength i.e. increase with photon energy implies that the normal dispersion occurred before the absorption edge followed by anomalous dispersion.

6. The electrical resistivity measurements were made on number of films from the room temperature up to 430K. The figure shows that the resistivity gradually decreases with the increase of temperature, which indicates the semiconducting nature of the materials. Resistivity also increases with the increasing doping concentration. The conductivity decreases with the increasing of Cu concentration. Incorporation of Cu into ZnO reduces its conductivity as Cu

introduces deep acceptor level and it traps electrons from the conduction band. The activation energy is increasing up to 9% and then it decreases with the higher percentage of copper concentration.

In this study, the results obtained from optical, electrical and structural measurements are found to be in good agreement with the results obtained by previous worker on this material.

6.2 Suggestions for Future Work

This is the first time that transition metal such as Cu doped ZnO thin films have been prepared in our laboratory. We have deposited ZnO and Cu doped ZnO thin films on glass substrate at 350^0C substrate temperature and studied some of their structural, electrical and optical properties. To prepare high quality films and for their details characterization more studies are necessary. Hence to get better performance from the as deposited pure and Cu doped ZnO thin films by spray pyrolysis technique, the following research work may be extended:

i) Study the magnetic properties.

ii) Measurements of Hall effect.

iii) Study of electrical properties at low temperature.

APPENDIX

Table. 1: Variation of absorbance as a function of wavelength for $Zn_{1-x}Cu_xO$ film for different concentrations.

wavelength	x=0.00	x=0.05	x=0.09	x=0.15	x=0.20	x=0.25
1100	0.008722	0.009424	0.007719	0.006817	0.003784	0.007619
1080	0.009273	0.009674	0.008145	0.007193	0.004035	0.008045
1060	0.00985	0.010075	0.008596	0.007569	0.004311	0.008421
1040	0.010551	0.010551	0.009098	0.00802	0.004612	0.008872
1020	0.010852	0.010727	0.009298	0.008195	0.004737	0.009123
1000	0.011328	0.011178	0.009724	0.008622	0.005038	0.009123
980	0.011679	0.011479	0.010075	0.008897	0.005288	0.009524
960	0.012055	0.011805	0.010401	0.009248	0.005514	0.009875
940	0.012456	0.012105	0.010702	0.009524	0.005739	0.010251
920	0.012857	0.012456	0.011053	0.00985	0.006015	0.010677
900	0.013283	0.012857	0.011404	0.010226	0.006266	0.011053
880	0.013684	0.013258	0.011805	0.010576	0.006566	0.011479
860	0.014185	0.013709	0.012206	0.011003	0.006892	0.01188
840	0.014687	0.014236	0.012632	0.011404	0.007193	0.012356
820	0.015213	0.014862	0.013083	0.01193	0.007569	0.012857
800	0.015815	0.015614	0.013609	0.012381	0.007895	0.01391
780	0.016491	0.016391	0.014135	0.012932	0.008346	0.014536
760	0.017168	0.017243	0.014687	0.013484	0.008747	0.015113
740	0.01792	0.01817	0.015213	0.014085	0.009123	0.015664
720	0.018797	0.019123	0.015714	0.014662	0.009449	0.016165
700	0.019724	0.020125	0.016241	0.015113	0.009749	0.016642
680	0.020702	0.021153	0.016717	0.015539	0.01	0.016892
660	0.021905	0.022306	0.017193	0.01594	0.010175	0.017093
640	0.023133	0.023559	0.017619	0.016241	0.010251	0.017193
620	0.024486	0.024837	0.017995	0.016491	0.010251	0.017218
600	0.026065	0.026316	0.018622	0.016892	0.010351	0.017368
580	0.02782	0.02782	0.019248	0.017318	0.010451	0.017594
560	0.029774	0.029624	0.02	0.01792	0.010652	0.01787
540	0.032105	0.031754	0.021028	0.018747	0.010977	0.018346
520	0.034612	0.034236	0.02218	0.019799	0.011479	0.018897
500	0.037594	0.037268	0.023659	0.021103	0.012105	0.019549
480	0.041128	0.040852	0.025489	0.022757	0.012907	0.020251
460	0.045639	0.045213	0.02817	0.025063	0.014135	0.021153
440	0.051203	0.050226	0.032281	0.028296	0.01604	0.021955
420	0.059724	0.056992	0.040902	0.034662	0.02015	0.023709
400	0.076767	0.069474	0.060551	0.048571	0.029674	0.026792
380	0.145313	0.103258	0.099023	0.076667	0.048546	0.032105
360	0.350201	0.21198	0.188672	0.14	0.088847	0.043484
340	0.37619	0.262281	0.309298	0.247118	0.154436	0.064035
320	0.391629	0.272907	0.344336	0.288446	0.181454	0.071529
300	0.355439	0.245213	0.326466	0.26792	0.146717	0.038922

Table2: Variation of transmittance as a function of wavelength for $Zn_{1-x}Cu_xO$ film for different concentrations.

wavelength	x=0.00	x=0.05	x=0.09	x=0.15	x=0.20	x=0.25
1100	0.9225	0.9178	0.9304	0.9402	0.9653	0.9316
1080	0.9182	0.9158	0.9272	0.9371	0.9635	0.9282
1060	0.9133	0.9121	0.9233	0.9336	0.9609	0.9248
1040	0.9073	0.9078	0.9193	0.9292	0.9583	0.9211
1020	0.9047	0.9056	0.9176	0.9272	0.9569	0.9191
1000	0.9008	0.9021	0.9137	0.9237	0.9543	0.9154
980	0.8975	0.8993	0.9108	0.921	0.9523	0.9124
960	0.8943	0.8966	0.9081	0.9182	0.9503	0.9092
940	0.8911	0.8939	0.9054	0.9158	0.9481	0.9058
920	0.8878	0.8912	0.9025	0.913	0.9458	0.9025
900	0.8846	0.8883	0.8995	0.9099	0.9436	0.899
880	0.881	0.8848	0.8962	0.9065	0.9409	0.8958
860	0.877	0.8811	0.8931	0.9033	0.9382	0.8918
840	0.873	0.8767	0.8893	0.9	0.9355	0.8879
820	0.8688	0.8716	0.8854	0.8958	0.9324	0.8839
800	0.8639	0.8658	0.8813	0.8916	0.9293	0.8792
780	0.8586	0.8593	0.8772	0.8871	0.9255	0.8744
760	0.8533	0.8524	0.8729	0.8823	0.922	0.8695
740	0.8474	0.8453	0.8689	0.8778	0.9189	0.8649
720	0.8409	0.8381	0.8646	0.8735	0.916	0.8611
700	0.8336	0.8303	0.8605	0.8694	0.9135	0.8578
680	0.8259	0.8226	0.8568	0.8661	0.9114	0.8555
660	0.8171	0.8138	0.853	0.8629	0.9098	0.8538
640	0.808	0.8047	0.8497	0.8605	0.9093	0.853
620	0.7982	0.795	0.8466	0.8585	0.9094	0.8529
600	0.7866	0.7847	0.8419	0.8555	0.9084	0.8517
580	0.7743	0.7738	0.837	0.8521	0.9075	0.8501
560	0.7607	0.7614	0.8312	0.8472	0.9059	0.8479
540	0.7449	0.7468	0.8236	0.8408	0.903	0.8442
520	0.728	0.73	0.8149	0.833	0.899	0.8398
500	0.7083	0.7098	0.8041	0.8229	0.8937	0.8348
480	0.6857	0.6869	0.7909	0.8104	0.8872	0.8297
460	0.6578	0.66	0.7716	0.7936	0.8772	0.8226
440	0.6252	0.6307	0.7434	0.7706	0.8621	0.8167
420	0.5782	0.5928	0.6869	0.7273	0.8298	0.8038
400	0.4929	0.5284	0.574	0.6404	0.7609	0.7811
380	0.26	0.3868	0.4025	0.4941	0.6406	0.7446
360	0.0403	0.1427	0.1766	0.2761	0.4418	0.671
340	0.0319	0.0898	0.0583	0.1028	0.2421	0.5558
320	0.028	0.0815	0.0422	0.0706	0.1887	0.5184
300	0.0411	0.1064	0.0508	0.0856	0.261	0.701

Table3: Variation of $(\alpha h\nu)^2$ as a function of $h\nu$ for $Zn_{1-x}Cu_xO$ film for different concentrations.

hν	x=0.00	x=0.05	x=0.09	x=0.15	x=0.20	x=0.25
1.130114	5.913E+09	6.9E+09	4.63E+09	3.62E+09	1.11E+09	4.51E+09
1.151042	6.934E+09	7.54E+09	5.35E+09	4.18E+09	1.31E+09	5.21E+09
1.172759	8.121E+09	8.49E+09	6.18E+09	4.8E+09	1.56E+09	5.93E+09
1.195313	9.681E+09	9.67E+09	7.19E+09	5.6E+09	1.85E+09	6.84E+09
1.21875	1.065E+10	1.04E+10	7.81E+09	6.08E+09	2.03E+09	7.51E+09
1.243125	1.207E+10	1.17E+10	8.89E+09	7E+09	2.39E+09	7.82E+09
1.268495	1.336E+10	1.29E+10	9.93E+09	7.76E+09	2.74E+09	8.87E+09
1.294922	1.483E+10	1.42E+10	1.1E+10	8.74E+09	3.1E+09	9.94E+09
1.322473	1.652E+10	1.56E+10	1.22E+10	9.66E+09	3.51E+09	1.12E+10
1.351223	1.837E+10	1.72E+10	1.36E+10	1.08E+10	4.02E+09	1.27E+10
1.38125	2.049E+10	1.92E+10	1.51E+10	1.22E+10	4.56E+09	1.42E+10
1.412642	2.274E+10	2.13E+10	1.69E+10	1.36E+10	5.24E+09	1.6E+10
1.445494	2.559E+10	2.39E+10	1.89E+10	1.54E+10	6.04E+09	1.79E+10
1.479911	2.875E+10	2.7E+10	2.12E+10	1.73E+10	6.9E+09	2.03E+10
1.516006	3.237E+10	3.09E+10	2.39E+10	1.99E+10	8.01E+09	2.31E+10
1.553906	3.675E+10	3.58E+10	2.72E+10	2.25E+10	9.16E+09	2.84E+10
1.59375	4.204E+10	4.15E+10	3.09E+10	2.59E+10	1.08E+10	3.26E+10
1.635691	4.799E+10	4.84E+10	3.51E+10	2.96E+10	1.25E+10	3.71E+10
1.679899	5.515E+10	5.67E+10	3.97E+10	3.41E+10	1.43E+10	4.21E+10
1.726563	6.41E+10	6.63E+10	4.48E+10	3.9E+10	1.62E+10	4.73E+10
1.775893	7.468E+10	7.77E+10	5.06E+10	4.39E+10	1.82E+10	5.31E+10
1.828125	8.717E+10	9.1E+10	5.68E+10	4.92E+10	2.03E+10	5.8E+10
1.883523	1.036E+11	1.07E+11	6.38E+10	5.49E+10	2.24E+10	6.3E+10
1.942383	1.229E+11	1.27E+11	7.12E+10	6.06E+10	2.41E+10	6.78E+10
2.00504	1.467E+11	1.51E+11	7.92E+10	6.66E+10	2.57E+10	7.24E+10
2.071875	1.775E+11	1.81E+11	9.05E+10	7.46E+10	2.8E+10	7.87E+10
2.143319	2.164E+11	2.16E+11	1.03E+11	8.39E+10	3.05E+10	8.64E+10
2.219866	2.659E+11	2.63E+11	1.2E+11	9.64E+10	3.4E+10	9.56E+10
2.302083	3.325E+11	3.25E+11	1.42E+11	1.13E+11	3.89E+10	1.08E+11
2.390625	4.167E+11	4.07E+11	1.71E+11	1.36E+11	4.58E+10	1.24E+11
2.48625	5.317E+11	5.22E+11	2.1E+11	1.68E+11	5.51E+10	1.44E+11
2.589844	6.905E+11	6.81E+11	2.65E+11	2.12E+11	6.8E+10	1.67E+11
2.702446	9.258E+11	9.08E+11	3.52E+11	2.79E+11	8.88E+10	1.99E+11
2.825284	1.274E+12	1.22E+12	5.06E+11	3.89E+11	1.25E+11	2.34E+11
2.959821	1.902E+12	1.73E+12	8.91E+11	6.41E+11	2.16E+11	2.99E+11
3.107813	3.464E+12	2.84E+12	2.15E+12	1.39E+12	5.18E+11	4.21E+11
3.271382	1.375E+13	6.94E+12	6.38E+12	3.83E+12	1.53E+12	6.7E+11
3.453125	8.9E+13	3.26E+13	2.58E+13	1.42E+13	5.73E+12	1.37E+12

Table 4: Variation of refractive index (n) as a function of wavelength for $Zn_{1-x}Cu_xO$ film for different concentrations.

wavelength	x=0.00	x=0.05	x=0.09	x=0.15	x=0.20	x=0.25
1100	1.710936	1.738832	1.662233	1.597989	1.426669	1.654388
1080	1.737098	1.750974	1.681918	1.617858	1.439551	1.675549
1060	1.767055	1.773777	1.706209	1.640418	1.458559	1.696903
1040	1.803501	1.800072	1.730666	1.668632	1.477026	1.719682
1020	1.819243	1.813945	1.741098	1.681566	1.487134	1.731886
1000	1.842614	1.834776	1.765162	1.703228	1.505153	1.757571
980	1.862687	1.851807	1.782738	1.720209	1.518693	1.775519
960	1.881866	1.867953	1.799052	1.73728	1.532291	1.795118
940	1.900842	1.884241	1.81549	1.752025	1.547272	1.815843
920	1.920467	1.900166	1.832908	1.769135	1.562482	1.835475
900	1.939224	1.917085	1.850963	1.787899	1.576998	1.856756
880	1.960836	1.938043	1.870676	1.808822	1.5947	1.875607
860	1.984459	1.959993	1.888993	1.827793	1.612057	1.900014
840	2.008076	1.986147	1.91185	1.847563	1.629451	1.92319
820	2.032877	2.016343	1.935179	1.872545	1.649036	1.946842
800	2.061913	2.050431	1.959325	1.897975	1.668822	1.971474
780	2.093179	2.089121	1.983454	1.924704	1.692516	1.999647
760	2.1245	2.130094	2.008758	1.95342	1.714278	2.028833
740	2.159458	2.17204	2.032209	1.979745	1.733292	2.056178
720	2.197762	2.214662	2.057868	2.00488	1.751172	2.078477
700	2.241359	2.261265	2.082028	2.029513	1.766386	2.097584
680	2.287599	2.307279	2.103847	2.048923	1.779141	2.111465
660	2.340206	2.360389	2.126374	2.067837	1.788943	2.121629
640	2.395165	2.415353	2.145881	2.082033	1.791863	2.126376
620	2.454704	2.474929	2.1644	2.093871	1.791177	2.126886
600	2.526185	2.538045	2.192148	2.111471	1.797356	2.134008
580	2.602504	2.606152	2.221343	2.131636	1.802843	2.14334
560	2.688219	2.684138	2.255956	2.160835	1.812431	2.156416
540	2.789433	2.777673	2.301246	2.198804	1.830029	2.178355
520	2.900299	2.887643	2.353613	2.244977	1.853875	2.204607
500	3.032934	3.023474	2.418888	2.30557	1.885624	2.234355
480	3.189823	3.182069	2.499528	2.381007	1.924215	2.264551
460	3.391438	3.375767	2.619685	2.483308	1.983475	2.307302
440	3.638762	3.596236	2.799531	2.626095	2.072583	2.342662
420	4.02162	3.899298	3.181661	2.905392	2.264558	2.420656
400	4.813837	4.466417	4.057131	3.521766	2.687501	2.560607
380	7.739551	5.995403	5.803303	4.799703	3.520168	2.791738
360	8.119347	9.168459	8.837397	7.479239	5.351012	3.294922
340	7.670557	9.252623	8.766893	9.323711	7.961618	4.2161
320	7.396205	9.177164	8.226198	9.029518	8.691114	4.561194
300	7.96113	9.26802	8.484294	9.205887	7.680433	3.081431

Table 5: Variation of Extinction coefficient (k) as a function of wavelength for $Zn_{1-x}Cu_xO$ film for different concentrations.

wavelength	x=0.00	x=0.05	x=0.09	x=0.15	x=0.20	x=0.25
1100	0.005954	0.006431	0.005267	0.004655	0.002583	0.005197
1080	0.006215	0.006482	0.005457	0.004823	0.002704	0.005388
1060	0.006479	0.006625	0.005652	0.004981	0.002835	0.005536
1040	0.00681	0.006807	0.005869	0.005178	0.002976	0.005722
1020	0.006869	0.006788	0.005883	0.00519	0.002998	0.005771
1000	0.00703	0.006934	0.006032	0.005352	0.003126	0.005658
980	0.007103	0.006978	0.006125	0.005413	0.003216	0.005788
960	0.007182	0.00703	0.006194	0.005512	0.003285	0.005879
940	0.007266	0.007059	0.00624	0.005558	0.003348	0.005976
920	0.00734	0.007109	0.006307	0.005626	0.003434	0.006091
900	0.007419	0.007178	0.006366	0.005713	0.003499	0.006169
880	0.007473	0.007238	0.006444	0.005778	0.003586	0.006264
860	0.007571	0.007314	0.006511	0.005874	0.003678	0.006336
840	0.007656	0.007418	0.006582	0.005947	0.003749	0.006437
820	0.007741	0.00756	0.006654	0.006073	0.003851	0.006538
800	0.007851	0.007749	0.006753	0.006149	0.003919	0.006901
780	0.007982	0.007931	0.006839	0.006262	0.00404	0.007032
760	0.008097	0.00813	0.006924	0.006362	0.004125	0.007123
740	0.008229	0.008341	0.006983	0.006471	0.004189	0.007188
720	0.008399	0.008541	0.007018	0.006553	0.004222	0.007218
700	0.008568	0.008739	0.007052	0.006567	0.004235	0.007224
680	0.008736	0.008923	0.007051	0.00656	0.00422	0.007124
660	0.008972	0.009133	0.007039	0.006531	0.004167	0.006996
640	0.009187	0.009354	0.006995	0.006453	0.004071	0.006824
620	0.009421	0.009553	0.006921	0.006347	0.003944	0.00662
600	0.009705	0.009795	0.006931	0.006292	0.003854	0.006463
580	0.010013	0.01001	0.006925	0.006236	0.003761	0.006328
560	0.010347	0.010291	0.006947	0.00623	0.003701	0.006206
540	0.010759	0.010637	0.007043	0.006285	0.003678	0.006144
520	0.011169	0.011044	0.007154	0.006392	0.003704	0.006094
500	0.011665	0.01156	0.007338	0.00655	0.003756	0.006062
480	0.012251	0.012165	0.007589	0.006781	0.003845	0.006028
460	0.013028	0.012902	0.008038	0.007157	0.004035	0.006034
440	0.013981	0.013709	0.00881	0.007729	0.00438	0.005991
420	0.015566	0.014849	0.010656	0.009038	0.005252	0.006175
400	0.019055	0.017239	0.015024	0.012061	0.007366	0.006646
380	0.034267	0.024342	0.023341	0.018086	0.011447	0.007566
360	0.078235	0.047341	0.042132	0.031289	0.019848	0.009708
340	0.079373	0.055321	0.065231	0.05216	0.032583	0.013502
320	0.07777	0.054176	0.068349	0.057302	0.036031	0.014195
300	0.066171	0.045636	0.060752	0.049898	0.027313	0.007241

Table 6: Variation of optical conductivity (σ) as a function of hν for $Zn_{1-x}Cu_xO$ film for different concentrations.

hν	x=0.00	x=0.05	x=0.09	x=0.15	x=0.20	x=0.25
1.130114	2.77809E+12	3.04955E+12	2.38775E+12	2.02884E+12	1.00511E+12	2.34508E+12
1.151042	2.99888E+12	3.15251E+12	2.54938E+12	2.16734E+12	1.08135E+12	2.50789E+12
1.172759	3.24023E+12	3.32595E+12	2.72943E+12	2.31242E+12	1.17049E+12	2.65854E+12
1.195313	3.54268E+12	3.53478E+12	2.92999E+12	2.49239E+12	1.268E+12	2.83856E+12
1.21875	3.67546E+12	3.62124E+12	3.01262E+12	2.56665E+12	1.31137E+12	2.93946E+12
1.243125	3.88602E+12	3.81687E+12	3.19421E+12	2.73487E+12	1.41153E+12	2.98305E+12
1.268495	4.05003E+12	3.95595E+12	3.34241E+12	2.85046E+12	1.49509E+12	3.14598E+12
1.294922	4.22344E+12	4.10371E+12	3.48208E+12	2.99228E+12	1.57282E+12	3.29789E+12
1.322473	4.40793E+12	4.24496E+12	3.6155E+12	3.10763E+12	1.65317E+12	3.46297E+12
1.351223	4.59681E+12	4.40492E+12	3.76986E+12	3.24533E+12	1.74961E+12	3.6459E+12
1.38125	4.79553E+12	4.58721E+12	3.92786E+12	3.40493E+12	1.83944E+12	3.81804E+12
1.412642	4.99536E+12	4.78199E+12	4.10928E+12	3.56298E+12	1.94937E+12	4.00548E+12
1.445494	5.24072E+12	5.00071E+12	4.29048E+12	3.74539E+12	2.06837E+12	4.19935E+12
1.479911	5.49048E+12	5.26199E+12	4.49398E+12	3.92388E+12	2.18191E+12	4.42095E+12
1.516006	5.75748E+12	5.57711E+12	4.71127E+12	4.16049E+12	2.32355E+12	4.65688E+12
1.553906	6.07061E+12	5.95831E+12	4.96195E+12	4.37646E+12	2.45265E+12	5.10189E+12
1.59375	6.42636E+12	6.37282E+12	5.21732E+12	4.63574E+12	2.62961E+12	5.40789E+12
1.635691	6.79016E+12	6.83561E+12	5.48999E+12	4.9055E+12	2.79139E+12	5.70441E+12
1.679899	7.20416E+12	7.34507E+12	5.75312E+12	5.19339E+12	2.94366E+12	5.99222E+12
1.726563	7.69086E+12	7.88174E+12	6.01771E+12	5.47457E+12	3.08024E+12	6.25103E+12
1.775893	8.23036E+12	8.46948E+12	6.29228E+12	5.71235E+12	3.2059E+12	6.49433E+12
1.828125	8.81643E+12	9.08307E+12	6.54465E+12	5.92956E+12	3.31206E+12	6.63576E+12
1.883523	9.5433E+12	9.79859E+12	6.80315E+12	6.13874E+12	3.38873E+12	6.74685E+12
1.942383	1.0315E+13	1.05901E+13	7.0357E+12	6.2975E+12	3.41934E+12	6.8016E+12
2.00504	1.11899E+13	1.144E+13	7.24784E+12	6.43104E+12	3.41803E+12	6.81315E+12
2.071875	1.22583E+13	1.24302E+13	7.59635E+12	6.64279E+12	3.46337E+12	6.89567E+12
2.143319	1.34787E+13	1.34931E+13	7.95652E+12	6.87538E+12	3.50759E+12	7.01577E+12
2.219866	1.49009E+13	1.47983E+13	8.39614E+12	7.21163E+12	3.59389E+12	7.16917E+12
2.302083	1.66724E+13	1.64153E+13	9.00475E+12	7.67704E+12	3.73978E+12	7.4351E+12
2.390625	1.86883E+13	1.83986E+13	9.7146E+12	8.27837E+12	3.96151E+12	7.75085E+12
2.48625	2.12269E+13	2.09704E+13	1.06496E+13	9.06141E+12	4.24929E+12	8.12632E+12
2.589844	2.44235E+13	2.41929E+13	1.18557E+13	1.00914E+13	4.62355E+12	8.53179E+12
2.702446	2.88155E+13	2.84053E+13	1.37329E+13	1.15914E+13	5.2194E+12	9.08017E+12
2.825284	3.4686E+13	3.36152E+13	1.6817E+13	1.38392E+13	6.1888E+12	9.56887E+12
2.959821	4.47155E+13	4.13587E+13	2.4217E+13	1.87557E+13	8.49481E+12	1.06775E+13
3.107813	6.87973E+13	5.77487E+13	4.57154E+13	3.18581E+13	1.48462E+13	1.27634E+13
3.271382	2.09376E+14	1.15214E+14	1.06937E+14	6.85329E+13	3.18132E+13	1.66752E+13
3.453125	5.29351E+14	3.61705E+14	3.10278E+14	1.95013E+14	8.85047E+13	2.66558E+13
3.65625	5.37205E+14	4.51642E+14	5.04595E+14	4.29113E+14	2.28896E+14	5.02283E+13
3.884766	5.39249E+14	4.66108E+14	5.27109E+14	4.85074E+14	2.93581E+14	6.06987E+13
4.14375	5.26799E+14	4.22954E+14	5.15434E+14	4.59355E+14	2.09775E+14	2.23137E+13

Table 7: Variation of real part of dielectric constant as a function of wavelength for $Zn_{1-x}Cu_xO$ film for different concentrations.

wavelength	x=0.00	x=0.05	x=0.09	x=0.15	x=0.20	x=0.25
1100	2.927266	3.023494	2.762991	2.553546	2.035378	2.736972
1080	3.017472	3.065868	2.82882	2.61744	2.072299	2.807434
1060	3.122441	3.146242	2.911116	2.690948	2.127385	2.879449
1040	3.252571	3.240214	2.995171	2.784305	2.181596	2.957274
1020	3.309599	3.290349	3.031389	2.827639	2.211559	2.999395
1000	3.395176	3.366354	3.115762	2.900957	2.265475	3.089024
980	3.469551	3.42914	3.178117	2.959089	2.306419	3.152434
960	3.541369	3.489198	3.23655	3.01811	2.347905	3.222413
940	3.613147	3.550316	3.295966	3.069562	2.394041	3.297249
920	3.688139	3.610581	3.359511	3.129806	2.44134	3.368931
900	3.760534	3.675165	3.426025	3.196549	2.486909	3.447505
880	3.844823	3.755959	3.499388	3.271804	2.543057	3.517862
860	3.93802	3.84152	3.568252	3.340792	2.598716	3.610013
840	4.03231	3.944726	3.655127	3.413452	2.655095	3.698619
820	4.132529	4.065583	3.744873	3.506389	2.719305	3.790152
800	4.251424	4.204206	3.838909	3.60227	2.784952	3.886662
780	4.381336	4.364364	3.934044	3.704446	2.864595	3.998538
760	4.513434	4.537235	4.035061	3.81581	2.938732	4.116114
740	4.663191	4.71769	4.129825	3.91935	3.004283	4.227816
720	4.830086	4.904657	4.234771	4.019502	3.066584	4.320014
700	5.023616	5.113242	4.334791	4.118882	3.120102	4.399806
680	5.233032	5.323457	4.426124	4.198042	3.165324	4.458232
660	5.476485	5.571355	4.521417	4.275908	3.2003	4.501261
640	5.736733	5.833845	4.604757	4.33482	3.210757	4.521428
620	6.025482	6.125184	4.684578	4.384254	3.2083	4.523599
600	6.381518	6.441574	4.805466	4.458272	3.230475	4.553949
580	6.772927	6.79193	4.934319	4.543832	3.250229	4.593866
560	7.226413	7.204489	5.089287	4.669169	3.284894	4.650092
540	7.780821	7.715353	5.295686	4.8347	3.348992	4.745194
520	8.411612	8.338358	5.539442	5.039882	3.43684	4.860254
500	9.198551	9.141262	5.850966	5.315611	3.555565	4.992307
480	10.17482	10.12542	6.247584	5.669147	3.702587	5.128155
460	11.50169	11.39563	6.862687	6.166768	3.934157	5.323607
440	13.24039	12.93273	7.837294	6.896315	4.29558	5.488031
420	16.17319	15.20431	10.12286	8.441223	5.128193	5.859536
400	23.17266	19.94858	16.46008	12.40269	7.222605	6.556666
380	59.89948	35.94427	33.67779	23.03683	12.39145	7.793746
360	65.9177	84.0584	78.09781	55.93804	28.63294	10.85642
340	58.83116	85.60798	76.85417	86.92887	63.3863	17.77532
320	54.69781	84.21741	67.66566	81.52892	75.53417	20.80429
300	63.37521	85.89411	71.97956	84.74586	58.98831	9.495168

Table 8: Variation of imaginary part of dielectric constant as a function of wavelength for $Zn_{1-x}Cu_xO$ film for different concentrations.

wavelength	x=0.00	x=0.05	x=0.09	x=0.15	x=0.20	x=0.25
1100	0.020373	0.022363	0.01751	0.014878	0.007371	0.017197
1080	0.021592	0.022698	0.018356	0.015605	0.007786	0.018057
1060	0.022898	0.023503	0.019288	0.016341	0.008271	0.018787
1040	0.024563	0.024508	0.020315	0.017281	0.008791	0.019681
1020	0.024993	0.024624	0.020486	0.017453	0.008917	0.019988
1000	0.025907	0.025446	0.021295	0.018232	0.00941	0.019887
980	0.02646	0.025846	0.021837	0.018623	0.009768	0.020554
960	0.02703	0.026264	0.022285	0.019151	0.010066	0.021106
940	0.027623	0.026602	0.022657	0.019474	0.01036	0.021701
920	0.028194	0.027017	0.023122	0.019905	0.010731	0.022362
900	0.028773	0.027523	0.023567	0.02043	0.011037	0.022908
880	0.029306	0.028054	0.024108	0.020903	0.011436	0.023499
860	0.030047	0.028671	0.024599	0.021474	0.011859	0.024076
840	0.030747	0.029467	0.025166	0.021974	0.012219	0.024757
820	0.031474	0.030488	0.025755	0.022744	0.012702	0.025458
800	0.032377	0.031778	0.026464	0.023341	0.013081	0.02721
780	0.033417	0.033139	0.02713	0.024106	0.013674	0.028121
760	0.034403	0.034634	0.027816	0.024855	0.014143	0.028902
740	0.035541	0.036236	0.028382	0.025621	0.014522	0.029562
720	0.036916	0.037832	0.028885	0.026278	0.014785	0.030005
700	0.038408	0.039524	0.029364	0.026658	0.014961	0.030307
680	0.039968	0.041177	0.029669	0.026881	0.015015	0.030082
660	0.04199	0.043114	0.029934	0.02701	0.01491	0.029686
640	0.044011	0.045184	0.030019	0.026869	0.014589	0.02902
620	0.046252	0.047285	0.029958	0.026582	0.014128	0.028161
600	0.049033	0.049721	0.030385	0.026571	0.013853	0.027583
580	0.052118	0.052173	0.030765	0.026585	0.013563	0.027128
560	0.05563	0.055247	0.031346	0.026923	0.013417	0.026765
540	0.060021	0.059095	0.032417	0.027637	0.013463	0.026766
520	0.064786	0.063782	0.033677	0.028698	0.013733	0.02687
500	0.070756	0.069901	0.035499	0.030205	0.014164	0.027088
480	0.078155	0.077417	0.037938	0.032293	0.014795	0.027302
460	0.088368	0.087109	0.042114	0.035547	0.016006	0.027846
440	0.101746	0.098605	0.04933	0.040595	0.018154	0.028069
420	0.125203	0.115804	0.067808	0.052516	0.023785	0.029897
400	0.183459	0.153997	0.121908	0.084955	0.03959	0.034036
380	0.530419	0.291876	0.270908	0.173617	0.080593	0.042244
360	1.270442	0.868091	0.744666	0.468032	0.212411	0.063974
340	1.217666	1.023721	1.143748	0.972655	0.51883	0.113851
320	1.150399	0.994364	1.1245	1.034824	0.626307	0.129491
300	1.053598	0.845908	1.030868	0.918711	0.419549	0.044627

Table 9: Variation of electrical resistivity (ρ) with temperature for as deposited $Zn_{1-x}Cu_xO$ thin films for different concentrations

Temp(K)	x=0.00 $\rho\ x10^{-2}$	x=0.05 $\rho\ x10^{-2}$	x=0.09 $\rho\ x10^{-2}$	x=0.15 $\rho\ x10^{-2}$	x=0.20 $\rho\ x10^{-2}$	x=0.25 $\rho\ x10^{-2}$
320	1.3742	1.5324	1.8023	2.2413	2.5021	2.8025
330	1.1523	1.3221	1.6354	2.0342	2.3425	2.6212
340	0.9544	1.1532	1.4282	1.8313	2.1523	2.4325
350	0.8521	0.9511	1.2212	1.6442	1.9542	2.2153
360	0.7813	0.8524	1.0135	1.4134	1.7517	2.0164
370	0.7072	0.7713	0.8524	1.2145	1.5432	1.8134
380	0.6507	0.6942	0.8048	1.1132	1.4413	1.7221
390	0.6021	0.6435	0.7535	1.0317	1.3621	1.6435
400	0.5413	0.5944	0.7021	0.9523	1.2873	1.5623
410	0.4834	0.5413	0.6542	0.8734	1.2003	1.4889
420	0.4242	0.4942	0.6073	0.7921	1.1213	1.4031
430	0.3621	0.4428	0.5563	0.7142	1.0442	1.3217

Table 10: Variation of electrical conductivity (σ) with temperature for as deposited $Zn_{1-x}Cu_xO$ thin films for different concentrations

Temp(K)	x=0.00 $\sigma\ x10^{2}$	x=0.05 $\sigma\ x10^{2}$	x=0.09 $\sigma\ x10^{2}$	x=0.15 $\sigma\ x10^{2}$	x=0.20 $\sigma\ x10^{2}$	x=0.25 $\sigma\ x10^{2}$
320	0.7277	0.65257	0.55485	0.44617	0.39966	0.35682
330	0.86783	0.75637	0.61147	0.49159	0.42689	0.3815
340	1.04778	0.86715	0.70018	0.54606	0.46462	0.4111
350	1.17357	1.05141	0.81887	0.6082	0.51172	0.45141
360	1.27992	1.17316	0.98668	0.70751	0.57087	0.49593
370	1.41403	1.29651	1.17316	0.82338	0.648	0.55145
380	1.53681	1.44051	1.24254	0.89831	0.69382	0.58069
390	1.66085	1.554	1.32714	0.96927	0.73416	0.60846
400	1.8474	1.68237	1.4243	1.05009	0.77682	0.64008
410	2.06868	1.8474	1.52858	1.14495	0.83313	0.67164
420	2.35738	2.02347	1.64663	1.26247	0.89182	0.71271
430	2.76167	2.25836	1.79759	1.40017	0.95767	0.7566

Table 11: Variation lnσ as a function of 1/T for the as-deposited $Zn_{1-x}Cu_xO$ thin films for different concentrations.

Temp(K)	x=0.00	x=0.05	x=0.09	x=0.15	x=0.20	x=0.25
3.33333	-0.31787	-0.42684	-0.58906	-0.80706	-0.91713	-1.03051
3.22581	-0.14176	-0.27922	-0.49189	-0.7101	-0.85122	-0.96363
3.125	0.04667	-0.14254	-0.35641	-0.60503	-0.76654	-0.88892
3.0303	0.16005	0.05014	-0.19983	-0.49725	-0.66998	-0.79539
2.94118	0.2468	0.1597	-0.01341	-0.346	-0.56059	-0.70131
2.85714	0.34644	0.25968	0.1597	-0.19433	-0.43386	-0.5952
2.77778	0.42971	0.365	0.21716	-0.10724	-0.36555	-0.54354
2.7027	0.50733	0.44083	0.28303	-0.03121	-0.30903	-0.49683
2.63158	0.61378	0.5202	0.35368	0.04888	-0.25255	-0.44616
2.5641	0.72691	0.61378	0.42434	0.13536	-0.18257	-0.39804
2.5	0.85755	0.70481	0.49873	0.23307	-0.11449	-0.33868
2.43902	1.01583	0.81464	0.58645	0.33659	-0.04325	-0.27892